FLORIDA INTERNATIONAL UNIVERSITY

Miami, Florida

MODIFIED GUANIDINE-CONTAINING POLYMERS FOR INTRACELLULAR PROTEIN DELIVERY

A dissertation submitted in partial fulfillment of

the requirements for the degree of

DOCTOR OF PHILOSOPHY

in

CHEMISTRY

by

Alfonso Barrios

2022

To: Dean Michael R. Heithaus
College of Arts, Sciences and Education

This dissertation, written by Alfonso Barrios, and entitled Modified Guanidine-Containing Polymers for Intracellular Protein Delivery, having been approved in respect to style and intellectual content, is referred to you for judgment.

We have read this dissertation and recommend that it be approved.

_____
Yuan Liu

_____
Bruce McCord

_____
Anthony McGoron

_____
Stanislaw Wnuk

_____
Joong Ho Moon, Major Professor

Date of Defense: June 13, 2022

The dissertation of Alfonso Barrios is approved.

_____
Dean Michael R. Heithaus
College of Arts, Sciences and Education

_____
Andres G. Gil
Vice President for Research and Economic Development
and Dean of the University Graduate School

Florida International University, 2022

ACKNOWLEDGMENTS

First and foremost, I would like to thank my advisor, Dr. Joong Ho Moon, without whom this work would not have been possible. The continuous support and endless guidance throughout my studies have taught me valuable lessons that I will carry with me throughout my life.

I would like to thank the members of my dissertation committee, Dr. Yuan Liu, Dr. Bruce McCord, Dr. Anthony McGoron, and Dr. Stanislaw Wnuk. The feedback, input, and questions received every meeting solidified my scientific understanding and presented me with an opportunity to grow, for which I am very grateful.

A special thanks goes out to Kyle Martin and the rest of the wonderful scientists at the Translational Glycobiology Institute at HWCOM. Their welcoming spirit and kind hospitality made me feel like part of their team. This work would be incomplete without their guidance, expertise, and unique perspectives.

I am forever thankful to all past and present members of Dr. Moon's research group. Our tight knit and collegial environment made this process so much better. Michelle, thank you for research advice, eagerness to help, and always willingness to listen. These past years would not have been the same without you. Sabbir, thank you for your kindness and inclination to help in any way possible. Mario, thank you for your continuous stream of jokes, you brought a lot of laughs to the lab. Patricia, Marilen, and Elianny – it has been a pleasure to have you as undergraduate researchers. Your motivation for research and enthusiasm to learn will always be remembered.

I would like to thank my family - my father, mother, and sister, for their love and support throughout my studies and life. I was fortunate enough to see them every day after

lab, and being surrounded by loved ones made this process possible. Finally, I must express my very profound gratitude to my forever partner, Vivi. Your lasting support and continuous encouragement made this possible. Thank you for being the reassuring voice whenever things got difficult.

ABSTRACT OF THE DISSERTATION

MODIFIED GUANIDINE-CONTAINING POLYMERS FOR INTRACELLULAR PROTEIN DELIVERY

by

Alfonso Barrios

Florida International University, 2022

Miami, Florida

Professor Joong Ho Moon, Major Professor

Protein-based therapeutics have gained significant attention for treating or curing various diseases, especially those untreatable by small molecule-drugs. Despite their widespread success and adoption, the cellular membrane remains a major obstacle for proteins to reach the inner compartments of the cell and have had limited applicability spanning only extracellular targets. Consequently, the efficient intracellular delivery of proteins offers tremendous potential to reach new, unexplored, and otherwise "undruggable" targets. Acknowledging the therapeutic need, research efforts aimed at facilitating the delivery of proteins using polymer-based nanoparticles have emerged.

Guanidine-containing polymers provide a promising platform to address the common hurdles associated with protein delivery. Specifically, this work focuses on the design, synthesis, and development of polymeric carriers featuring a rational guanidine modification. A new class of carbamoylated guanidine-containing polymers were characterized, optimized, and evaluated for their efficacy in protein delivery. The developed functional group aided the biophysical properties of complexes, resulting in a dramatic increase in protein delivery compared to commercially available carriers. The

planarity and rigidity of the developed side chains aided complexation with cargo, stability in the harsh physiological environment, and subsequent cellular entry. Additionally, therapeutically relevant proteins were intracellularly delivered and assayed for their retained function, revealing the potential these carriers have for translational applications. Key insights into the fundamental identity of the carbamoylated guanidine functional group revealed novel design features that can be incorporated into delivery systems moving forward, expanding the field of protein delivery.

TABLE OF CONTENTS

LIST OF TABLES

TABLE PAGE

LIST OF FIGURES

FIGURE PAGE

LIST OF SCHEMES

SCHEME PAGE

ABBREVIATIONS AND ACRONYMS

BSA	bovine serum albumin
$CDCl_3$	deuterated chloroform
CG	carbamoylated guanidine
CPP	cell penetrating peptide
DCM	dichloromethane
DMF	dimethylformamide
DMSO	dimethylsulfoxide
EGFP	enhanced green fluorescent protein
FBS	fetal bovine serum
FP	fluorescent protein
HB	hydrogen bond
HD	hydrodynamic diameter
K_d	dissociation constant
MeOH	methanol
MFI	mean/median fluorescent intensity
M_n	number average molecular weight
MTT	(3-(4,5-dimethylthiazol-2-yl)-2,5-diphenyltetrazolium bromide
M_w	weight average molecular weight
NMR	nuclear magnetic resonance
NTA	nanoparticle tracking analysis
PAA	poly(amidoamine)
PBAE	poly(beta-amino ester)

PBS	phosphate buffered saline
PCC	Pearson’s correlation coefficient
PEI	polyethyleneimine
PLGA	poly(lactic-co-glycolic acid)
PLL	polylysine
PN	polynorbornene
PTD	protein transduction domain
PTDM	protein transduction domain mimic
PTFE	polytetrafluoroethylene
R-PE	R-phycoerythrin
ROMP	ring opening metathesis polymerization
TFA	trifluoroacetic acid
THF	tetrahydrofuran

CHAPTER I

Intracellular Delivery of Therapeutic Proteins

1.1. Introduction

Protein-based drugs are one of the fastest growing class of therapeutics.[1,2] The protein therapeutics market size was valued at $280 Billion in 2020 and is projected to reach over $560 Billion by 2030, indicating the significant and continued growth in the space. Their significant advantages over conventional small-molecule drug therapy has revolutionized the pharmaceutical industry. Owing to the highly specific action of proteins, the off-target effects encountered in therapy is limited.[3] Additionally, the endogenous nature of proteins means they are generally well tolerated and less likely to elicit immune responses.[1] These factors contribute to the faster clinical development and regulatory approval timeline for protein-based drugs, increasing their attractiveness in the field.[1]

Currently used protein-based therapeutics can be broadly classified into two categories: proteins with enzymatic or regulatory activity and proteins with special targeting activity.[1] Proteins with enzymatic or regulatory activity are generally used by replacing a protein that is deficient or abnormal or by augmenting biological pathways linked to disease states. Proteins with special targeting activity are designed to interfere with a known molecule by binding and blocking their function or stimulating a signaling pathway.[1,2,4] Nevertheless, proteins have the therapeutic potential to address issues in cancer therapy, metabolic diseases, and vaccine development.[1,3] Despite this, all currently used protein-based drugs were developed for targeting extracellular targets, such as cell membrane associated proteins and secretory proteins.[5] This restraint is caused by the membrane impermeability of proteins and limited cellular entry. The physical properties of proteins, such as size and hydrophilicity make proteins generally incapable of diffusion across cellular membranes and therefore lack the ability to reach intracellular sites. It is

estimated only 30% of genome-encoded proteins are extracellularly available to proteins, leaving a plethora of "undruggable" intracellular targets.[6,7] To address these issues, a wide array of intracellular delivery methods have been developed for therapeutic proteins.

For successful protein delivery, the carrier must efficiently complex the protein cargo, maintain the complex stability in the harsh extracellular environment, internalize the complex intracellularly, and finally, release the cargo in the cell.[8] Factors regarding the inter-macromolecular interactions between the carrier and cargo, mechanism of cellular entry, and temporal release of the therapeutic protein cargo dictate the success of a developed system.

1.2. Delivery Methods

Intracellular protein delivery has gained significant attention in recent times and many of the concepts stem from the field of nucleic acid delivery. The field began with the use of physical delivery methods such as electroporation but quickly shifted toward the use of lipids, peptides, and polymeric systems to facilitate the transport of proteins to the intracellular space in cells. A description of each of these methods is discussed, with a specific focus on the key structural and chemical identities of these.

1.2.1. Peptide-based Delivery

Cell penetrating peptides (CPPs) are short amino acid sequences (10-30 residues), primarily composed of cationic and hydrophobic residues.[9] These peptide sequences have been shown to translocate across the cell membrane using various mechanisms, including both endocytotic and non-endocytotic, energy-independent pathways. The mechanism of uptake is highly dependent on the type of cargo delivered with the CPP, yet most

applications show entry via endocytosis mechanisms such as clathrin mediated and macropinocytosis pathways.[10,11]

Intracellular delivery using CPPs has mainly been achieved via the direct conjugation of CPP sequences to the cargo, requiring modification of the protein itself.[4,11] Few examples of CPPs being used to delivery proteins non-covalently are reported in the literature, attempting to circumvent the protein modification steps required with covalent conjugation. Nevertheless, the discovery of HIV-1 Tat led to the entire field of CPPs for delivery[9,12,13], and various methods are discussed here.

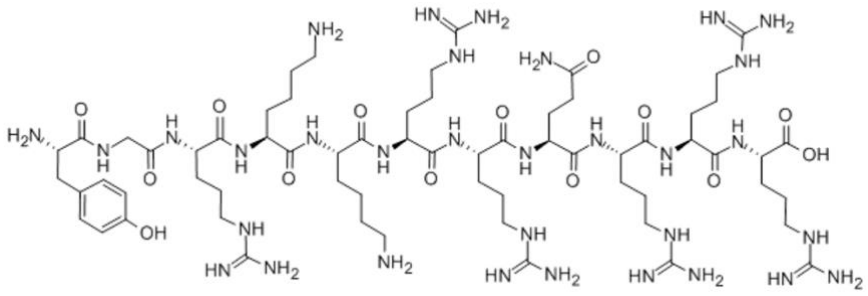

Figure 1.1. Chemical structure of HIV-1 Tat Peptide.

Both naturally occurring CPPs and their synthetic mimics have been explored for delivery. Transportan, a 27 amino acid-long CPP was shown to deliver large proteins, such as antibodies (150 kDa) either by covalent attachment or non-covalent complexation.[14] The transportan carriers were initially biotinylated in order to improve carrier-protein interactions and intracellular delivery. In a similar approach, a peptide carrier, Pep-1, was developed for the non-covalent delivery of proteins.[15] Pep-1 is a 21-residue peptide, consisting of three domains: a hydrophobic tryptophan-rich sequence, a hydrophilic lysine rich motif, and a flexible proline segment. Green fluorescent protein (GFP) was delivered to greater than 80% of the cell population using this non-covalent approach. In both

examples, the need of a hydrophobic segment or specific binding motif was needed to complex the cargo protein effectively.

The use of CPPs has proven to be an effective tool for the delivery of proteins, but challenges remain for their widespread use. For those using covalent modification of proteins, problems arising from the altered protein structure and loss of activity are persistent.[4,7,11] Additionally, the mechanism of entry is variable depending on the cargo delivered and endosomal entrapment is a hurdle to be addressed. Taken together, the naturally occurring CPPs and their synthetic mimics are highly biocompatible and a promising platform for the delivery of proteins to the intracellular compartment of cells.

1.2.2. Lipid-based Delivery

Lipid-based carriers, such as liposomes, have traditionally been used as nanocarriers for the delivery of various macromolecules including proteins, antibodies, peptides, and nucleic acids. Liposomes are generally composed of phospholipids forming a spherical vesicle with at least one lipid bilayer. The liposomal bilayer forms a hydrophilic core that encapsulates and stabilizes cargo and facilitates internalization typically via electrostatic interactions by the addition of cationic charges on the lipid membrane.[16–18] The high compatibility and biodegradability of liposomes have made them attractive carriers for delivery applications.

Significant efforts have been made to develop liposomes with stimuli responsiveness (pH[19], redox[20], light[21], temperature[22]), improved circulation life (via PEGylation[23]), and specific cell targeting.[24] Additionally, the desirable aspects of liposome-based platforms have led to several commercially available lipids for protein delivery.[4]

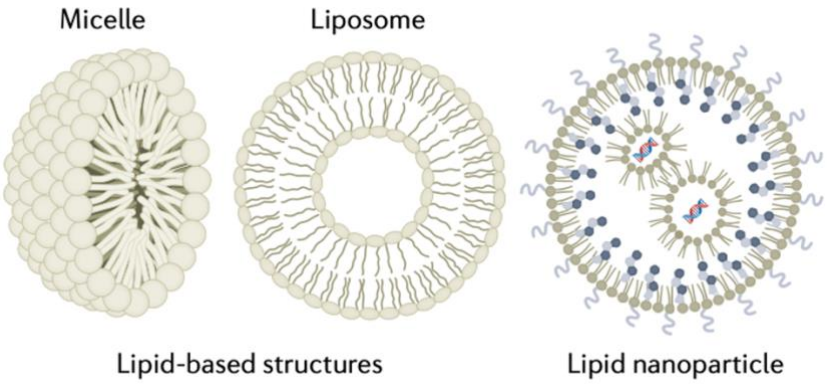

Figure 1.2. Schematic representation of lipid-based structures and lipid nanoparticles. Adapted from Dahlman et. al.[25]

An example of a commercially available solution for protein delivery mediated by a cationic lipid is PULSin (Polyplus-transfection (France)). PULSin has been widely used to deliver fluorescent proteins, antibodies, and enzymes to a wide array of cell types. Other type of cationic liposomes, Pierce (ThermoFisher Scientific, USA) and BioPORTER (Gene Therapy Systems, USA) have also demonstrated ability to delivery functional proteins to cells.[4]

In general, complimentary electrostatic and hydrophobic interactions have been leveraged to assist in lipid-protein assembly and subsequent internalization into cells. Cationic lipids containing ammonium and guanidiniums groups have been used extensively and balanced with helper co-lipids.[26] Similarly, the incorporation of cell penetrating peptides in liposomal delivery systems has been reported in the literature.[27] Although with some success, the use of cell penetrating peptides in these formulations has been associated with significant endosomal entrapment, hindering its efficacy. Formulations with specific targeting has also been explored. In one example, an anti-CD44 antibody was decorated on liposomal formulations, and demonstrated efficient targeting and functional antibody delivery.[28]

The success of liposomes as protein carriers stems from their tunable composition and ease of use. The ability to add surface functionality and encapsulate differing cargo has made them an attractive platform. Additionally, the previous clinical use of liposomal systems offer a competitive advantage. Despite this, various hurdles limit their use. In addition to endosomal entrapment, common liposome preparation protocols require the use of organic solvents, sonication, and detergents, that can cause problems of protein denaturation. Low protein loading efficiency and the stability of liposomal preparations is another area needing significant improvement. Disruption of liposome vesicles by serum proteins leads to poor serum-stability and delivery efficacy. Many protocols for lipid carriers require serum-free conditions leading to high cellular toxicity and making them unfavorable carriers for sensitive cell lines such as primary cells. Nonetheless, lipid-based carriers remain widely used as carriers for the delivery of proteins.

1.2.3. Polymeric Nanocarriers

Polymer-based nanoparticles offer great tunability in molecular weight, particle size, and functional groups, making them attractive candidates for protein delivery systems. Hurdles associated with protein carriers have been continuously addressed with novel structure and polymer designs. Enhancement of circulation time[29,30], complex stability[31,32], and tissue-specific targeting[33] have aided the in vivo translation of this technology.

Generally, non-covalent complexation approaches have gained significant attention due to the ease of preparation and the lack of protein modification steps involved with covalent conjugation. Inter-macromolecular interactions such as electrostatic, hydrophobic, and hydrogen bonding interactions have dictated the self-assembly of

polymer-protein complexes. A variety of classes of polymers and architectures have been explored and reviewed extensively. Here, representative examples are discussed.

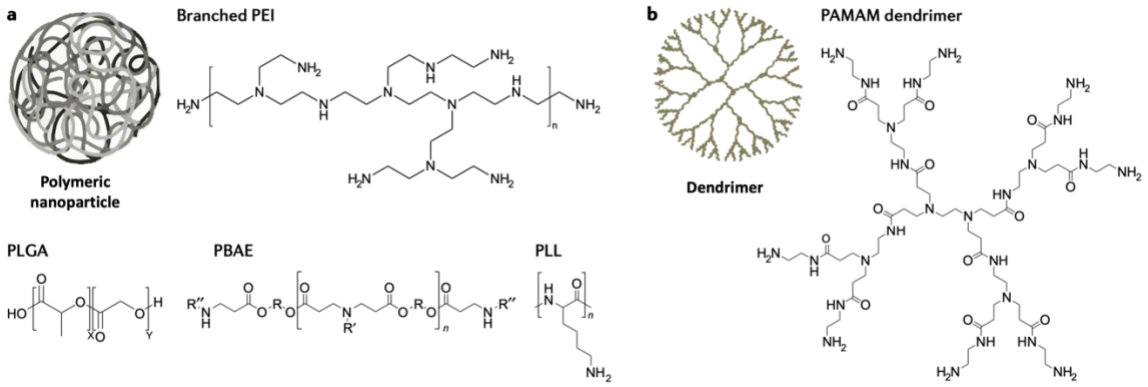

Figure 1.3. Schematic representation of polymeric nanoparticle (a) and dendrimer (b) structure. PEI: polyethyleneimine, PLGA: poly(lactic-co-glycolic acid), PBAE: poly(beta-amino ester), PLL: polylysine, PAMAM: polyamidoamine. Adapted from Dahlman et. al.[25]

Various biodegradable polymers commonly used for gene delivery have been modified and repurposed for protein delivery purposes. Poly(lactic-*co*-glycolic acid) (PLGA) is a copolymer used in various FDA-approved formulations recently shown to non-covalently deliver anti-annexinA2 (AnxA2) antibody.[34] Release kinetics demonstrated the slow degrading features of the formulation had sustained antibody release and maintained functionality Given the lack of hydrophobic segment in this carrier, encapsulation efficacy of only about 20% was achieved. Another commonly used biodegradable polymer, polyethyleneimine (PEI) was modified for protein delivery.[35] PEI was grafted with fluoroalkanes to varying degrees via amine-isocyanate reactions. The high complexation ability and subsequent delivery of fluorinated carriers was shown, indicating the importance of hydrophobicity in the assembly. Similarly, other PEI[36], poly(amidoamine)s (PAAs)[37], and other biodegradable polymers and their derivatives have been studied for protein delivery. Another class of polymers, hyperbranched poly(β-amino

ester)s (PBAEs) have gained significant attention for gene delivery.[8] In one approach, PBAEs were modified with hydrophobic, cationic, and anionic segments in order to encapsulate proteins with simple mixing. The robust platform was able to complex proteins of varying sizes and enable functional protein delivery.

Dendrimers are a type of highly ordered branched polymers. In general, dendrimers are symmetric around their central core and have a three-dimensional morphology. Surface groups of dendrimers are modified with various functional groups to alter their surface properties and ultimately tailor their biological properties. Similar to some biodegradable polymers previously discussed, the field of gene delivery has advanced with the use of dendrimer carriers and recently been applied for protein delivery. Cheng et. al. has designed various dendrimers with surface functionalities and stimuli responsiveness for the delivery of peptides and proteins. In one example, the hydrophilic surface amines of a generation 5 poly(amidoamine) (PAMAM) dendrimer were reacted with guanidinobenzoic acid to increase hydrophobicity via the aromatic pendant and protein complexation with the inclusion of the guanidinium group.[38] Various antibodies, enzymes, and peptides were successfully delivered in vitro and in vivo. Mice bearing PC-9 tumors showed tumor growth reduction when the dendrimer delivered an apoptosis-inducing protein compared to controls. Despite these positive results, administration was done with intratumoral injections, indicating the challenges associated with systemic administration. In another example, the serum stability of dendrimer-protein complexes was improved by engineering a pH-responsive assembly-disassembly process.[31] The surface modification of dendrimer with motifs having varying solubility at the physiological pH range allowed complexes to

maintain stability in the presence of serum and allowed dissociation of the cargo from carrier at the endosomal pH.

Synthetic polymers can readily be designed to mimic the key structural features of naturally occurring macromolecules. Specifically, features of CPPs have been incorporated into synthetic protein carriers by various groups. Short sequences within proteins or peptides termed protein transduction domains (PTDs) have been extensively studied to determine their role in cellular entry. Cationic residues such as lysine and arginine, together with hydrophobic residues such as tryptophan, compose the structure of various CPPs, such as Pep-1 previously discussed. Polymers with side chains resembling these amino acid side chains have been used for protein delivery. In one example, Tew et. al. developed ring opening metathesis polymerization (ROMP)-based polymers mimicking PTD.[39] These PTD mimics (PTDMs) demonstrated delivery of various fluorescent and functional proteins. PTMDs with arginine-like, guanidinium moieties performed better than those with primary amines, consistent with what is observed in CPPs. The architecture of PTDMs has also been explored.[40] Polymers with random- or block-copolymer architecture were studied for their efficacy in protein delivery. PTDMs with isolated hydrophobic and hydrophilic segments performed significantly when EGFP was delivered to Jurkat T cells.

An important characteristic to understand regarding polymeric carriers is the strength of interaction between the two macromolecules. The interaction between these two macromolecular entities can dictate stability, cellular entry, and finally, the release of the cargo inside the cell. Using fluorescence-based assays, the binding interaction and strength for polymers has been extensively studied.[41,42] Although binding strength was not directly correlated to delivery efficacy, the intracellular function of the functional protein

was dictated by the unbinding of protein from the carrier. Overall, the understanding of interactions at the interface of the carrier and cargo is vital to enable more effective methods for protein delivery.

Polymer-based nanocarriers are one of the most attractive methods for protein delivery due to their facile synthesis and endless modification strategies. The ability to synthesize and formulate varying polymer designs allows researchers to tackle the hurdles of poor complex stability and cellular entry, biodegradability, and biocompatibility. An improved understanding of the structure-activity relationship of polymer design and protein delivery is critical for the continued expansion of the field.

1.3. Functional Group Design for Protein Carriers

1.3.1. Guanidine and Guanidinium

Guanidine-containing compounds are highly valued in many biological applications. Lessons learned from the field of CPPs and their mimics have demonstrated the importance of guanidinium groups and their interaction with biological membranes and macromolecular entities. Among CPPs, arginine-rich sequences have been shown to be highly efficient in cellular entry and have therefore been exploited for protein delivery. Various studies have demonstrated that guanidinium headgroups are primarily responsible for the uptake into cells.[12] When other cationic residues, such as lysine, are replaced with guanidine-containing arginine, cellular uptake is enhanced. Various differing mechanisms can explain their importance on cellular entry, given both energy dependent and independent pathways lead to entry. A passive diffusion across the nonpolar cellular membrane is difficult to explain given the polarity of charged arginine residues. However, it is believed the polarity of the guanidinium groups is decreased through association with

surface associated oxyanionic groups, such as carboxylate and phosphate ions.[12,43] These less polar ion pair complexes are capable of diffusing through the membrane. Methylation of guanidinium-rich oligomers demonstrate they are less efficient in cellular entry. Despite this, as mentioned previously, depending on the cargo carried across the membrane, the mechanism of entry may vary. Additionally, when association constants (K_{assoc}) are measured between anions and guanidinium/ammonium-containing compounds, it is revealed the K_{assoc} is significantly stronger for guanidinium, indicating the strong bidentate interactions present.[43] The high pK_a (~13) of guanidinium provides a delocalized positive charge that can lead to efficient electrostatic interactions. The hydrogen bonding (HB) interactions present are also enhanced due to the strong ionic interaction, thus both interactions work dependently on one another.[44]

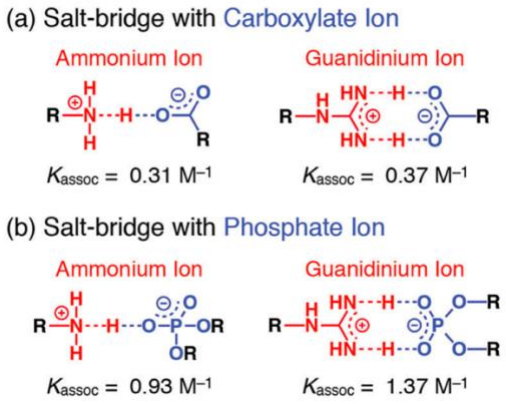

Figure 1.4. Association constants (K_{assoc}) of interaction of ammonium and guanidinium ions with carboxylate (a) and phosphate (b) ions. Adapted from Aida et. al.[43]

To date, various classes of carriers rich in guanidine have been developed to transport biological macromolecules, such as proteins, across the cell membrane. The attractive properties of guanidinium have led researchers to incorporate this distinctive and unique functional group into the carrier design.

1.3.2. Guanidine Derivatives

As previously discussed, guanidine-containing compounds are highly valued for many biological applications. Despite the beneficial properties of guanidine-rich carriers, such as their cellular entry, this functional group has also been associated with various hurdles holding back protein carriers. Their cationic nature is in part responsible for poor stability in serum and high toxicity seen in various applications. Naturally, this had led many researchers to design and develop guanidine-based derivatives with improved and tailored biological properties.

The strong ionic, and bidentate hydrogen bonding interactions possible with guanidine-rich compounds have been significantly studied and are the main driving forces behind guanidine's attractiveness. In many regards, a derivative that tailors these forces are possible through many approaches.

In one example discussed briefly earlier, guanidine octamers were momo- or dimethylated and their cellular entry was studied.[12] The alkylated guanidiniums had an attenuated ability to form strong HBs and therefore their cellular entry suffered. A reduction of 80 and 95% cellular entry, for mono- and dimethylated octamers, respectively, was observed. These results indicate how modification that restricts hydrogen bonds may negatively impact cellular entry and subsequently, delivery.

A common derivative of guanidine commonly used, especially in medicinal chemistry, are acylguanidine's. Acylguanidines have shown improved pharmacokinetic properties compared to those of the parent guanidine.[45] The pK_a of acylguanidine is lowered from ~13 down to ~8, significantly decreasing the basicity.[46] The increased acidity of the acylguanidinium NH proton results in improved interactions and stronger binding to

carboxylates compared to guanidine. Given the prevalence of carboxylated on cellular membranes, acylguandine's seem like an attractive derivative for delivery purposes.

In another regard, some groups have attempted to enhance HBs by increasing the number of HB donors and acceptors available via guanidine-derivates. Namely, a guanidiniocarbonyl pyrrole (GCP) moiety was developed by Carsten Schmuck, et al., and used for the delivery of various macromolecules.[47–49] A novel, zwitterionic moiety was designed by the acylation of guanidine and addition of a carboxyl pyrrole group. Initially, self-assembly binding behavior or GCP dimers was studied, revealing how complementary electrostatic interactions, extended HB sites, and hydrophobic interactions would aid in binding.[47,49] This GCP moiety was grafted on various polymeric carriers and shown to condense nucleic acids efficiently, adding to the field of gene delivery. Overall, tailoring the features of guanidine, such as their electrostatic potential and HB ability, has led to various derivatives with enhanced properties.

1.4. Dissertation Overview

The aim of the following dissertation was to design, develop, and test polymer-based carriers for the delivery of functional proteins. The work presented here aims to overcome the hurdles typically associated with protein delivery systems and aid the advancement of this new era of protein-based therapeutics.

Specifically, Chapter 2 focuses on the design of a novel functional group and its structure-activity relationship for the delivery of various model system proteins and functional proteins. While commonly used approaches performed well in the absence of serum, the newly designed functional group demonstrated excellent stability and delivery

efficacy a serum-containing medium. This added stability provides significant promise to the development of functional materials with possible translational applications.

Chapter 3 dives deeper into understanding how a key structural component in responsible for high efficacy in protein delivery. A series of polymeric carriers with tuned planarity, rigidity, and flexibility were used to delivery various proteins. The results indicated that while the rigidity and planarity did not influence the inter-macromolecular interactions between the carrier and the protein, the cellular entry was severely affected. Specifically, the planar conformation along the polymer side chain group led to the best delivery efficacy.

Finally, the closing remarks briefly describe the translational applications for therapeutic protein delivery are currently ongoing. Direct uses that go a step-further than in vivo experiments show promise and provide insight on how this research is expected to move forward.

1.5. References

(1) Benjamin Leader, Q. J. B. and D. E. G. Protein Therapeutics: A Summary and Pharmacological Classification. *Nat. Rev. Drug Discov.* **2008**, *7* (1), 21–39.

(2) Carter, P. J.; Lazar, G. A. Next Generation Antibody Drugs: Pursuit of the "High-Hanging Fruit." *Nat. Rev. Drug Discov.* **2018**, *17* (3), 197–223. https://doi.org/10.1038/nrd.2017.227.

(3) Slastnikova, T. A.; Ulasov, A. V.; Rosenkranz, A. A.; Sobolev, A. S. Targeted Intracellular Delivery of Antibodies: The State of the Art. *Front. Pharmacol.* **2018**, *9* (OCT), 1–21. https://doi.org/10.3389/fphar.2018.01208.

(4) Singh, K.; Ejaz, W.; Dutta, K.; Thayumanavan, S. Antibody Delivery for Intracellular Targets: Emergent Therapeutic Potential. *Bioconjug. Chem.* **2019**, *30* (4), 1028–1041. https://doi.org/10.1021/acs.bioconjchem.9b00025.

(5) Cheng, Y. Design of Polymers for Intracellular Protein and Peptide Delivery. *Chinese J. Chem.* **2021**, *39* (6), 1443–1449. https://doi.org/10.1002/cjoc.202000655.

(6) Diehn, M.; Bhattacharya, R.; Botstein, D.; Brown, P. O. Genome-Scale Identification of Membrane-Associated Human MRNAs. *PLoS Genet.* **2006**, *2* (1), 39–50. https://doi.org/10.1371/journal.pgen.0020011.

(7) Lv, J.; Fan, Q.; Wang, H.; Cheng, Y. Polymers for Cytosolic Protein Delivery. *Biomaterials* **2019**, *218* (July), 119358. https://doi.org/10.1016/j.biomaterials.2019.119358.

(8) Rui, Y.; Wilson, D. R.; Choi, J.; Varanasi, M.; Sanders, K.; Karlsson, J.; Lim, M.; Green, J. J. Carboxylated Branched Poly(β-Amino Ester) Nanoparticles Enable Robust Cytosolic Protein Delivery and CRISPR-Cas9 Gene Editing. *Sci. Adv.* **2019**, *5* (12). https://doi.org/10.1126/sciadv.aay3255.

(9) Stanzl, E. G.; Trantow, B. M.; Vargas, J. R.; Wender, P. A. Fifteen Years of Cell-Penetrating, Guanidinium-Rich Molecular Transporters: Basic Science, Research Tools, and Clinical Applications. *Acc. Chem. Res.* **2013**, *46* (12), 2944–2954. https://doi.org/10.1021/ar4000554.

(10) Torchilin, V. Intracellular Delivery of Protein and Peptide Therapeutics. *Drug Discov. Today Technol.* **2008**, *5* (2–3). https://doi.org/10.1016/j.ddtec.2009.01.002.

(11) Fu, A.; Tang, R.; Hardie, J.; Farkas, M. E.; Rotello, V. M. Promises and Pitfalls of Intracellular Delivery of Proteins. *Bioconjug. Chem.* **2014**, *25* (9), 1602–1608. https://doi.org/10.1021/bc500320j.

(12) Rothbard, J. B.; Jessop, T. C.; Lewis, R. S.; Murray, B. A.; Wender, P. A. Role of Membrane Potential and Hydrogen Bonding in the Mechanism of Translocation of Guanidinium-Rich Peptides into Cells. *J. Am. Chem. Soc.* **2004**, *126* (31), 9506–9507. https://doi.org/10.1021/ja0482536.

(13) Wender, P. A.; Cooley, C. B.; Geihe, E. I. Beyond Cell Penetrating Peptides: Designed Molecular Transporters. *Drug Discov. Today Technol.* **2012**, *9* (1), e49–e55. https://doi.org/10.1016/j.ddtec.2011.07.004.

(14) Pooga, M.; Kut, C.; Kihlmark, M.; Hällbrink, M.; Fernaeus, S.; Raid, R.; Land, T.; Hallberg, E.; Bartfai, T.; Langel, Ü. Cellular Translocation of Proteins by Transportan. *FASEB J.* **2001**, *15* (8), 1451–1453. https://doi.org/10.1096/fj.00-0780fje.

(15) Morris, M. C.; Depollier, J.; Heitz, F.; Divita, G. A Peptide Carrier for the Delivery of Biologically Active Proteins into Mammalian Cells: Application to the Delivery of Antibodies and Therapeutic Proteins. *Cell Biol. Four-Volume Set* **2006**, *4* (December), 13–18. https://doi.org/10.1016/B978-012164730-8/50187-8.

(16) Qin, X.; Yu, C.; Wei, J.; Li, L.; Zhang, C.; Wu, Q.; Liu, J.; Yao, S. Q.; Huang, W. Rational Design of Nanocarriers for Intracellular Protein Delivery. *Adv. Mater.* **2019**, *31* (46), 1–32. https://doi.org/10.1002/adma.201902791.

(17) Li, Y.; Li, P.; Li, R.; Xu, Q. Intracellular Antibody Delivery Mediated by Lipids, Polymers, and Inorganic Nanomaterials for Therapeutic Applications. *Adv. Ther.* **2020**, *3* (12), 1–22. https://doi.org/10.1002/adtp.202000178.

(18) Rurik, J. G.; Tombácz, I.; Yadegari, A.; Méndez Fernández, P. O.; Shewale, S. V; Li, L.; Kimura, T.; Soliman, O. Y.; Papp, T. E.; Tam, Y. K.; et al. CAR T Cells Produced in Vivo to Treat Cardiac Injury. *Science* **2022**, *375* (6576), 91–96. https://doi.org/10.1126/science.abm0594.

(19) Karanth, H.; Murthy, R. S. R. PH-Sensitive Liposomes-Principle and Application in Cancer Therapy. *J. Pharm. Pharmacol.* **2010**, *59* (4), 469–483. https://doi.org/10.1211/jpp.59.4.0001.

(20) Falsini, S.; Ristori, S. Non-Viral Gene Delivery Vectors. **2016**, *1445*, 33–43. https://doi.org/10.1007/978-1-4939-3718-9.

(21) Yavlovich, A.; Smith, B.; Gupta, K.; Blumenthal, R.; Puri, A. Light-Sensitive Lipid-Based Nanoparticles for Drug Delivery: Design Principles and Future Considerations for Biological Applications. *Mol. Membr. Biol.* **2010**, *27* (7), 364–381. https://doi.org/10.3109/09687688.2010.507788.

(22) Kono, K.; Ozawa, T.; Yoshida, T.; Ozaki, F.; Ishizaka, Y.; Maruyama, K.; Kojima, C.; Harada, A.; Aoshima, S. Highly Temperature-Sensitive Liposomes Based on a Thermosensitive Block Copolymer for Tumor-Specific Chemotherapy. *Biomaterials* **2010**, *31* (27), 7096–7105. https://doi.org/10.1016/j.biomaterials.2010.05.045.

(23) Milla, P.; Dosio, F.; Cattel, L. PEGylation of Proteins and Liposomes: A Powerful and Flexible Strategy to Improve the Drug Delivery. *Curr. Drug Metab.* **2011**, *13* (1), 105–119. https://doi.org/10.2174/138920012798356934.

(24) Deshpande, P. P.; Biswas, S.; Torchilin, V. P. Current Trends in the Use of Liposomes for Tumor Targeting. *Nanomedicine* **2013**, *8* (9), 1509–1528. https://doi.org/10.2217/nnm.13.118.

(25) Paunovska, K.; Loughrey, D.; Dahlman, J. E. Drug Delivery Systems for RNA Therapeutics. *Nat. Rev. Genet.* **2022**. https://doi.org/10.1038/s41576-021-00439-4.

(26) Chatin, B.; Mével, M.; Devallière, J.; Dallet, L.; Haudebourg, T.; Peuziat, P.; Colombani, T.; Berchel, M.; Lambert, O.; Edelman, A.; et al. Liposome-Based Formulation for Intracellular Delivery of Functional Proteins. *Mol. Ther. - Nucleic Acids* **2015**, *4* (April), e244. https://doi.org/10.1038/mtna.2015.17.

(27) Yamada, Y.; Perez, S. M. V.; Tabata, M.; Abe, J.; Yasuzaki, Y.; Harashima, H. Efficient and High-Speed Transduction of an Antibody into Living Cells Using a Multifunctional Nanocarrier System to Control Intracellular Trafficking. *J. Pharm. Sci.* **2015**, *104* (9), 2845–2854. https://doi.org/10.1002/jps.24310.

(28) Guo, C.; Chen, Y.; Gao, W.; Chang, A.; Ye, Y.; Shen, W.; Luo, Y.; Yang, S.; Sun, P.; Xiang, R.; et al. Liposomal Nanoparticles Carrying Anti-IL6R Antibody to the Tumour Microenvironment Inhibit Metastasis in Two Molecular Subtypes of Breast Cancer Mouse Models. *Theranostics* **2017**, *7* (3), 775–788. https://doi.org/10.7150/thno.17237.

(29) Gulati, N. M.; Stewart, P. L.; Steinmetz, N. F. Bioinspired Shielding Strategies for Nanoparticle Drug Delivery Applications. *Mol. Pharm.* **2018**, *15* (8), 2900–2909. https://doi.org/10.1021/acs.molpharmaceut.8b00292.

(30) Wu, D.; Qin, M.; Xu, D.; Wang, L.; Liu, C.; Ren, J.; Zhou, G.; Chen, C.; Yang, F.; Li, Y.; et al. A Bioinspired Platform for Effective Delivery of Protein Therapeutics to the Central Nervous System. *Adv. Mater.* **2019**, *31* (18), 1–7. https://doi.org/10.1002/adma.201807557.

(31) Zhang, S.; Lv, J.; Gao, P.; Feng, Q.; Wang, H.; Cheng, Y. A PH-Responsive Phase-Transition Polymer with High Serum Stability in Cytosolic Protein Delivery. *Nano Lett.* **2021**. https://doi.org/10.1021/acs.nanolett.1c03031.

(32) Barrios, A.; Estrada, M.; Moon, J. H. Carbamoylated Guanidine-Containing Polymers for Non-Covalent Functional Protein Delivery in Serum-Containing Media. *Angew. Chemie Int. Ed.* **2022**, *33199*. https://doi.org/10.1002/anie.202116722.

(33) Chen, W.; Zuo, H.; Zhang, E.; Li, L.; Henrich-Noack, P.; Cooper, H.; Qian, Y.; Xu, Z. P. Brain Targeting Delivery Facilitated by Ligand-Functionalized Layered Double Hydroxide Nanoparticles. *ACS Appl. Mater. Interfaces* **2018**, *10* (24), 20326–20333. https://doi.org/10.1021/acsami.8b04613.

(34) Gdowski, A.; Ranjan, A.; Mukerjee, A.; Vishwanatha, J. Development of Biodegradable Nanocarriers Loaded with a Monoclonal Antibody. *Int. J. Mol. Sci.* **2015**, *16* (2), 3990–3995. https://doi.org/10.3390/ijms16023990.

(35) Zhang, Z.; Shen, W.; Ling, J.; Yan, Y.; Hu, J.; Cheng, Y. The Fluorination Effect of Fluoroamphiphiles in Cytosolic Protein Delivery. *Nat. Commun.* **2018**, *9* (1). https://doi.org/10.1038/s41467-018-03779-8.

(36) Lv, J.; Tan, E.; Wang, Y.; Fan, Q.; Yu, J.; Cheng, Y. Tailoring Guanidyl-Rich Polymers for Efficient Cytosolic Protein Delivery. *J. Control. Release* **2020**, *320* (January), 412–420. https://doi.org/10.1016/j.jconrel.2020.01.056.

(37) Dubois, J. L. N.; Lavignac, N. Cationic Poly(Amidoamine) Promotes Cytosolic Delivery of Bovine RNase A in Melanoma Cells, While Maintaining Its Cellular Toxicity. *J. Mater. Chem. B* **2015**, *3* (31), 6501–6508. https://doi.org/10.1039/c4tb02065k.

(38) Chang, H.; Lv, J.; Gao, X.; Wang, X.; Wang, H.; Chen, H.; He, X.; Li, L.; Cheng, Y. Rational Design of a Polymer with Robust Efficacy for Intracellular Protein and Peptide Delivery. *Nano Lett.* **2017**, *17* (3), 1678–1684. https://doi.org/10.1021/acs.nanolett.6b04955.

(39) Tezgel, A. Ö.; Jacobs, P.; Backlund, C. M.; Telfer, J. C.; Tew, G. N. Synthetic Protein Mimics for Functional Protein Delivery. *Biomacromolecules* **2017**, *18* (3), 819–825. https://doi.org/10.1021/acs.biomac.6b01685.

(40) Sgolastra, F.; Backlund, C. M.; Ilker Ozay, E.; deRonde, B. M.; Minter, L. M.; Tew, G. N. Sequence Segregation Improves Non-Covalent Protein Delivery. *J. Control. Release* **2017**, *254* (March), 131–136. https://doi.org/10.1016/j.jconrel.2017.03.387.

(41) Posey, N. D.; Hango, C. R.; Minter, L. M.; Tew, G. N. The Role of Cargo Binding Strength in Polymer-Mediated Intracellular Protein Delivery. *Bioconjug. Chem.* **2018**, *29* (8), 2679–2690. https://doi.org/10.1021/acs.bioconjchem.8b00363.

(42) Davis, H. C.; Posey, N. D.; Tew, G. N. Protein Binding and Release by Polymeric Cell-Penetrating Peptide Mimics. *Biomacromolecules* **2022**, *23* (1), 57–66. https://doi.org/10.1021/acs.biomac.1c00929.

(43) Mogaki, R.; Hashim, P. K.; Okuro, K.; Aida, T. Guanidinium-Based "Molecular Glues" for Modulation of Biomolecular Functions. *Chem. Soc. Rev.* **2017**, *46* (21), 6480–6491. https://doi.org/10.1039/c7cs00647k.

(44) Rozas, I.; Alkorta, I.; Elguero, J. Hydrogen Bonds and Ionic Interactions in Guanidine/Guanidinium Complexes: A Computational Case Study. *Struct. Chem.* **2008**, *19* (6), 923–933. https://doi.org/10.1007/s11224-008-9377-9.

(45) Kleinmaier, R.; Keller, M.; Igel, P.; Buschauer, A.; Gschwind, R. M. Conformations, Conformational Preferences, and Conformational Exchange of N′-Substituted N -Acylguanidines: Intermolecular Interactions Hold the Key. *J. Am. Chem. Soc.* **2010**, *132* (32), 11223–11233. https://doi.org/10.1021/ja103756y.

(46) Keller, M.; Kuhn, K. K.; Einsiedel, J.; Hübner, H.; Biselli, S.; Mollereau, C.; Wifling, D.; Svobodová, J.; Bernhardt, G.; Cabrele, C.; et al. Mimicking of Arginine by Functionalized Nω-Carbamoylated Arginine As a New Broadly Applicable Approach to Labeled Bioactive Peptides: High Affinity Angiotensin, Neuropeptide Y, Neuropeptide FF, and Neurotensin Receptor Ligands As Examples. *J. Med. Chem.* **2016**, *59* (5), 1925–1945. https://doi.org/10.1021/acs.jmedchem.5b01495.

(47) Schmuck, C.; Wienand, W. Highly Stable Self-Assembly in Water: Ion Pair Driven Dimerization of a Guanidiniocarbonyl Pyrrole Carboxylate Zwitterion. *J. Am. Chem. Soc.* **2003**, *125* (2), 452–459. https://doi.org/10.1021/ja028485+.

(48) Samanta, K.; Jana, P.; Bäcker, S.; Knauer, S.; Schmuck, C. Guanidiniocarbonyl Pyrrole (GCP) Conjugated PAMAM-G2, a Highly Efficient Vector for Gene Delivery: The Importance of DNA Condensation. *Chem. Commun.* **2016**, *52* (84), 12446–12449. https://doi.org/10.1039/c6cc06404c.

(49) Hatai, J.; Schmuck, C. Diverse Properties of Guanidiniocarbonyl Pyrrole-Based Molecules: Artificial Analogues of Arginine. *Acc. Chem. Res.* **2019**, *52* (6), 1709–1720. https://doi.org/10.1021/acs.accounts.9b00142.

CHAPTER II

Carbamoylated Guanidine-Containing Polymers for Non-Covalent Functional Protein Delivery in Serum-Containing Media

This chapter has been published in full in Angewandte Chemie International Edition, **2022**, *61*, e202116722.

Alfonso Barrios,[a] Marilen Estrada,[b] and Joong Ho Moon[a]

[a]Department of Chemistry and Biochemistry, Biomolecular Sciences Institute, Florida International University, 11200 SW 8th St., Miami, FL 33199, USA
[b]Department of Natural and Applied Sciences, Florida International University, 11200 SW 8th St., Miami, FL 33199, USA

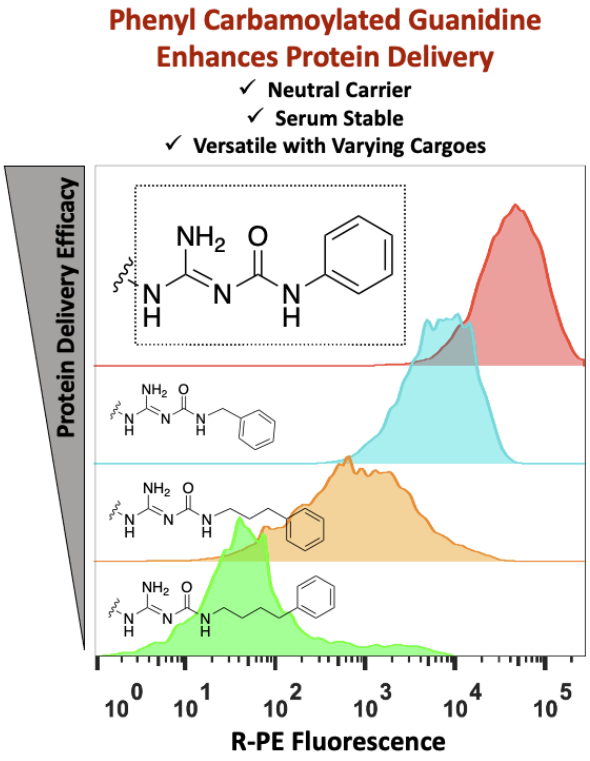

2.1. Abstract

Despite the high potential of controlling cellular processes and treating various diseases by intracellularly delivered proteins, current delivery systems exhibit poor efficiency due to poor serum stability, cellular entry, and cytosolic availability of proteins. Here, we report a novel functional group, phenyl carbamoylated guanidine (Ph-CG), that greatly enhances the delivery efficiency to various types of cells. Owing to the substantially lowered pKa, the hydrophobic Ph-CG offers optimized inter-macromolecular interactions via enhanced hydrogen bonding and hydrophobic interactions. The coplanarity of Ph-CG also leads to the better intracellular entry of protein complexes. Intracellularly delivered apoptosis-inducing enzymes and antibodies significantly induce cell viability inhibitions in a serum-containing medium. The newly developed Ph-CG can be introduced to various existing carriers, leading to the realization of future therapeutic protein delivery.

2.2. Introduction

Abnormalities in the structure or inadequate concentrations of functional proteins are closely tied to numerous disorders such as diabetes,[1] cancers,[2] and inflammatory diseases.[3] The cytosolic delivery of functional proteins could lead to efficient and specific control of cellular processes for various disease treatments.[4] Despite the success and promise of the first protein-based drugs, current protein-based therapeutics are mainly designed to target the extracellular receptors or secretory proteins due to the cell membrane impermeability of most proteins.[5] Therefore, the lack of effective approaches to delivering proteins to otherwise “undruggable” intracellular targets has sparked significant interest in developing versatile delivery systems.

While covalent coupling of cell membrane translocating moieties to proteins can be used, various non-covalent methods using lipids, peptides, and polymers have gained much attention due to the facile complex formation, without the risk of altered native function.[6–8] The synergistic and balanced inter-macromolecular ionic, hydrophobic, and hydrogen bond (HB) interactions are essential to achieve complex stability, interactions with the cell membranes, and protein release to the cytosol.[9,10] As the active functional group of cell-penetrating peptides,[11,12] protein transduction domains,[13,14] and numerous synthetic mimics,[15–17] the guanidine group has played a pivotal role in translocating numerous biologically active substances across cellular membranes. The unique delocalized positive charge on a trigonal planar structure creates strong positive charges in a unique hydrophobic core, leading to efficient ionic and hydrophobic interactions with biomacromolecules.[18] The charge-assisted bidentate HB interaction also offers additional binding strength, especially when multiple guanidine units collectively interact with biomacromolecules in a relatively hydrophobic environment.[19,20] Despite the advantages, the same positive charge is often responsible for non-specific binding with serum proteins, resulting in destabilization of protein/carrier complexes, alternation of cellular entry pathways, and diminishing overall intracellular entry efficiency.[21,22] The HB interactions in aqueous environments are also dramatically weakened as a large excess of water molecules strongly interacts with guanidine.[23] Therefore, most guanidine-based protein delivery systems perform poorly in serum-containing media.[24–27] To address the serum stability issue, protein delivery carriers have been modified with fluorous ligands,[28] zwitterionic moieties,[29] and decreased positive charge density.[26]

Herein, we report a rational guanidine modification approach that greatly enhances the efficiency of protein delivery in serum-containing media. We hypothesized that a direct conjugation of planar carbamoyl (Cbm) group to guanidine (G) (i.e., CG) (Figure 2.1) will decrease pKa of guanidine, leading to decreased positive charge density in physiological environments.[30,31] This reduced charge density is expected to increase the local hydrophobicity, which significantly enhances the efficiency of HB interactions in combination with the increased number (i.e., tridentate) of HB sites of CG.[32] Recently, Cheng et al. reported that the nature (i.e., aliphatic versus aromatic) of local hydrophobicity at guanidine plays a significant role in enhancing complex stability and cellular delivery.[33] Several CG-functionalized model polymers were synthesized and tested for delivery of various proteins to various types of cells. Our results indicate that the coplanar phenyl group connected CG (i.e., Ph-CG) exhibits efficient delivery of proteins with various sizes and isoelectric points. The Ph-CG successfully delivers apoptosis-inducing proteins even in a serum-containing medium, as compared with most protein delivery systems showing a sharp efficiency decrease in the presence of serum.[24,27]

2.3. Results and Discussion

Polynorbornenes (PNs) were selected as a model polymeric system to test the CG hypothesis because their physical properties (i.e., molecular weights and narrow molecular weight distributions) are well defined and several PN-based random and block copolymers containing both guanidine and hydrophobic units have been used for protein delivery.[14,27,34,35] After synthesizing a guanidine-containing poly(oxanorbornene imide) (G, Figure 2.1), phenyl isocyanate was reacted with guanidine to synthesize the Ph-CG

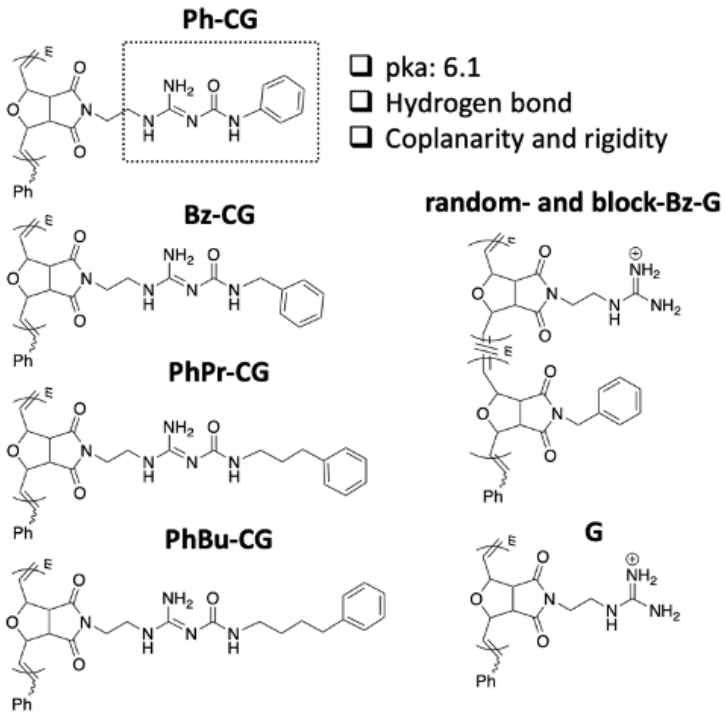

Figure 2.1. Chemical structures of PNs containing various functional groups. CG: Carbamoylated (Cbm) Guanidine (G); Ph: Phenyl; Bz: Benzyl; PhPr: Phenylpropyl; and PhBu: Phenylbutyl.

containing PN. Synthesis of Bz, PhPr, and PhBu was done via the reaction of the respective primary amines and the N,N'-di-boc-guanidine containing PN.[36] Random and block copolymers with repeating units bearing both guanidine and aromatic benzyl side chains (random-Bz-G and block-Bz-G) were also synthesized as control PNs (Scheme 2.1 and 2.2).

Before complexation, PNs dissolved in DMSO were diluted with water to make aqueous PN stock solutions. Complexation was achieved by mixing the corresponding PN and protein in an aqueous solution. Nanoparticle tracking analysis (NTA) and zeta potential

Table 2.1. Summary of molecular weights (M_n and M_w, kDa) and acidity constant (pK_a) of polymers and the hydrodynamic diameters (HD, nm), zeta potentials (ξ), and dissociation constants (K_d, μM) of PN/BSA complexes.

PNs	M_n	M_w	HD[a]	ξ[a]	K_d[b]	pK_a[c]
G	4.8	5.4	NA	NA	NA	NA
Ph-CG	5.5	5.9	200 ± 55	-14.3	3.7 ± 0.8	6.1
Bz-CG	5.7	6.1	179 ± 31	-15.3	3.8 ± 0.6	6.1
PhPr-CG	5.7	6.1	168 ± 44	-11.6	3.1 ± 04	6.3
PhBu-CG	5.7	6.1	175 ± 36	-13.4	5.7 ± 1.2	6.1
random-Bz-G (5k)	5.0	5.6	230 ± 50	-8.9	3.3 ± 0.6	NA
block-Bz-G (5k)	4.5	5.1	178 ± 45	-6.1	5.3 ± 1.3	NA
random-Bz-G	10.3	11.4	208 ± 54	-11.9	-	NA
block-Bz-G	8.9	10.3	209 ± 48	-14.5	-	NA

[a] Concentrations of polymer and BSA in the complexes were 10 μM and 100 nM, respectively. Values represent mean ± standard deviation of the arithmetic values calculated for all nanoparticles recorded by the NTA software. [b] Dissociation constants were calculated using rhodamine labelled BSA. [c] Effective pK_a was determined by pH titration. NA: Not able to determine under the titration condition.

measurements indicate that all PNs form relatively uniform nanometer size complexes with slightly negative zeta potentials (Table 2.1, Figure 2.2), despite the excess amounts of PNs used in the complex. Considering the negatively charged bovine serum albumin (BSA) in neutral pH,[37] the negative zeta potentials of PN/BSA complexes suggest the possible neutral (or slightly positive) charge of PNs, especially for Ph-CG. It is reported that the acylation on guanidine results in a sharp pKa decrease from 12-13 to ~8.[38] The pKa values of CG derivatives were measured as ~6.1 using the pH titration method (Figure 2.3);[26,39] therefore, Ph-CG exists as neutral in the physiological environment. Nevertheless, fluorescence quenching assays using rhodamine-labeled BSA (Rho-BSA) confirm the high protein affinity of Ph-CG. The fluorescence intensity of Rho-BSA will be decreased as the

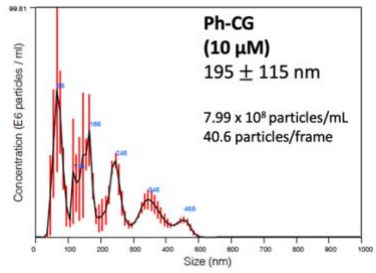
Ph-CG
(10 µM)
195 ± 115 nm
7.99 x 10⁸ particles/mL
40.6 particles/frame
Concentration (E6 particles / ml)
Size (nm)

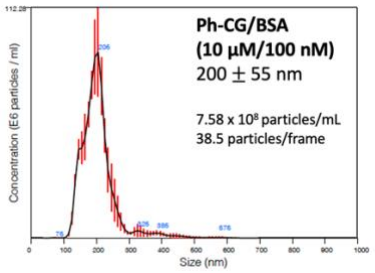
Ph-CG/BSA
(10 µM/100 nM)
200 ± 55 nm
7.58 x 10⁸ particles/mL
38.5 particles/frame
Concentration (E6 particles / ml)
Size (nm)

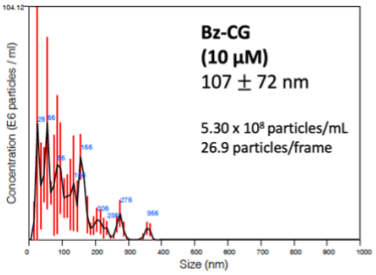
Bz-CG
(10 µM)
107 ± 72 nm
5.30 x 10⁸ particles/mL
26.9 particles/frame
Concentration (E6 particles / ml)
Size (nm)

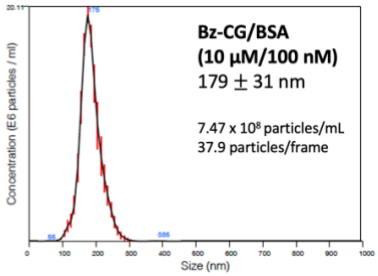
Bz-CG/BSA
(10 µM/100 nM)
179 ± 31 nm
7.47 x 10⁸ particles/mL
37.9 particles/frame
Concentration (E6 particles / ml)
Size (nm)

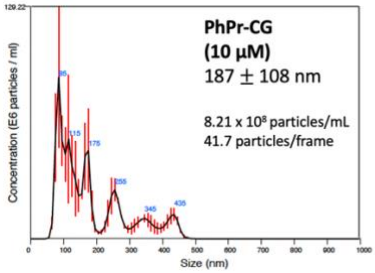
PhPr-CG
(10 µM)
187 ± 108 nm
8.21 x 10⁸ particles/mL
41.7 particles/frame
Concentration (E6 particles / ml)
Size (nm)

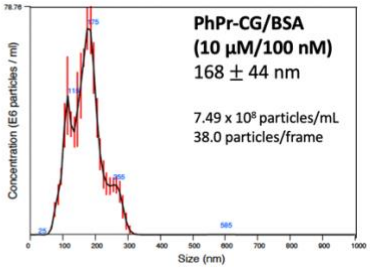
PhPr-CG/BSA
(10 µM/100 nM)
168 ± 44 nm
7.49 x 10⁸ particles/mL
38.0 particles/frame
Concentration (E6 particles / ml)
Size (nm)

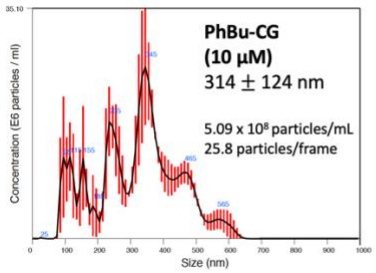
PhBu-CG
(10 µM)
314 ± 124 nm
5.09 x 10⁸ particles/mL
25.8 particles/frame
Concentration (E6 particles / ml)
Size (nm)

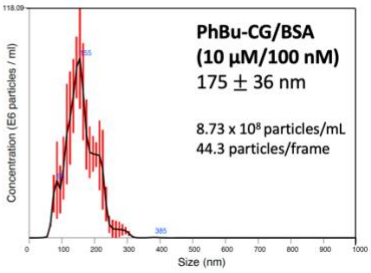
PhBu-CG/BSA
(10 µM/100 nM)
175 ± 36 nm
8.73 x 10⁸ particles/mL
44.3 particles/frame
Concentration (E6 particles / ml)
Size (nm)

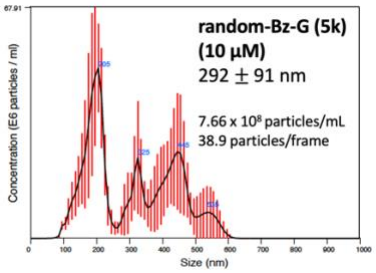
random-Bz-G (5k)
(10 µM)
292 ± 91 nm
7.66 x 10⁸ particles/mL
38.9 particles/frame
Concentration (E6 particles / ml)
Size (nm)

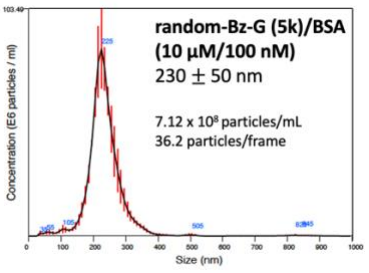
random-Bz-G (5k)/BSA
(10 µM/100 nM)
230 ± 50 nm
7.12 x 10⁸ particles/mL
36.2 particles/frame
Concentration (E6 particles / ml)
Size (nm)

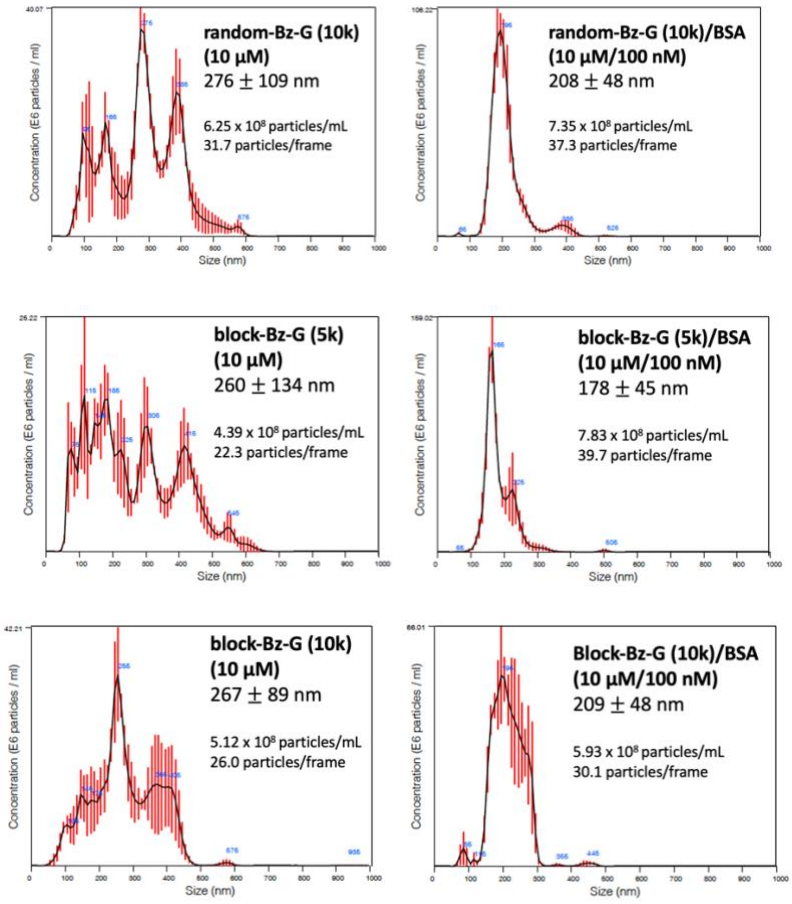

Figure 2.2. HD plots for PNs (left) and PN/BSA complexes (right), demonstrating formation off relatively monodisperse nanoparticles after complexation.

Rho-BSA concentration increases in the complex due to self-quenching. By monitoring the fluorescence quenching of Rho-BSA as a function of PN concentrations, the dissociation constants (K_d) of PN/BSA complexes were determined as ~3-5 µM (Figure 2.4 and 2.5).[34] The protein loading efficiency was also determined by measuring the amount of red algae-phycoerythrin (R-PE) in the supernatant after centrifugation of PN/R-PE complexes.[5] Most CbmG derivatives and control random-Bz-G complex ~90% of R-PE (Figure 2.6). Despite similar K_d values and R-PE loading ratios, the complex stability in phosphate-buffered saline (PBS) containing 10% fetal bovine serum (FBS) is significantly different depending

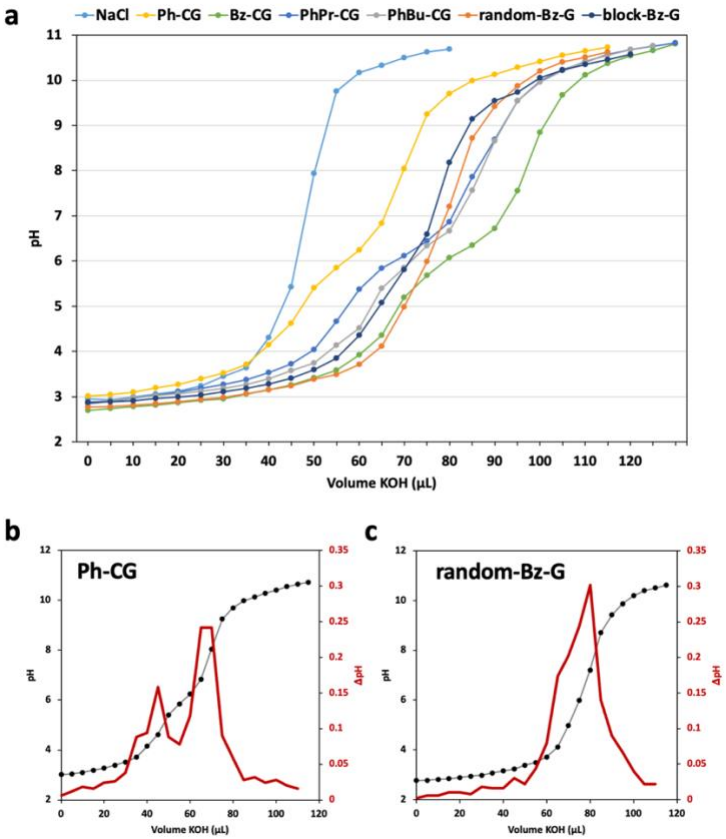

Figure 2.3. (a) pH titration curves of PNs with KOH from pH 3 to 11. (b-c) Method for pKa determination of Ph-CG (b) and random-Bz-G (c). No value was determined using this method for random-Bz-G as there is only maximum ΔpH.

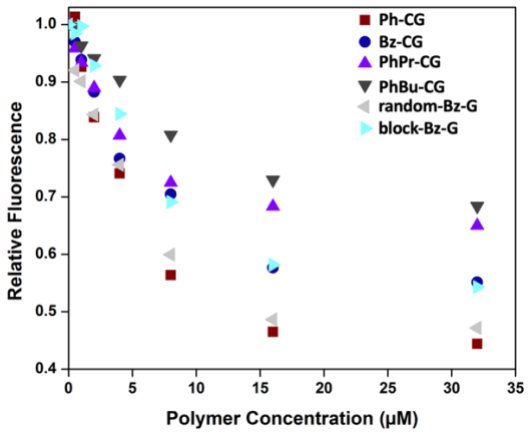

Figure 2.4. Relative fluorescent quenching of Rho-BSA complexed with various PNs. Data represents the average of 3 independent experiments. Errors bars were omitted for clarity of data.

on the functional group. The amounts of free R-PE released from complexes (i.e., in the supernatant after centrifugation) over time were monitored via fluorescence measurements.[5,40] Both Ph-CG and random-Bz-G exhibit full complexation of R-PE over the incubation time in a serum-free medium, although the block-Bz-G only exhibits ~60% complexation efficiency (Figure 2.7a). In the presence of serum, the Ph-CG/complex exhibits minimal loss of R-PE over the incubation time, indicating the complex stability was not compromised by the serum proteins (Figure 2.7b). Meanwhile, both random and block-Bz-G complexes had a sharp loss of complexed R-PE after 30 min, suggesting substantial complex dissociation.

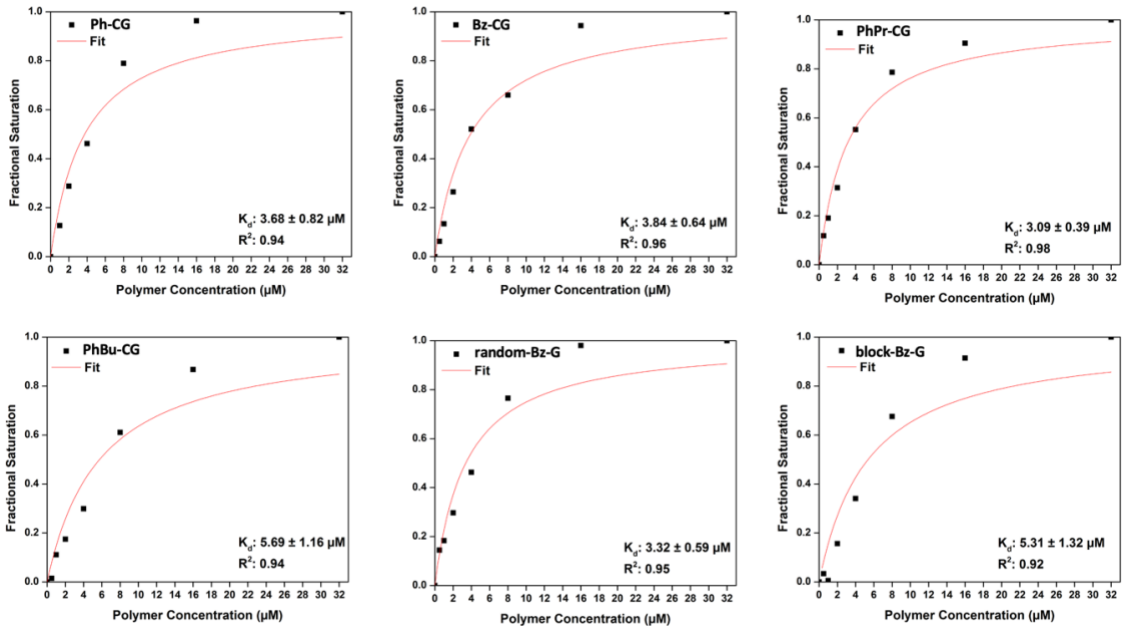

Figure 2.5. Fractional saturation and fitting curves of PNs with Rho-BSA.

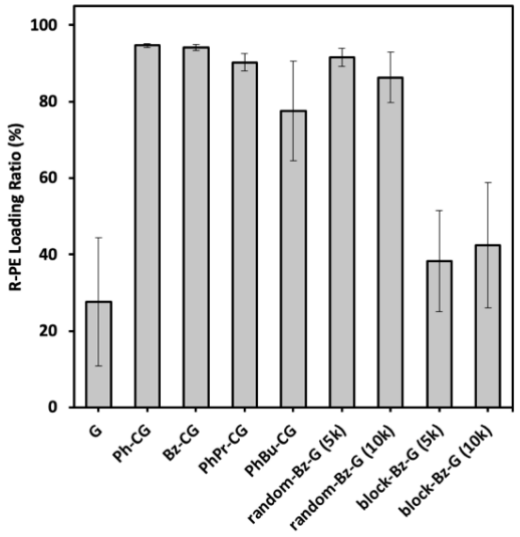

Figure 2.6. Loading ratio of R-PE by PNs. Data represents mean of three independent experiments +/- standard deviation.

Another CbmG derivative, Bz-CG, also exhibits excellent serum stability similarly to Ph-CG (Figure 2.8). Complex stability was also studied using Rho-BSA and fluorescence quenching experiments, demonstrating similar results (Figure 2.9).[24,41] Considering the similar physical properties of the PN/protein complexes, this substantial serum stability difference between CbmG- and conventional guanidine-containing PNs is due to enhanced HB interactions of CbmG from low pKa value and attached hydrophobicity.[23]

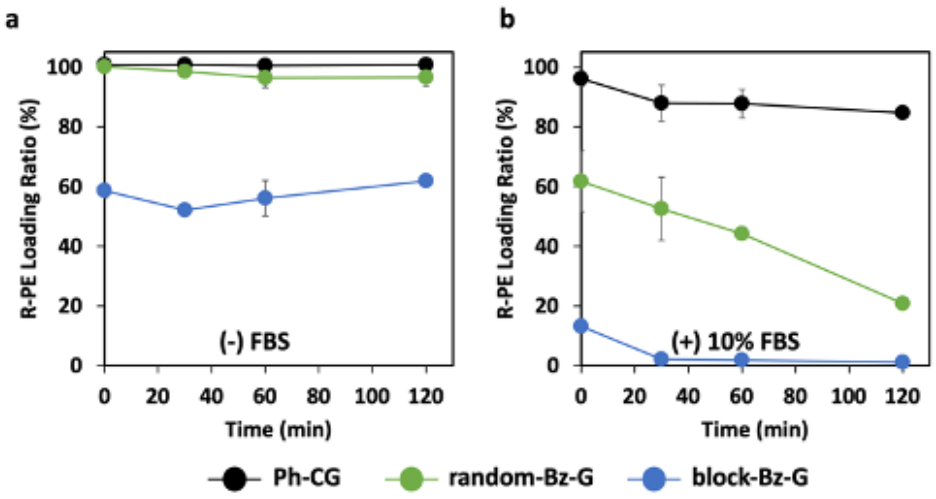

Figure 2.7. Stability of R-PE complexes of Ph-CG, random-Bz-G, and block-Bz-G in PBS (a) and PBS with 10% FBS (b). While all complexes show a relatively good stability in PBS, the complex stability in the serum-containing medium is substantially different. Ph-CG/protein complex exhibits high serum stability over the extended incubation time.

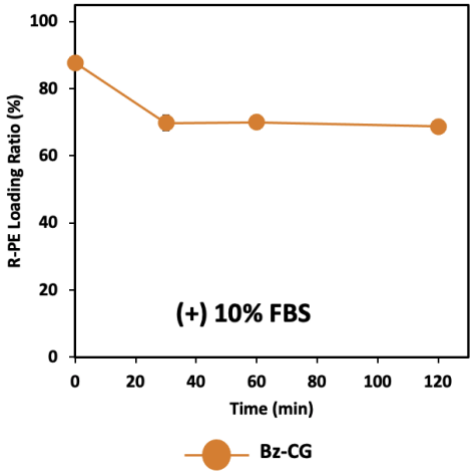

Figure 2.8. Stability of Bz-CG/R-PE complexes in PBS containing 10% FBS. Data represents mean of three independent experiments +/- standard deviation.

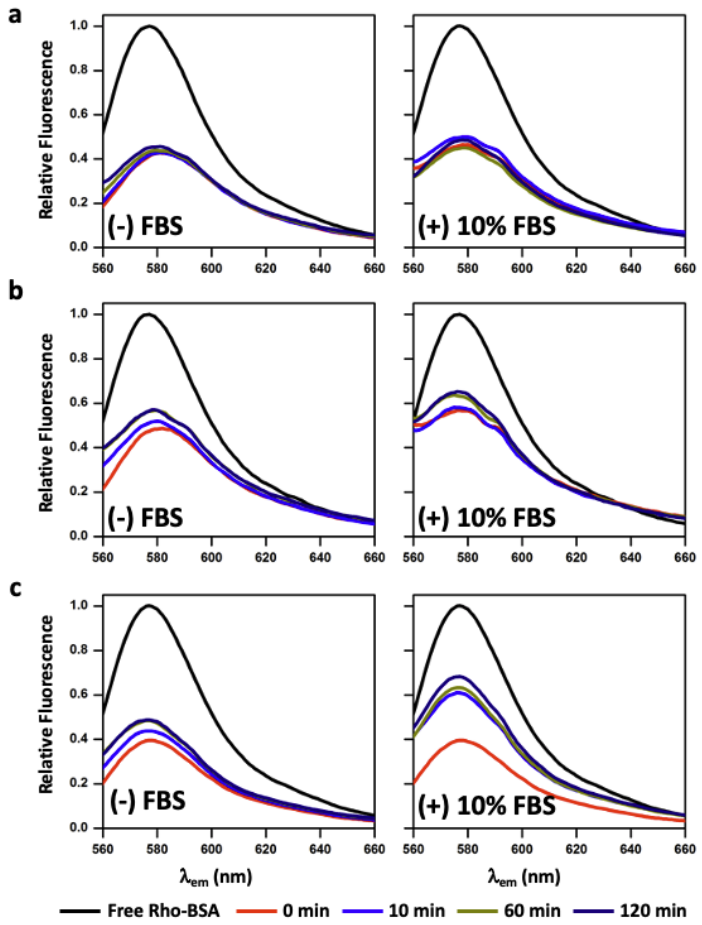

Figure 2.9. Stability of Ph-CG (a), Bz-CG (b), and random-Bz-G (c) complexes with Rho-BSA in PBS or in PBS containing 10% FBS. All PN/Rho-BSA complexes exhibits similar fluorescence intensity to that of the initial complex over time. In the presence of serum (right), the Ph-CG and Bz-CG/complex exhibits no fluorescence changes over the incubation time, indicating the complex stability was not compromised by the serum proteins. Meanwhile, the fluorescence intensity of random-Bz-G/protein complex was sharply increased within 10 min of incubation, suggesting complex dissociation.

All PNs exhibited no noticeable cell viability inhibition up to 40 μM, except the guanidine-containing PN (G) that showed a slight viability inhibition (~15%) at that concentration (Figure 2.10). Using flow cytometry, the cellular protein delivery efficiencies of PNs were evaluated by measuring the median fluorescent intensity (MFI) of HeLa cells incubated with PNs/R-PE complexes in a serum-containing medium overnight.

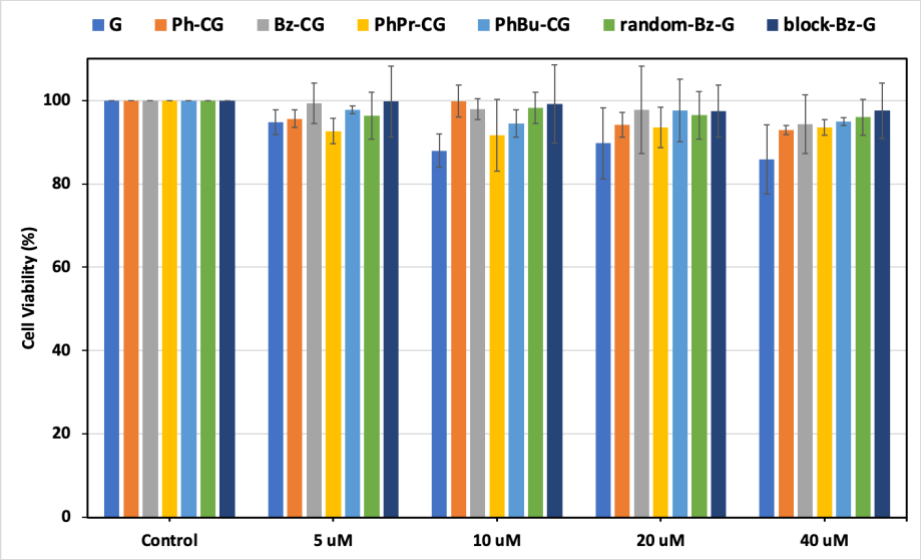

Figure 2.10. Cell viability inhibition of PNs at various concentrations.

As shown in Figure 2.11, Ph-CG with molecular weight (MW) of ~5,000 g/mol exhibits about 5- and 300-fold higher MFI than the control random-Bz-G and the commercially available PULSin reagent, respectively, despite all PN/R-PE treated cells being R-PE positive. Structurally, the hydrophobic phenyl group is directly introduced to guanidine via the Cbm extension in Ph-CG, whereas the charges and hydrophobic groups in the control PNs are segregated in either random or block backbone structures, similarly to other PN-based protein delivery systems.[35] The control PNs with doubled MWs, in which the PNs have the same numbers of guanidine and hydrophobic unit per repeating unit as those of Ph-CG, exhibit no improved delivery efficiency. Unlike previously reported systems,[35] the block copolymer exhibited poorer R-PE delivery than the random copolymer, likely due to their low efficiency in R-PE loading (Figure 2.6). Control polymers containing Ph side chains (i.e., random and block-Ph-G; Figure 2.12a) were also synthesized and tested for an appropriate comparison to Ph-CG. Because there was no efficiency difference observed

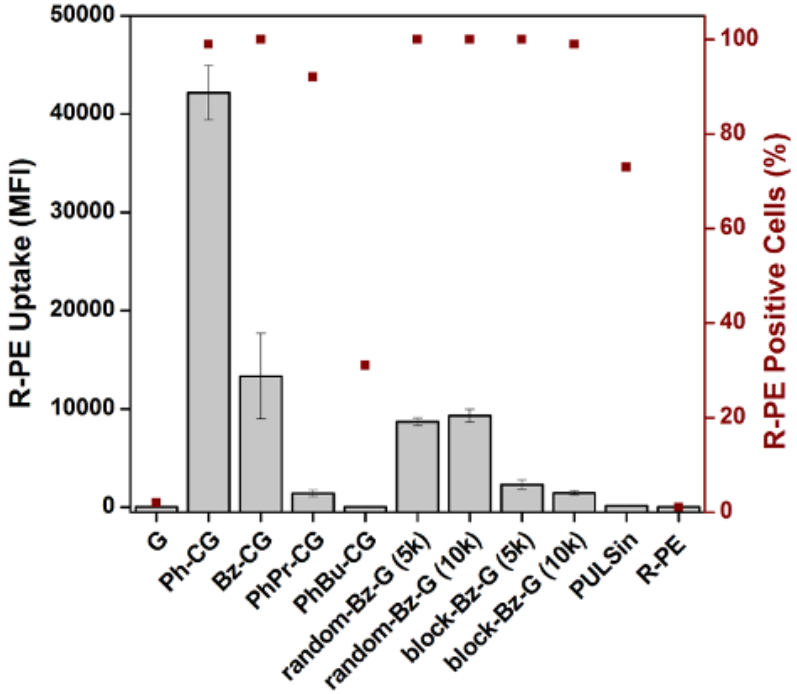

Figure 2.11. Median fluorescence intensity of HeLa cells treated with PN/R-PE complexes for 18 h. The percent R-PE positive cells are presented on the right axis. The concentration of polymer and R-PE was 10 μM and 15 nM, respectively. R-PE only was used as a negative control. PULSin was used as a positive control according to the suggested guidelines by the manufacturer. Data shown is the mean of three independent experiments ± standard deviation.

between Bz- and Ph-containing control polymers (Figure 2.12b), we selected random- and block-Bz-G as controls for subsequent experiments given their structural similarity to benzyl ester-containing polymers used in previous studies.[14] Most importantly, it is interesting to observe that the R-PE delivery efficiency decreases exponentially as the chain length between Ph and CG increases (Figure 2.11). The separation of the phenyl ring by 1 carbon unit (i.e., Bz-CG) decreases the protein uptake efficiency by ~75% and a further increase in the distance (i.e., PhPr and PhBu) eventually leads to minimal delivery.

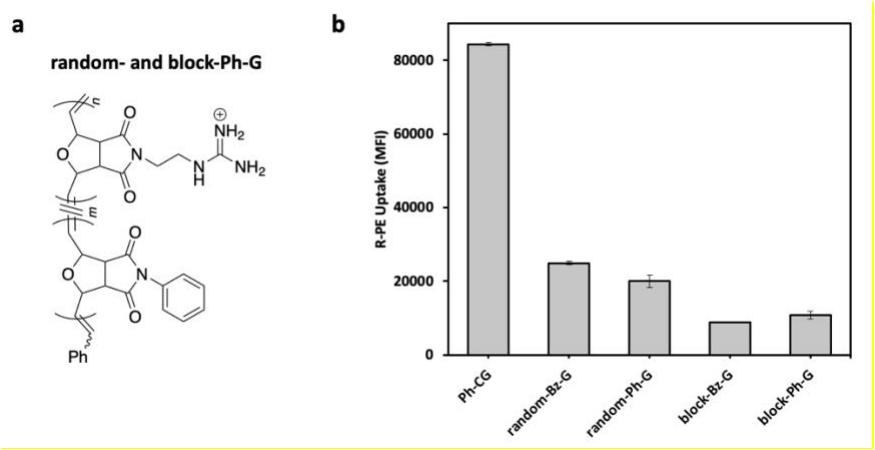

Figure 2.12. (a) Chemical structure of control polymers random- and block-Ph-G. (b) Median fluorescence intensity of HeLa cells treated with PN/R-PE complexes for 18 h. The concentration of polymer and R-PE were 10 μM and 15 nM, respectively. Data shown is the mean of three independent experiments +/- standard deviation.

Considering very similar pKa, complex serum stability, and amount of complexed R-PE among the CG derivatives, we believe that the coplanarity of Ph-CG contributes to better cellular entry through better interactions with the membranes, resulting in high protein delivery efficiency. While the Ph group maintains the coplanarity with CG in Ph-CG and thus the rigidity of the active group is maintained, no coplanarity is present when the phenyl group is connected to Cbm through methylene spacers due to the free rotation of the methylene group. It has been reported that the rigidity of delivery materials plays a crucial role in cellular entry due to enhanced membrane interactions.[42,43]

The robust design concept of Ph-CG for universal protein delivery was examined by treating primary human mesenchymal stem cells (MSC) and CD4+ T cells, respectively, with Ph-CG/fluorescent proteins (FPs) in serum-containing media. As shown in Figure 2.13, Ph-CG efficiently delivers various FPs with different sizes and surface properties to

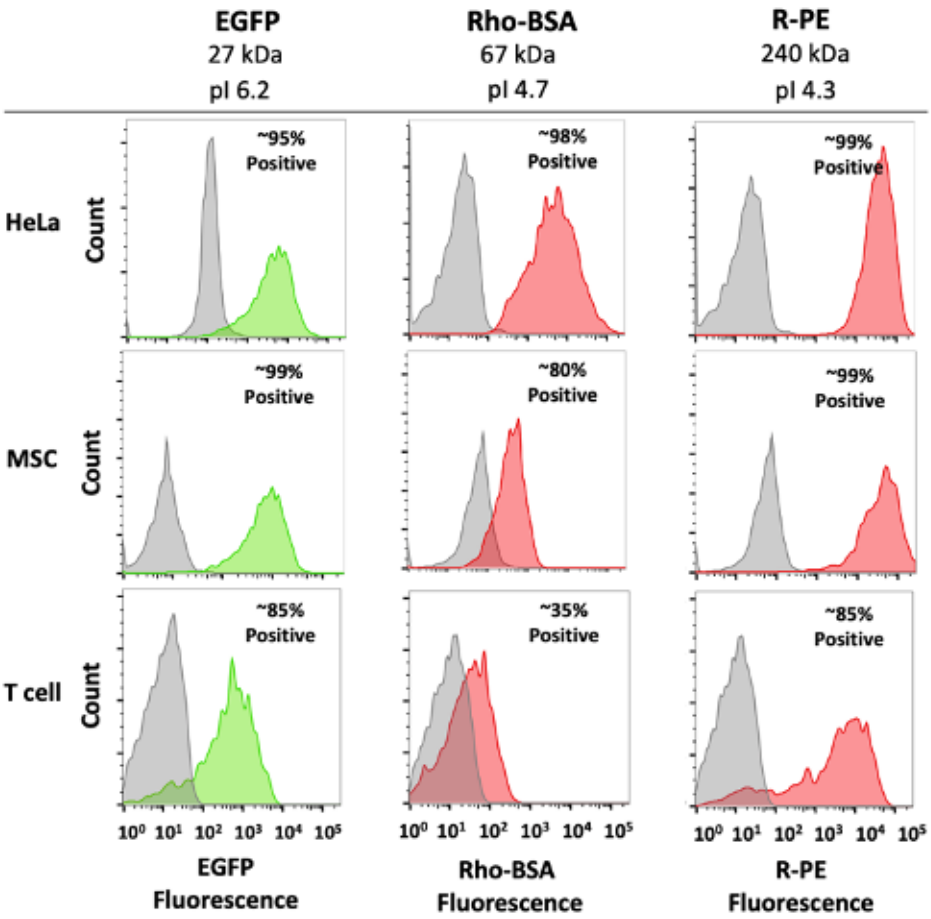

Figure 2.13. Flow cytometry histograms of Ph-CG mediated delivery of EGFP, Rho-BSA, and R-PE into HeLa, Mesenchymal Stem Cells (MSC), and T cells. Almost complete cell populations show signals from R-PE within 3 h of treatment. The concentrations of polymer, R-PE, EGFP, and Rho-BSA were 10 μM, 15 nM, 60 nM, and 100 nM, respectively.

hard-to-transfect cells with greater than 80% of the FP positive cell populations. Interestingly, Rho-BSA delivery efficiency was generally lower than that of the intrinsic FPs. We speculate that the altered surface functionalities from chemical conjugations of Rho to BSA could be responsible for the relatively low delivery efficiency. For those non-FPs with smaller size (e.g., 13.7 kDa RNase A) and positively charged surfaces [i.e., RNase (pI 8.6) and Saporin (pI 9.3)], functional assays were used to validate Ph-CG-mediated delivery in a serum-containing medium (see below). Cellular entry pathway studies

indicate that the internalization of the Ph-CG/R-PE complex primarily occurs via energy-dependent pathway (Figure 2.14). Ph-CG/R-PE entry was decreased under the pretreatment of various pharmacological endocytosis inhibitors, implying that those relatively well-studied endocytosis pathways (i.e., clathrin-mediated endocytosis and macropinocytosis) are also involved in Ph-CG/FPs entry to HeLa cells.

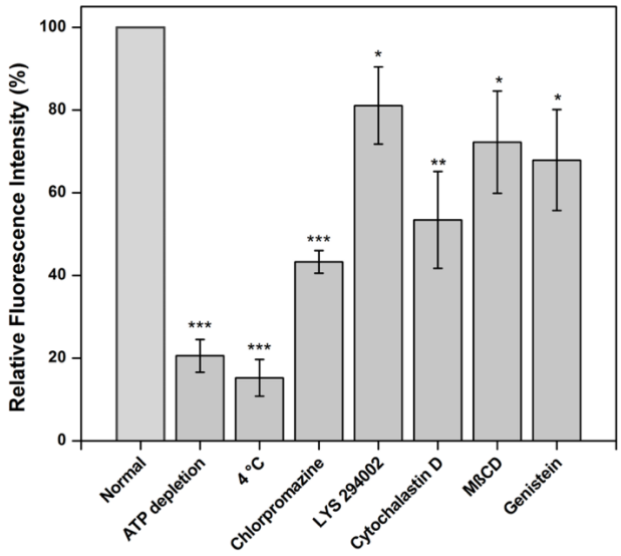

Figure 2.14. Relative median fluorescence intensity of HeLa cells in energy-independent conditions (ATP depletion and 4 ℃) or pre-treated with various pharmacological endocytosis inhibitors followed by incubation with Ph-CG/R-PE complex for 1 h. The concentration of polymer and R-PE were 10 μM and 15 nM, respectively. Data shown is the mean of three independent experiments +/- standard deviation.

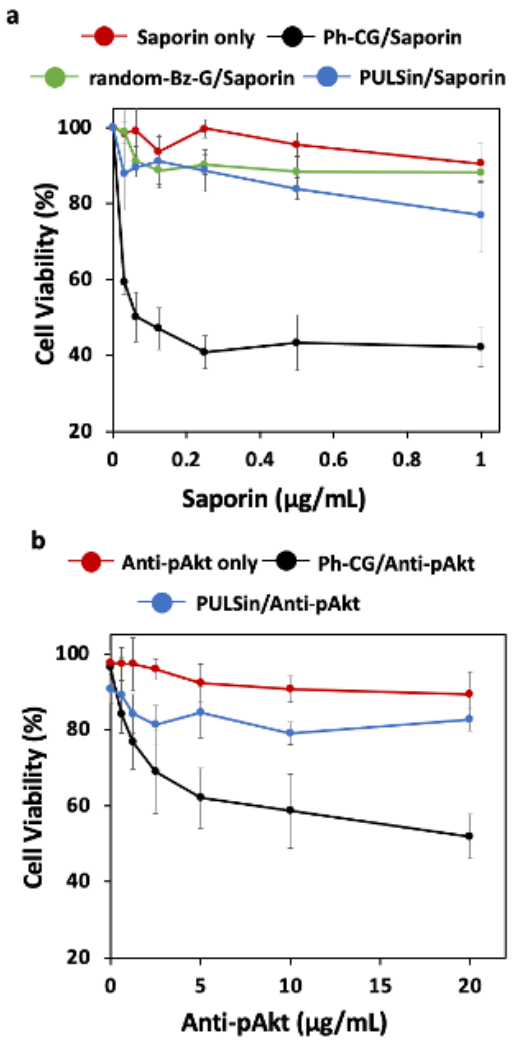

Figure 2.15. Viability of HeLa cells treated with Ph-CG/Saporin (a) and Ph-CG/Anti-pAkt (b) at various protein concentrations in a serum-containing medium. The concentration of polymer was kept constant at 10 μM. Data represents the mean of three independent experiments ± standard deviation.

We further tested the ability of Ph-CG for functional protein delivery. Saporin is a ribosome-inactivating protein that irreversibly blocks the synthesis of proteins in cells.[44] RNase A is an enzyme capable of degrading RNA chains and thus exhibiting toxic effects.[45] While both cell membrane-impermeable proteins show no toxicity on HeLa cells, an exponential cell viability inhibition was observed when Saporin (32.8 kDa) was

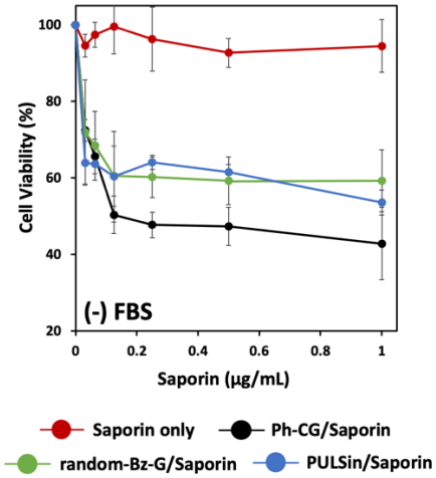

Figure 2.16. Viability of HeLa cells treated with saporin only and saporin complexes at various concentrations in a serum-free medium. The concentration of PNs was kept constant at 10 μM. Data represents the mean of 3 independent experiments +/- standard deviation.

delivered by Ph-CG at less than 0.03 μg/mL (Figure 2.15a). It is noteworthy that this functional protein delivery was conducted in a serum-containing medium and the efficiency is very similar regardless of the serum (Figure 2.16). The positive controls exhibit poor activities in the presence of serum, similarly to most of the reported systems.[24] Delivered RNase by Ph-CG also shows concentration-dependent exponential cell viability decrease (Figure 2.17). However, RNase delivery was more efficient in a serum-free medium, indicating that Ph-CG works better with larger proteins than RNase. Compared to Ph-CG/Saporin, NTA analysis indicates significantly larger HD for Ph-CG/RNase (Figure 2.18), suggesting potential loose complex formation that may be susceptible to serum proteins. Previously, a comparable PN-based system also reported poor complex formation with small proteins. Nevertheless, this viability inhibition result indicates that internalized proteins escape from endosomes and/or use different pathways (e.g., via leaky macropinosomes in macropinocytosis) to reach the cytosolic targets. We further sought to

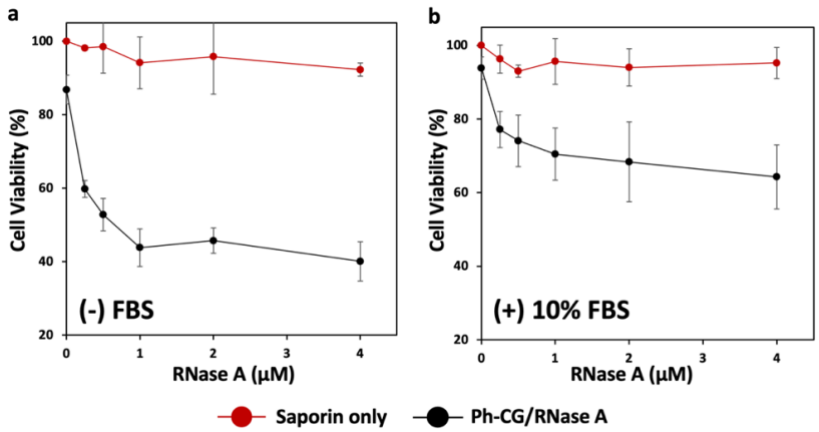

Figure 2.17. Viability of HeLa cells treated with RNase only and Ph-CG/RNase A complexes at various RNase concentrations in a serum-free (a) and a serum-containing medium (b). The concentration of polymer was kept constant at 10 μM. Data represents the mean of 3 independent experiments +/- standard deviation.

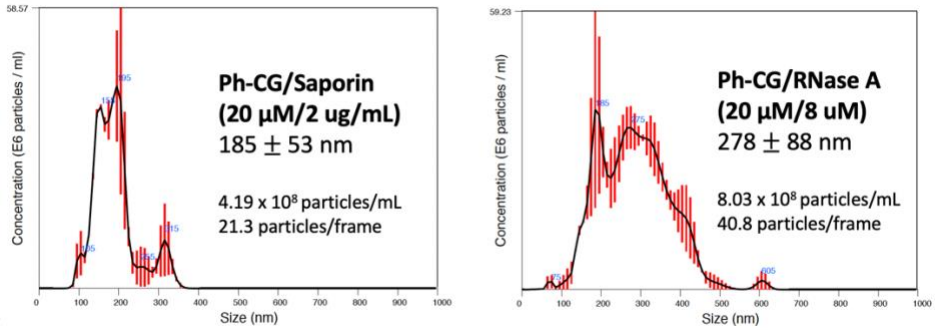

Figure 2.18. HD plots for saporin (left) and RNase A (right) complexes.

test the ability of Ph-CG in delivering a functional antibody. The phosphorylation of protein kinase B (i.e., pAkt) is closely tied to promoting growth factor-mediated cell growth and proliferation. Therefore, blocking the pathway could result in increased apoptosis.[46,47] Anti-pAkt was successfully delivered by Ph-CG by showing a dose-dependent cell viability decrease (Figure 2.15b). This antibody delivery result strongly supports that the internalized antibody retains its activity and reaches the epitope in the cytosol.

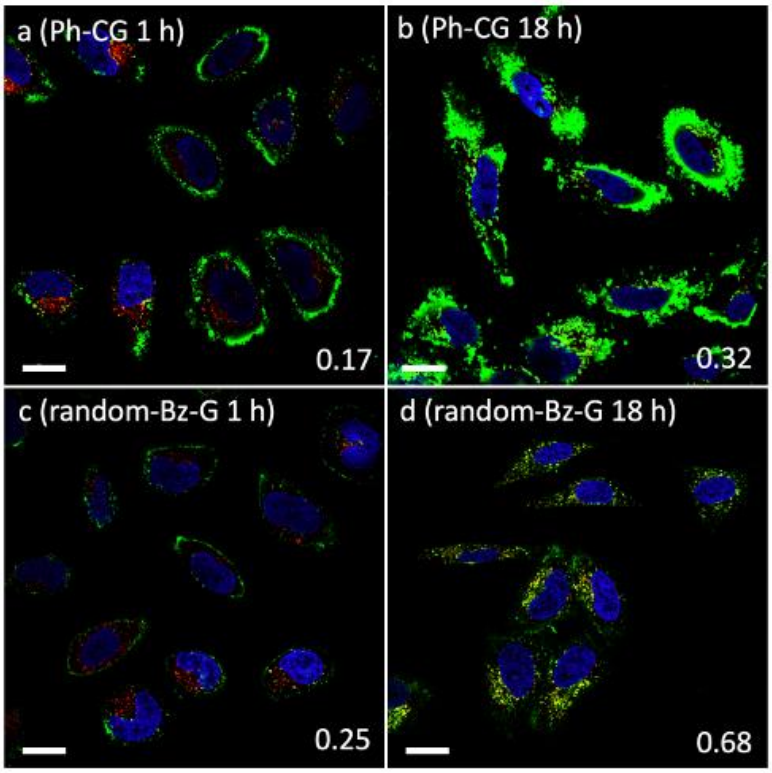

Figure 2.19. Confocal images of HeLa cells treated with Ph-CG/FITC-BSA (a: 1 h and b: 18h) and random-Bz-G/FITC-BSA (c: 1h and d: 18h). Blue: nucleus, green: FITC-BSA, red: Lysotracker. PCC scores are indicated in the lower right corner. Scale bar: 20 μm.

Confocal microscopic images of HeLa cells treated with Ph-CG/fluorescein isothiocyanate (FITC) labeled-BSA show a diffused but intense cytosolic staining pattern that is quite different from the characteristic puncta (Figure 2.19 and Figure 2.20 for other FPs). To determine whether FITC-BSA delivered by Ph-CG and random-Bz-G, respectively, are localized in acidic endosome/lysosome, we counter-stained cells with Lysotracker Red, and used the Pearson's correlation coefficient (PCC) method to quantitatively analyze the levels of overlap between green and red colors. Low PCC scores of 0.17 and 0.25 were calculated from cells treated for 1 h with Ph-CG and random-Bz-G, respectively, indicating FITC-BSAs are not in acidic organelles. When the treatment time increased to 18h, the PCC score from the control random-Bz-G treated cells increased substantially (i.e., 0.68),

indicating high FITC-BSAs localization in the endosome/lysosome. Meanwhile, the low PCC score (0.32) of 18 h Ph-CG/FITC-BSA treated cells indicates that the location of FITC-BSA is not in acidic organelles. From the unique imaging pattern and colocalization result, we assume that Ph-CG could use other entry pathways that are not heavily related to conventional well-studied endocytoses, although further mechanistic studies are required.

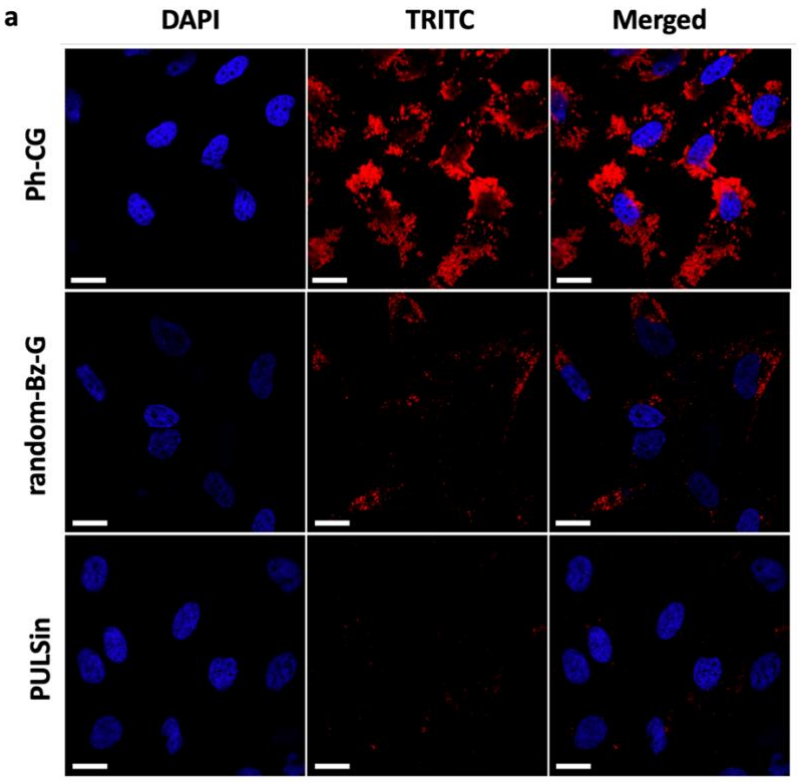

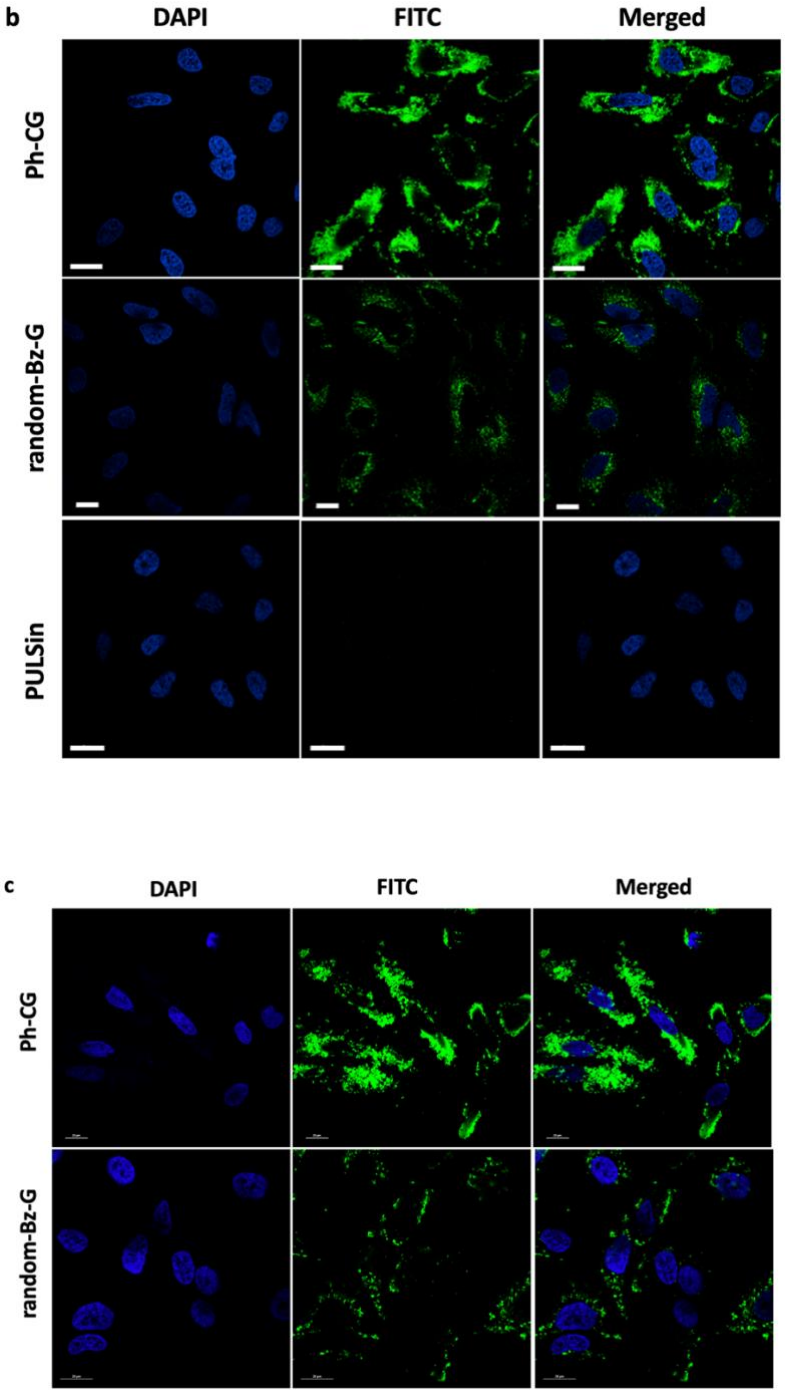

Figure 2.20. Confocal microscope images of HeLa cells incubated with PN and PULSin complexes of R-PE (a), FITC-BSA (b), and EGFP (c). Concentrations of PN, R-PE, FITC-BSA and EGFP were 10 µM, 15 nM, 100 nM and 100 nM, respectively.

2.4. Conclusion

In summary, we introduced a rational design concept of guanidine modification to substantially improve functional protein delivery efficiency. The decreased pKa of planar CG increases local hydrophobicity and HB interactions, allowing the formation of stable protein complexes with improved complex stability in a serum-containing medium. We also found that the coplanarity of the Ph group directly introduced to CG plays a significant role in the cellular entry. A PN containing Ph-CG efficiently delivers various proteins with different sizes and surface charges to multiple cells including hard-to-transfect cells in serum-containing media. The developed functional group can be introduced to many existing biologic delivery platforms, and our discovery can provide new insights to tackle the issues associated with therapeutic protein delivery.

2.5. Experimental and Supporting Information

2.5.1. Physical Characterization of PNs and PN/BSA Complexes

Molecular Weight Determination - Aliquots of polymer solutions in tetrahydrofuran (THF) or dichloromethane (DCM) were diluted in 1 mL of HPLC-grade THF and filtered through a 0.45 μm polytetrafluoroethylene (PTFE) syringe filter prior to injection.

Measurement of Hydrodynamic Diameters and Zeta Potential - Nanoparticle tracking analysis (NTA) was used to determine the hydrodynamic diameter (HD) of PN/protein complexes. Briefly, PN stock solutions were prepared by dissolving dried PN powders in DMSO and diluting to final concentrations of 1 mM in DMSO. Adequate volumes of PN stock solutions were diluted in water (20% v/v) and mixed with equal volumes of BSA solution for a final complex volume of 100 μL. Complexes were incubated for 30 min at room temperature before a ten-fold dilution in PBS to a final volume of 1 mL (final

PN/BSA concentration was 10 μM and 100 nM, respectively). 1 mL of this solution was then injected into the NTA chamber and videos of the scattering particles was recorded for 30 seconds. The software identified each individual particle and tracked its motion, relating the particle displacement as a function of Brownian motion, which relates to the particle size through the Stokes-Einstein equation. The concentrations of samples were chosen to meet the manufacturers' recommendation of 20-100 particles per frame and a concentration of 10^7-10^9 particles/mL. All measurements were performed in triplicate at 25 °C. HD plots are listed below for PNs (10 μM) and PN/BSA complexes (10 μM/100 nM), demonstrating the formation of monodisperse nanoparticles upon addition of BSA. Values given is the mean HD of three readings +/- mean standard deviation (SD). In this study, SD is defined as the arithmetic value calculated with the sizes of all of the particles analyzed by the software. Zeta Potential was acquired by preparing samples in the same way as for NTA prior to analysis.

2.5.2. pKa Determination

pKa was determined for the different PNs by preparing a 2 mM polymer solution in 1 mL of acidified (pH ~3) 100 mM NaCl solution and titrating from pH ~3 to 11 with 5 μL increments of a 25 mM KOH solution. For the titration, the pH was determined using a Mettler Toledo InLab Ultra-Micro pH Probe. pKa value for each polymer was determined by plotting the ΔpH/volume of KOH and identifying the largest ΔpH. For polymers with two maxima, the volume of the median point between the two maxima was chosen as the point where pH = pKa. For random-Bz-G and block-Bz-G, no deprotonation of the cationic moiety occurs and therefore titration curves are only representative of the change in pH of solution.

2.5.3. Fluorescent Quenching Titration

The complexation between the PNs and protein was studied by monitoring the fluorescence emission intensity (Ex: 540 nm; Em: 576 nm) of rhodamine-labelled bovine serum albumin (Rho-BSA) as a functional of increasing concentrations of PNs. Rhodamine quenching was indicative of protein binding. PN stock solutions were prepared by dissolving dried PN powders in DMSO and diluting to final concentrations of 3.2 mM in DMSO. Polymer solutions were serially diluted (1:1) in DMSO (from 3.2 to 0.5 mM) and further diluted in H2O (20% v/v). Emission of Rho-BSA solutions was taken before and after the addition of adequate volumes of polymer solutions, and the relative emission intensity as a function of polymer concentration was plotted. Final concentration of Rho-BSA was 100 nM and of polymers ranged from 32-0.5 μM.

2.5.4. Dissociation Constant Determination

The dissociation constant was determined by converting the relative fluorescence quenching plots to fractional saturation plots using equation 1 below:

$$Fractional\ Saturation\ (y) = \frac{F_P - F_0}{F_{sat} - F_0} \qquad (1)$$

where F_0, F_P, and F_{sat} were the relative emission intensities of Rho-BSA only, polymer/Rho-BSA complexes at the various concentrations tested, and polymer/Rho-BSA at saturation. The dissociation constant was determined by equation 2 below:

$$y = \frac{(P + c + K_d) - \sqrt{(P + c + K_d)^2 - 4Pc}}{4c} \qquad (2)$$

where y is the fractional saturation plot obtained with equation 1, P is the polymer concentration (x-axis) and c is the constant Rho-BSA concentration (100 nM). K_d was determined using the non-linear curve fitting module of Origin 8.5 and equation 2.

2.5.5. Protein Loading Ratio

The loading ratio of R-PE was determined by measuring the fluorescence of non-complexed R-PE in centrifuged complexes. PN stock solutions were prepared by dissolving dried PN powders in DMSO and diluting to final concentrations of 1 mM in DMSO. Adequate volumes of PN stock solutions were diluted in water (20% v/v) and mixed with equal volumes of R-PE solution for a final complex volume of 50 μL. Complexes were incubated for 30 min at room temperature before a ten-fold dilution in PBS to a final volume of 500 μL (final PN/R-PE concentration was 10 μM and 15 nM, respectively). The solutions were centrifuged at 22,000 x g for 10 min. The supernatant was collected in a cuvette and the fluorescence intensity of R-PE in the supernatant was measured at 574 nm. The amount of R-PE in supernatant was calculated according to the standard curve of R-PE in the same solvent composition.

2.5.6. Serum Stability Assay

R-PE release assay - The stability of complexes was studied by monitoring the fluorescence of the R-PE released from complexes. PN stock solutions were prepared by dissolving dried PN powders in DMSO and diluting to final concentrations of 1 mM in DMSO. Adequate volumes of PN stock solutions were diluted in water (20% v/v) and mixed with equal volumes of R-PE solution for a final complex volume of 50 μL. Complexes were incubated for 30 min at room temperature before a ten-fold dilution in PBS with 10% FBS to a final volume of 500 μL (final PN/R-PE concentration was 10 μM and 15 nM, respectively). The solutions were incubated at room temperature for the respective amounts of time before being centrifuged at 22,000 x g for 10 min. The supernatant was collected in a cuvette and the fluorescence intensity of R-PE in the supernatant was measured at 574

nm. The amount of R-PE in supernatant was calculated according to the standard curve of R-PE in same solvent composition.

Rho-BSA Quenching Assay - The stability of complexes in the presence of 10% fetal bovine serum (FBS) was studied by monitoring the fluorescence of PN/Rho-BSA complexes over 2 hours. Briefly, 40 μL of complexes were prepared by mixing equal volumes of polymer and Rho-BSA solutions and allowing them to complex for 30 min. These complexes were then diluted into 360 μL of either PBS or PBS with 10% FBS and the emission spectra was recorded immediately. Final concentration of PN and Rho-BSA was 10 μM and 100 nM, respectively. The complexes were allowed to sit at room temperature between readings.

2.5.7. Cell Culture

HeLa cells were cultured in Gibco DMEM High Glucose medium supplemented with 10% (v/v) FBS and 1% (v/v) Penicillin-Streptomycin mixture. Mesenchymal stem cell (MSC) and T cell were cultured and treated with PN/R-PE at Prof. Sackstein's laboratory at Florida International University with technical assistant. MSC were isolated from patient adipose samples and cultured in Gibco DMEM High Glucose medium supplemented with 10% FBS. T cells were isolated from a PMCB suspension and cultured in RPMI supplemented with 10% FBS.

2.5.8. PN Toxicity Assay

HeLa cells were seeded in a 96-well plate (~10,000/well) in 200 μL of complete medium and allowed to attach for one day at 37 °C under a humidified atmosphere of 5% CO_2 prior to sample treatment. Final concentrations of 40, 20, 10, and 5 μM were added into the complete media by dilution of the polymer stock solutions. After addition of the samples,

cells were incubated for 18 h prior to treatment with 10 μL of methylthiazole tetrazolium (MTT) (5 mg/mL in PBS) and incubated for 4 h at 37 °C. After incubation, 200 μL of medium was gently removed and 100 μL of biological grade DMSO was added to solubilize the purple formazan crystals. Absorbance was measured by microwell plate reader. Cell viability was determined as a function of absorbance of each sample relative to control wells. All measurements represent the average of three independent measurements +/- standard deviation.

2.5.9. Flow Cytometry Analysis

Hela cells and MSCs were seeded into 12 or 6-well plates (~100,000/well or ~60,000/well, respectively) in complete media and allowed to attach for one day at 37 °C under a humidified atmosphere of 5% CO_2 prior to sample treatment. In contrast, T-cells were counted plated in 12-well plates (~400,000/well) in complete RPMI media and treated right away. R-PE, EGFP, FITC-BSA, and Rho-BSA stock solutions were diluted to working concentrations with 1X PBS. Polymer stock solutions were prepared at 1 mM in DMSO. 40 μL of polymer/protein complexes were prepared by mixing appropriate volumes of polymer and protein substock solutions and incubating for 30 min at room temperature in the dark. Complexes were added dropwise to each well to the cells in complete media and incubated for varying periods of time, depending on the experiment. After the incubation periods required, adherent cells were rinsed three times with full volumes of PBS, followed by washing with 1 μM heparan sulfate solution to remove any extracellular surface-bound complexes. The cells were harvested with TrypLE, transferred to centrifuge tubes, rinsed an additional three times with PBS before being finally resuspended in 300 μL of PBS. In the case of suspension cells, cells were transferred to centrifuge tubes, centrifuged, and

resuspended in PBS three times. Cells were analyzed by flow cytometry, in which data for 10,000 events were collected. Analysis for primary cells were performed with supervision and technical assistance of Dr. Sackstein group.

2.5.10. R-PE Uptake of Control Polymers

In order to study the R-PE uptake, HeLa cells were treated with PN/R-PE complexes (final concentration of PN and R-PE were 10 μM and 15 nM, respectively) before analyzed by flow cytometry analysis as described previously.

2.5.11. Cellular Entry Pathway

In order to study the mechanism of uptake, HeLa cells were treated with Ph-CG/R-PE complexes (10 μM/15 nM) for 1 h under energy-independent conditions or under pre-treatment with various pharmacological inhibitors. Briefly, HeLa cells seeded the day prior to sample treatment in 12-well plates (100,000/well). The day of experiment, cells were equilibrated for 30 minutes under 4 °C, ATP depletion conditions (NaN_3: 10 mM & 2-deoxyglucose: 50 mM), chlorpromazine (28 μM), LYS 294003 (3 μM), Cytochalastin D (10 μM), methyl-B-cyclodextrin (1 mM) and genistein (200 μM) or normal culture conditions. Complexes were added dropwise, and cells were incubated for 1 h prior to analysis via flow cytometry as described previously.

2.5.12. Functional Protein Delivery

MTT assay was performed with PN/protein complexes are described previously. In short, serial dilutions of saporin, RNase, or anti-pAkt were prepared and complexes with various PNs. For serum-containing media, complexes were added to HeLa cells and incubated overnight prior to MTT treatment. For serum-free experiments, complexes were added in

DMEM for 4 h and the media was replaced with complete media overnight prior to MTT treatment.

2.5.13. Confocal Imaging

Hela cells were seeded on 12-well plates (~60,000/well) containing glass coverslips one day before sample treatment. Complexes were prepared as described previously. After incubation for varying periods of time using same culture conditions discussed earlier, the medium was removed, and cells were washed three times with PBS and once with heparan sulfate. Cells were fixed with 4% PFA for 10 minutes and rinsed once with PBS. Nuclei were stained with Hoechst 33342 at final concentration of 1 µg/mL for 7 minutes. For cells with Lysotracker Red staining, the manufacturers protocol was followed. The coverslips were mounted on microscope slides using 1:1 glycerol/PBS mounting medium.

2.5.14. Synthesis

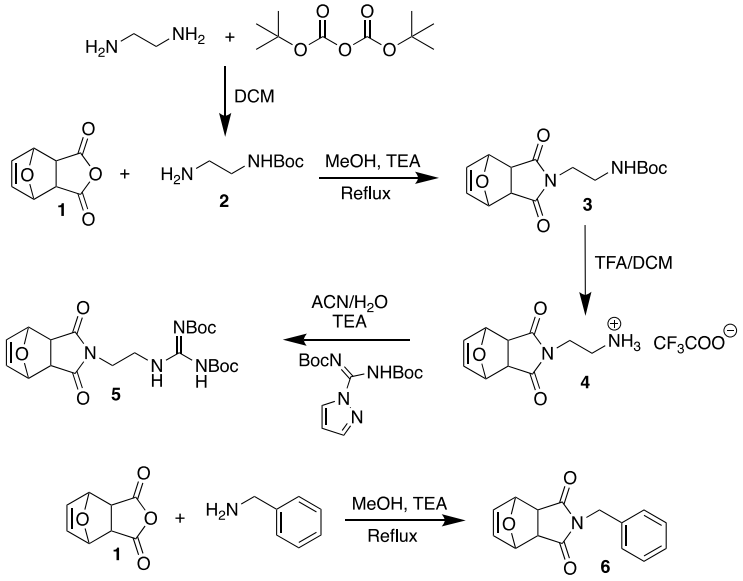

Scheme 2.1. Synthesis of monomer 5 and 6.

Monomer Synthesis - Monomers 5 and 6 were used for polymerization and synthesized following previously reported procedures. Briefly, synthesis of monomer 5 began with the

N-Boc protection of ethylenediamine with the addition of 0.1 equivalents of di-tert-butyl decarbonate dropwise overnight. N-Boc protected ethylenediamine was refluxed with compound 1 and was precipitated after reaction was complete, yielding compound 3. This compound was deprotected using TFA (compound 4) and the free amine was converted to Boc-protected guanidine (compound 5). Compound 6 was synthesized by refluxing compound 1 with benzylamine.

2: Yield: 83%. ^{1}H NMR (400 MHz, $CDCl_3$): δ 5.44 (br s, 1H), 2.96 (s, 2H), 2.59 (t, 2H), 1.25 (s, 9H), 1.04 (s, 2H).

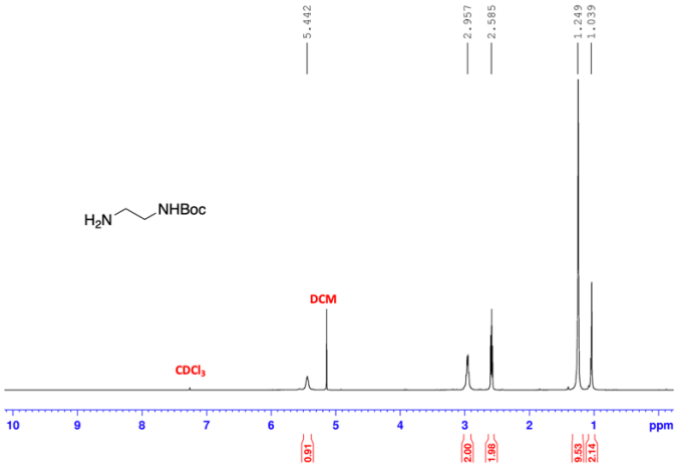

3: Yield: 50%. ^{1}H NMR (400 MHz, $CDCl_3$): δ 6.51 (s, 2H), 5.25 (s, 2H), 4.79 (s, 1H), 3.62 (t, 2H), 3.30 (t, 2H), 2.84 (s, 2H), 1.41 (s, 9H).

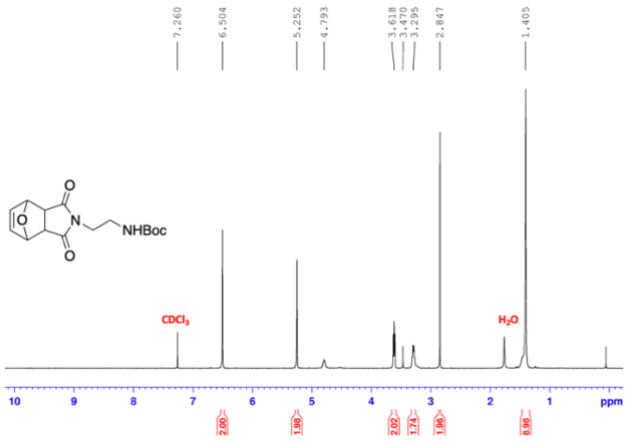

4: Yield: 85%. ^{1}H NMR (400 MHz, DMSO-d_6): δ 7.98 (s, 3H), 6.56 (s, 2H), 5.14 (s, 2H), 3.62 (t, 2H), 2.94 (m, 4H).

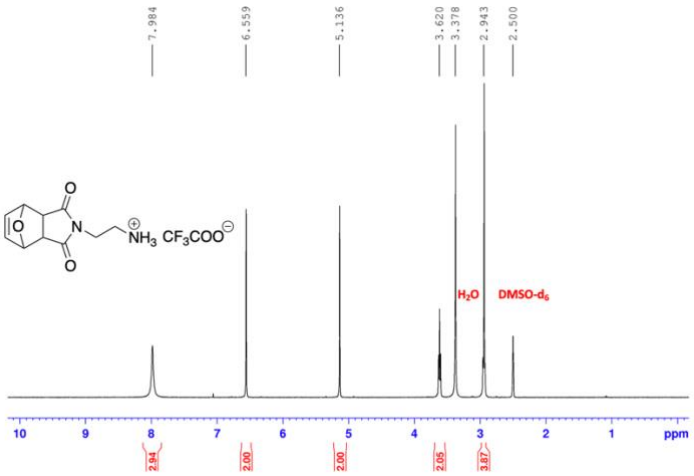

5: Yield: 68%. ^{1}H NMR (400 MHz, $CDCl_3$): δ 11.40 (s, 1H), 8.39 (s, 1H), 6.48 (s, 2H), 5.23 (s, 2H), 3.67 (t, 2H), 3.60 (t, 2H), 2.84 (s, 2H), 1.44 (m, 18H).

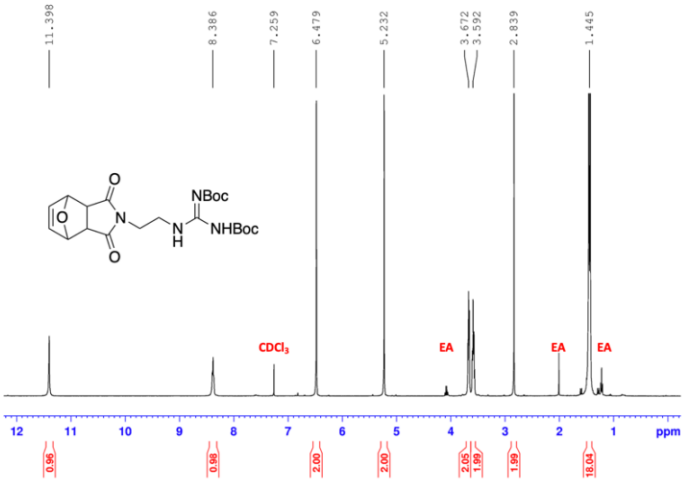

6: Yield: 70%. ^{1}H NMR (400 MHz, $CDCl_3$): δ 7.30 (m, 5H), 6.52 (s, 2H), 5.29 (s, 2H), 4.64 (s, 2H), 2.86 (s, 2H).

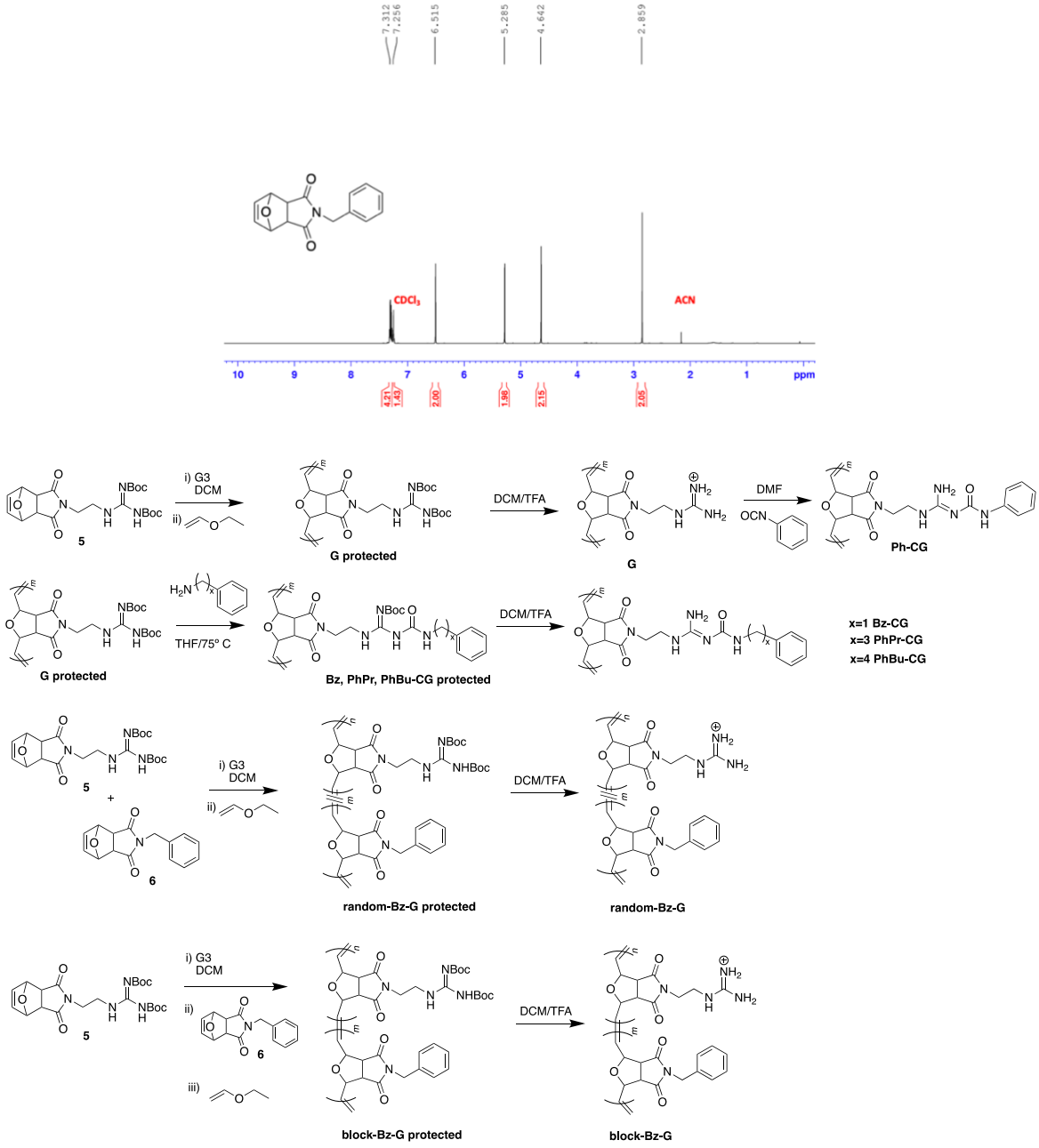

Scheme 2.2. Synthesis of polymers (G, Ph-CG, Bz-CG, PhPr-CG, PhBu-CG, random-Bz-G, block-Bz-G).

Synthesis of G. Monomer 5 was dissolved in DCM. Grubbs 3rd generation catalyst was dissolved in DCM and added to the stirring monomer solution. After 60 min, the living polymer was end-capped with 1 mL of ethyl vinyl ether. The polymer solution was

precipitated into stirring diethyl ether (3x) and dried. The dried solid was dissolved in a DCM/TFA mixture (1:1, v/v) and deprotected overnight. The reaction mixture was precipitated (3x) and collected via centrifugation.

G protected: ^{1}H NMR (400 MHz, $CDCl_3$): δ 11.45 (br, 1H), 8.46 (br, 1H), 6.06 (br, 1H), 5.73 (br, 1H), 4.98 (br, 1H), 4.48 (br, 1H), 3.65 (br, 4H), 3.35 (br, 2H), 1.47 (d, 18H).

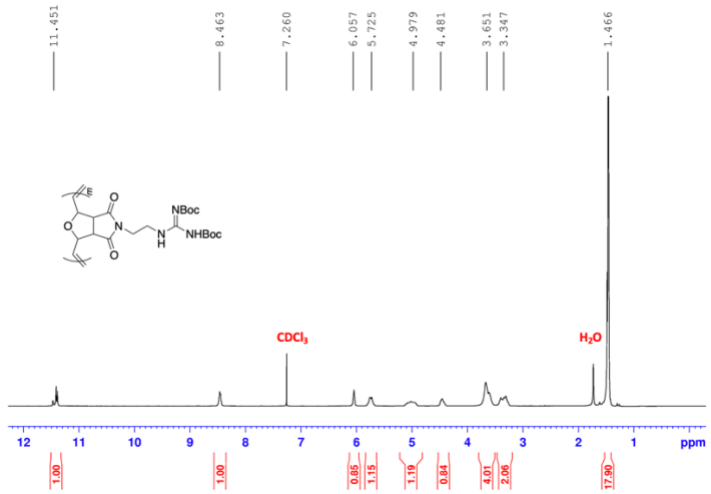

G: ^{1}H NMR (400 MHz, DMSO-d_6): δ 7.97 (br, 1H), 7.42 (br, 4H), 5.97 (br, 1H), 5.76 (br, 1H), 4.94 (br, 1H), 4.45 (br, 1H), 3.51 (br, 2H), 3.34 (br, 4H).

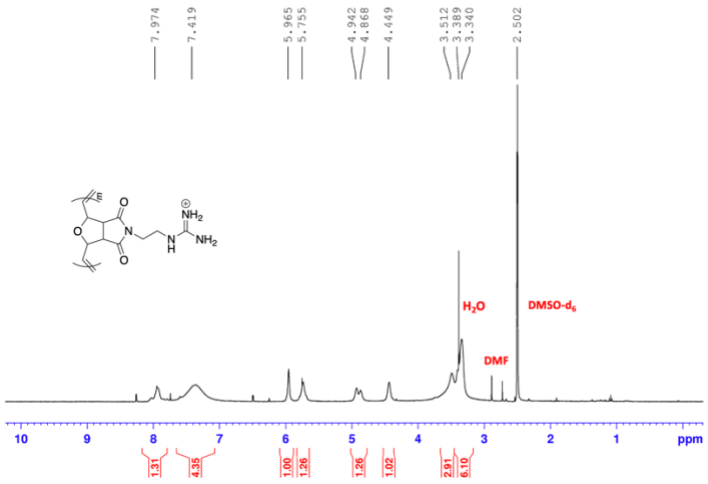

Synthesis of Ph-CG. G polymer was dissolved in dry DMF. 5 equivalents of phenyl isocyanate were added. The mixture was sealed in a vial and allowed to react overnight at

75 °C. The reaction mixture was precipitated into diethyl ether (3x) and the polymer was collected via centrifugation.

Ph-CG: ^{1}H NMR (400 MHz, DMSO-d$_6$): δ 11.70 (br, 1H), 9.59 (br, 1H), 9.15 (br, 2H), 7.91 (br, 2H), 7.69 (br, 1H), 7.55 (br, 2H), 5.75 (br, 2H), 4.91 (br, 1H), 4.41 (br, 1H), 3.60 (br, 4H), 3.24 (br, 2H).

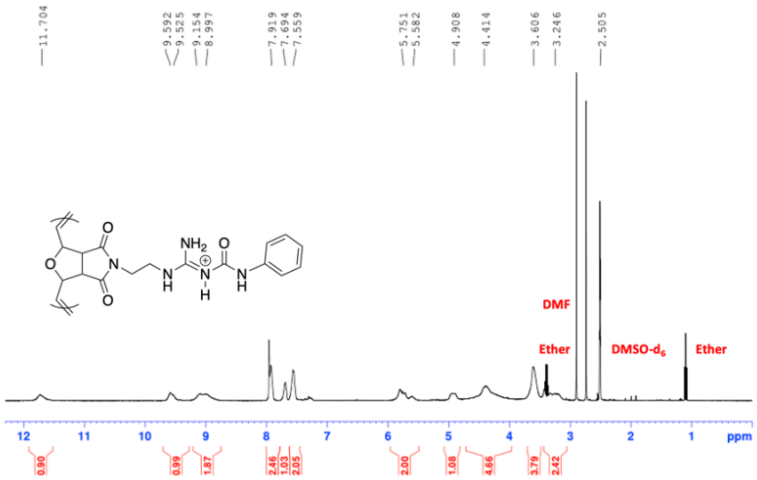

Synthesis of Bz, PhPr, PhBu-CG. Protected G polymer was dissolved in THF to which 2.5 equivalents of benzylamine, 3-Phenylpropylamine or 4-Phenylbutylamine were added. The mixture was sealed in a vial and allowed to react overnight at 75 °C. The reaction mixture was precipitated into diethyl ether (3x) and then deprotected in DCM/TFA mixture (1:1, v/v). Deprotected polymer solution was precipitated into diethyl ether (3x) and polymer collected via centrifugation.

Bz-CG protected: ^{1}H NMR (400 MHz, $CDCl_3$): δ 12.04 (br, 1H), 8.14 (br, 1H), 7.20 (br, 5H), 5.97 (br, 1H), 5.67 (br, 1H), 4.97 (br, 1H), 4.33 (br, 3H), 3.56 (br, 4H), 3.17 (br, 2H), 1.44 (s, 9H).

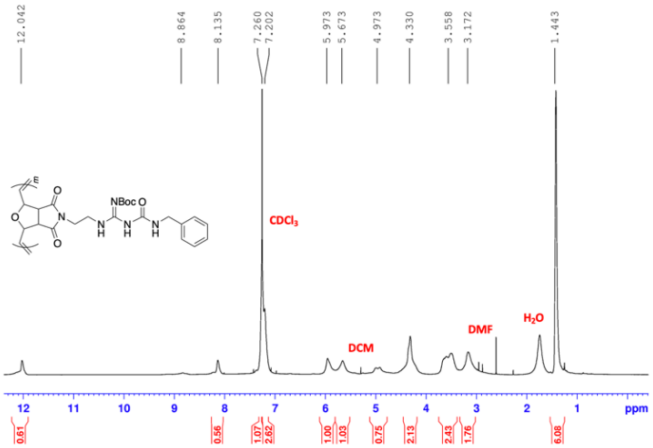

Bz-CG: ^{1}H NMR (400 MHz, DMSO-d_6): δ 9.15 (br, 1H), 8.61 (br, 2H), 7.99 (br, 1H), 7.27 (br, 5H), 5.92 (br, 1H), 5.71 (br, 2H), 4.94 (br, 1H), 4.41 (br, 1H), 4.25 (br, 4H), 3.75 (br, 4H).

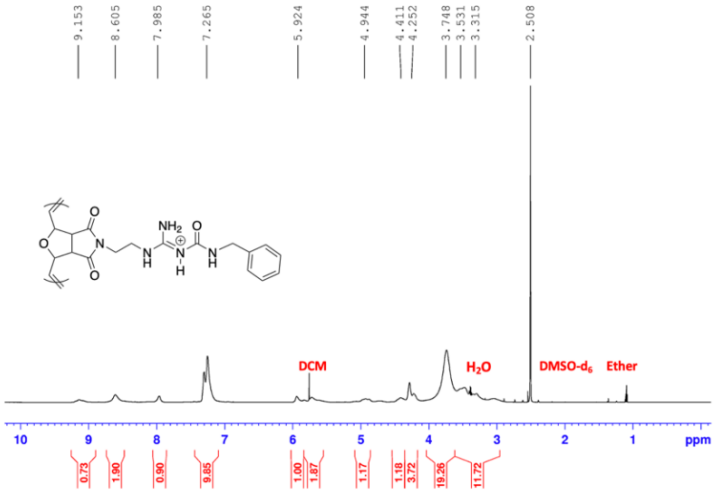

PhPr-CG protected: ^{1}H NMR (400 MHz, $CDCl_3$): δ 12.10 (br, 1H), 8.13 (br, 1H), 7.27 (br, 2H), 7.21 (br, 3H), 5.98 (br, 1H), 5.68 (br, 1H), 4.99 (br, 1H), 4.34 (br, 1H), 3.63 (br, 2H), 3.16 (br, 4H), 2.60 (br, 2H), 1.77 (br, 2H), 1.40 (s, 9H).

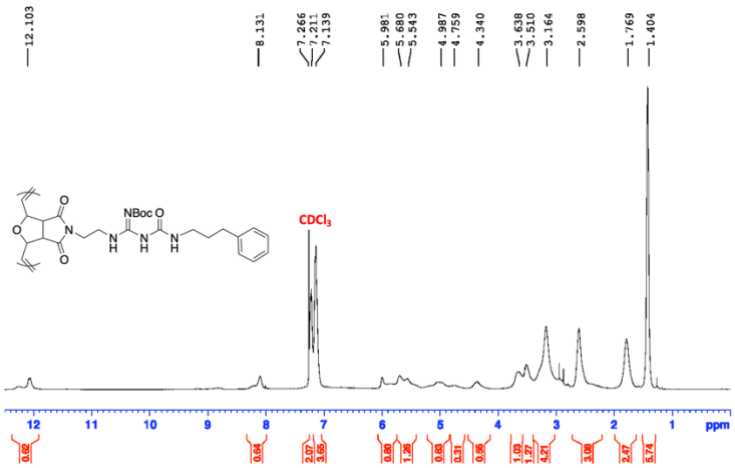

PhPr-CG: ^{1}H NMR (400 MHz, DMSO-d_6): δ 8.73 (br, 1H), 7.88 (br, 1H), 7.17 (br, 5H), 6.12 (br, 1H), 5.80 (br, 1H), 4.85 (br, 1H), 4.29 (br, 1H), 3.25 (br, 4H), 2.94 (br, 6H),1.58 (br, 2H).

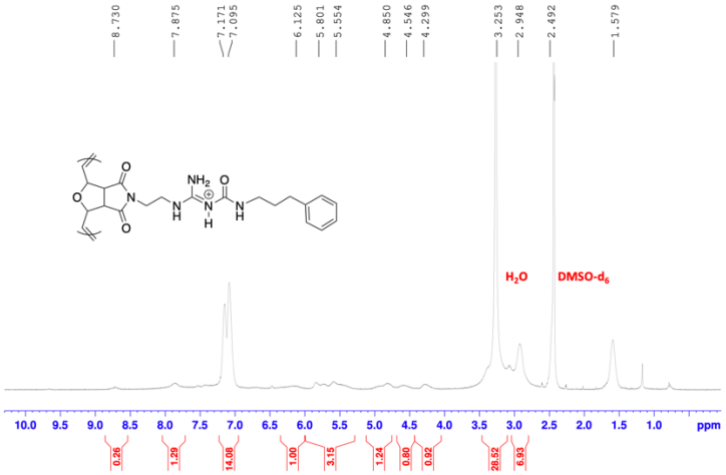

PhBu-CG protected: ^{1}H NMR (400 MHz, $CDCl_3$): δ 12.08 (br, 1H), 8.08 (br, 1H), 7.27 (br, 2H), 7.10 (br, 3H), 6.02 (br, 1H), 5.71 (br, 1H), 5.06 (br, 1H), 4.34 (br, 1H), 3.66 (br, 2H), 3.14 (br, 4H), 2.59 (br, 2H), 1.60 (br, 4H), 1.40 (s, 9H).

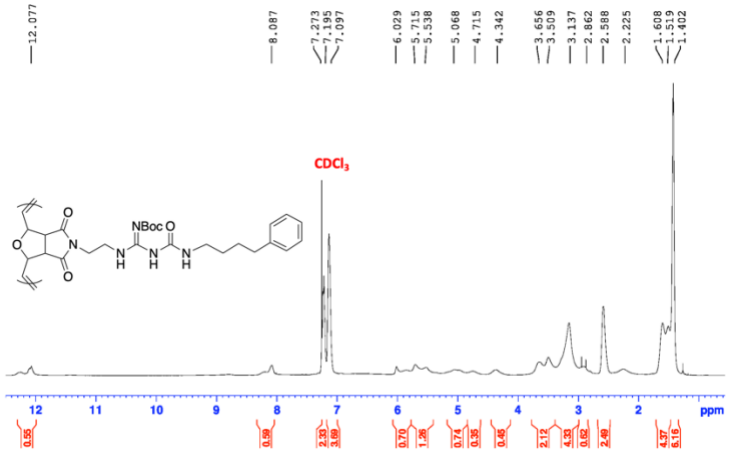

PhBu-CG: ^{1}H NMR (400 MHz, DMSO-d_6): δ 9.11 (br, 1H), 8.08 (br, 2H), 7.90 (br, 1H), 7.16 (br, 5H), 6.05 (br, 1H), 5.74 (br, 1H), 4.85 (br, 1H), 4.42 (br, 1H), 3.66 (br, 2H), 3.13 (br, 4H), 2.62 (br, 2H), 1.60 (br, 4H).

Synthesis of random-Bz-G. Molar equivalents of monomer 5 and 6 were dissolved in DCM. Grubbs 3rd generation catalyst was dissolved in DCM and added to the stirring monomer solution. After 60 min, the living polymer was end-capped with 1 mL of ethyl vinyl ether. The polymer solution was precipitated into stirring diethyl ether (3x) and dried. The dried solid was dissolved in a DCM/TFA mixture (1:1, v/v) and deprotected overnight. The reaction mixture was precipitated (3x) and collected via centrifugation.

random-Bz-G protected: ^{1}H NMR (400 MHz, $CDCl_3$): δ 11.43 (br, 0.5H), 8.46 (br, 0.5H), 7.27 (br, 2.5H), 6.04 (br, 1H), 5.75 (br, 1H), 4.99 (br, 1H), 4.64 (br, 1H), 4.47 (br, 1H), 3.65 (br, 2H), 3.32 (br, 2H), 1.44 (s, 9H).

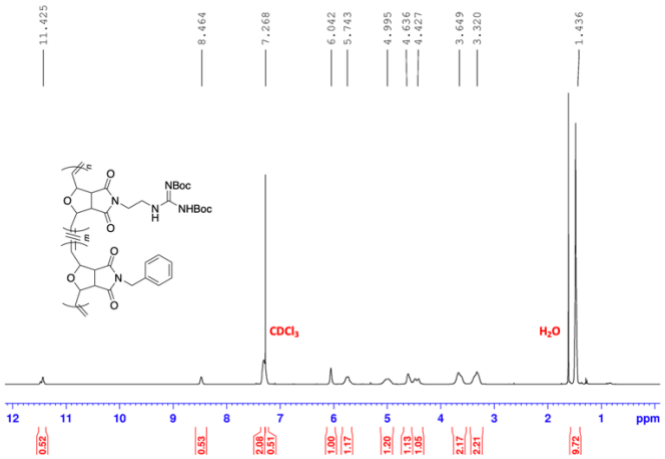

random-PN-Bz-G: ^{1}H NMR (400 MHz, DMSO-d_6): δ 7.73 (br, 1H), 7.26 (br, 4H), 5.96 (br, 1H), 5.71 (br, 1H), 4.88 (br, 1H), 4.55 (br, 1H), 4.41 (br, 1H), 3.47 (br, 2H), 3.33 (br, 2H).

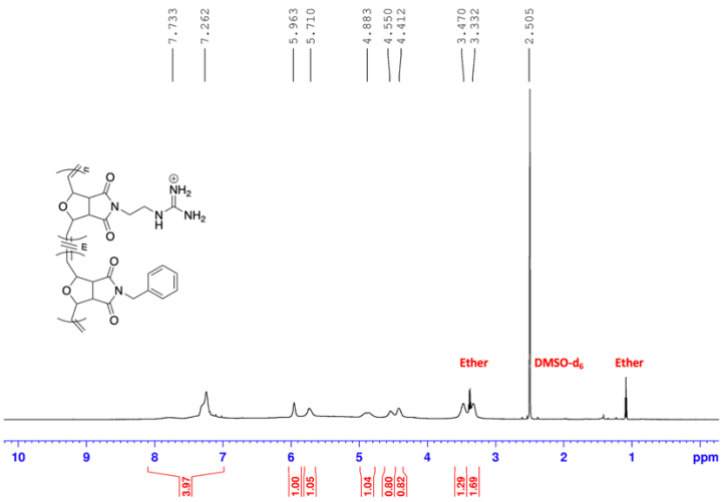

Synthesis of block-Bz-G. Monomer 5 was dissolved in DCM. Grubbs 3rd generation catalyst was dissolved in DCM and added to the stirring monomer solution. After 15 mins, monomer 6 solution was added to the stirring polymerization solution and allowed to stir for additional 45 mins. Afterwards, the living polymer was end-capped with 1 mL of ethyl vinyl ether. The polymer solution was precipitated into stirring diethyl ether (3x) and dried.

The dried solid was dissolved in a DCM/TFA mixture (1:1, v/v) and deprotected overnight.

The reaction mixture was precipitated (3x) and collected via centrifugation.

block-Bz-G protected: ^{1}H NMR (400 MHz, $CDCl_3$): δ 11.41 (br, 0.5H), 8.47 (br, 0.5H), 7.30 (br, 2.5H), 6.00 (br, 1H), 5.68 (br, 1H), 5.04 (br, 1H), 4.56 (br, 1H), 4.42 (br, 1H), 3.68 (br, 2H), 3.28 (br, 2H), 1.46 (s, 9H).

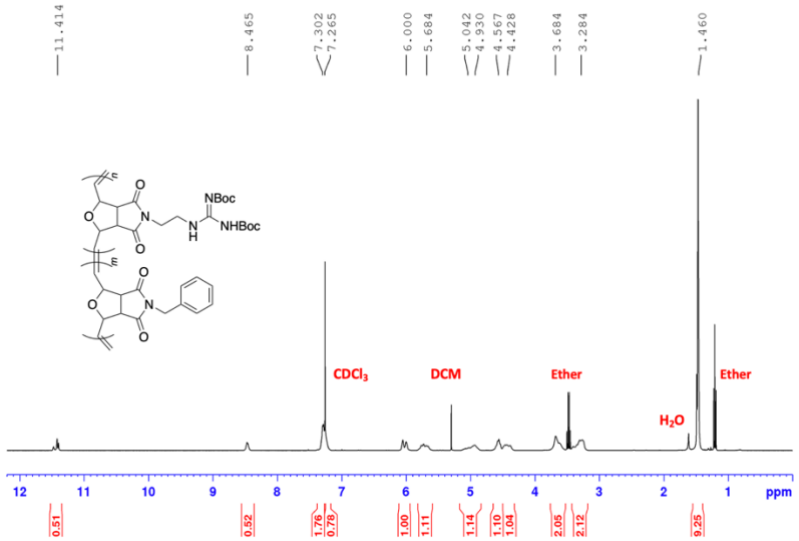

block-Bz-G: ^{1}H NMR (400 MHz, DMSO-d_6): δ 7.91 (br, 0.5H), 7.44 (br, 2H), 7.23 (br, 2.5H), 5.96 (br, 1H), 5.72 (br, 1H), 4.94 (br, 1H), 4.51 (br, 1H), 4.45 (br, 1H), 3.46 (br, 2H), 3.35 (br, 2H).

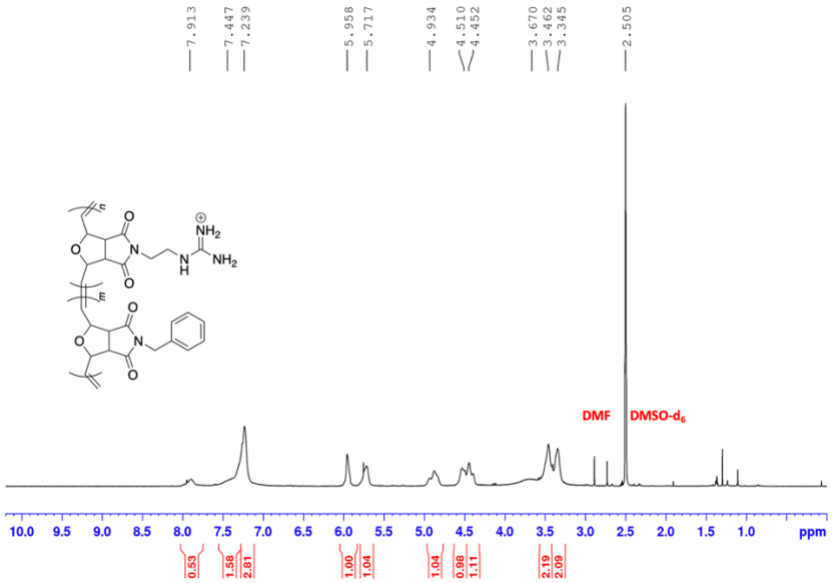

2.6. References

(1) Aguzzi, A.; O'Connor, T. Protein Aggregation Diseases: Pathogenicity and Therapeutic Perspectives. *Nat. Rev. Drug Discov.* **2010**, *9* (3), 237–248. https://doi.org/10.1038/nrd3050.

(2) Attwood, M. M.; Fabbro, D.; Sokolov, A. V.; Knapp, S.; Schiöth, H. B. Trends in Kinase Drug Discovery: Targets, Indications and Inhibitor Design. *Nat. Rev. Drug Discov.* **2021**, *0123456789*. https://doi.org/10.1038/s41573-021-00252-y.

(3) Bansal, A.; Schmidt, M.; Rennegarbe, M.; Haupt, C.; Liberta, F.; Stecher, S.; Puscalau-Girtu, I.; Biedermann, A.; Fändrich, M. AA Amyloid Fibrils from Diseased Tissue Are Structurally Different from in Vitro Formed SAA Fibrils. *Nat. Commun.* **2021**, *12* (1). https://doi.org/10.1038/s41467-021-21129-z.

(4) Singh, K.; Ejaz, W.; Dutta, K.; Thayumanavan, S. Antibody Delivery for Intracellular Targets: Emergent Therapeutic Potential. *Bioconjug. Chem.* **2019**, *30* (4), 1028–1041. https://doi.org/10.1021/acs.bioconjchem.9b00025.

(5) Ren, L.; Lv, J.; Wang, H.; Cheng, Y. A Coordinative Dendrimer Achieves Excellent Efficiency in Cytosolic Protein and Peptide Delivery. *Angew. Chemie - Int. Ed.* **2020**, *59* (12), 4711–4719. https://doi.org/10.1002/anie.201914970.

(6) Lv, J.; Fan, Q.; Wang, H.; Cheng, Y. Polymers for Cytosolic Protein Delivery. *Biomaterials* **2019**, *218* (July), 119358. https://doi.org/10.1016/j.biomaterials.2019.119358.

(7) Lv, J.; Wang, C.; Li, H.; Li, Z.; Fan, Q.; Zhang, Y.; Li, Y.; Wang, H.; Cheng, Y. Bifunctional and Bioreducible Dendrimer Bearing a Fluoroalkyl Tail for Efficient Protein Delivery Both in Vitro and in Vivo. *Nano Lett.* **2020**, *20* (12), 8600–8607. https://doi.org/10.1021/acs.nanolett.0c03287.

(8) Cheng, Y. Design of Polymers for Intracellular Protein and Peptide Delivery. *Chinese J. Chem.* **2021**, *39* (6), 1443–1449. https://doi.org/10.1002/cjoc.202000655.

(9) Fu, A.; Tang, R.; Hardie, J.; Farkas, M. E.; Rotello, V. M. Promises and Pitfalls of Intracellular Delivery of Proteins. *Bioconjug. Chem.* **2014**, *25* (9), 1602–1608. https://doi.org/10.1021/bc500320j.

(10) Rothbard, J. B.; Jessop, T. C.; Lewis, R. S.; Murray, B. A.; Wender, P. A. Role of Membrane Potential and Hydrogen Bonding in the Mechanism of Translocation of Guanidinium-Rich Peptides into Cells. *J. Am. Chem. Soc.* **2004**, *126* (31), 9506–9507. https://doi.org/10.1021/ja0482536.

(11) Wender, P. A.; Galliher, W. C.; Goun, E. A.; Jones, L. R.; Pillow, T. H. The Design of Guanidinium-Rich Transporters and Their Internalization Mechanisms. *Adv. Drug Deliv. Rev.* **2008**, *60* (4–5), 452–472. https://doi.org/10.1016/j.addr.2007.10.016.

(12) Stanzl, E. G.; Trantow, B. M.; Vargas, J. R.; Wender, P. A. Fifteen Years of Cell-Penetrating, Guanidinium-Rich Molecular Transporters: Basic Science, Research Tools, and Clinical Applications. *Acc. Chem. Res.* **2013**, *46* (12), 2944–2954. https://doi.org/10.1021/ar4000554.

(13) Caffrey, L. M.; Deronde, B. M.; Minter, L. M.; Tew, G. N. Mapping Optimal Charge Density and Length of ROMP-Based PTDMs for SiRNA Internalization. *Biomacromolecules* **2016**, *17* (10), 3205–3212. https://doi.org/10.1021/acs.biomac.6b00900.

(14) Tezgel, A. Ö.; Jacobs, P.; Backlund, C. M.; Telfer, J. C.; Tew, G. N. Synthetic Protein Mimics for Functional Protein Delivery. *Biomacromolecules* **2017**, *18* (3), 819–825. https://doi.org/10.1021/acs.biomac.6b01685.

(15) Wender, P. A.; Cooley, C. B.; Geihe, E. I. Beyond Cell Penetrating Peptides: Designed Molecular Transporters. *Drug Discov. Today Technol.* **2012**, *9* (1), e49–e55. https://doi.org/10.1016/j.ddtec.2011.07.004.

(16) Chang, H.; Lv, J.; Gao, X.; Wang, X.; Wang, H.; Chen, H.; He, X.; Li, L.; Cheng, Y. Rational Design of a Polymer with Robust Efficacy for Intracellular Protein and Peptide Delivery. *Nano Lett.* **2017**, *17* (3), 1678–1684. https://doi.org/10.1021/acs.nanolett.6b04955.

(17) Lee, Y. W.; Luther, D. C.; Goswami, R.; Jeon, T.; Clark, V.; Elia, J.; Gopalakrishnan, S.; Rotello, V. M. Direct Cytosolic Delivery of Proteins through Coengineering of Proteins and Polymeric Delivery Vehicles. *J. Am. Chem. Soc.* **2020**, *142* (9), 4349–4355. https://doi.org/10.1021/jacs.9b12759.

(18) Heyda, J.; Okur, H. I.; Hladílková, J.; Rembert, K. B.; Hunn, W.; Yang, T.; Dzubiella, J.; Jungwirth, P.; Cremer, P. S. Guanidinium Can Both Cause and Prevent the Hydrophobic Collapse of Biomacromolecules. *J. Am. Chem. Soc.* **2017**, *139* (2), 863–870. https://doi.org/10.1021/Jacs.6b11082.

(19) Feldblum, E. S.; Arkin, I. T. Strength of a Bifurcated H Bond. *Proc. Natl. Acad. Sci. U. S. A.* **2014**, *111* (11), 4085–4090. https://doi.org/10.1073/pnas.1319827111.

(20) Mogaki, R.; Hashim, P. K.; Okuro, K.; Aida, T. Guanidinium-Based "Molecular Glues" for Modulation of Biomolecular Functions. *Chem. Soc. Rev.* **2017**, *46* (21), 6480–6491. https://doi.org/10.1039/c7cs00647k.

(21) Monopoli, M. P.; Åberg, C.; Salvati, A.; Dawson, K. A. Biomolecular Coronas Provide the Biological Identity of Nanosized Materials. *Nat. Nanotechnol.* **2012**, *7* (12), 779–786. https://doi.org/10.1038/nnano.2012.207.

(22) Fleischer, C. C.; Payne, C. K. Nanoparticle-Cell Interactions: Molecular Structure of the Protein Corona and Cellular Outcomes. *Acc. Chem. Res.* **2014**, *47* (8), 2651–2659. https://doi.org/10.1021/ar500190q.

(23) Hatai, J.; Schmuck, C. Diverse Properties of Guanidiniocarbonyl Pyrrole-Based Molecules: Artificial Analogues of Arginine. *Acc. Chem. Res.* **2019**, *52* (6), 1709–1720. https://doi.org/10.1021/acs.accounts.9b00142.

(24) Weill, C. O.; Biri, S.; Adib, A.; Erbacher, P. A Practical Approach for Intracellular Protein Delivery. *Cytotechnology* **2008**, *56* (1), 41–48. https://doi.org/10.1007/s10616-007-9102-3.

(25) Fu, A.; Tang, R.; Hardie, J.; Farkas, M. E.; Rotello, V. M. Promises and Pitfalls of Intracellular Delivery of Proteins. *Bioconjug. Chem.* **2014**, *25* (9), 1602–1608. https://doi.org/10.1021/bc500320j.

(26) Rui, Y.; Wilson, D. R.; Choi, J.; Varanasi, M.; Sanders, K.; Karlsson, J.; Lim, M.; Green, J. J. Carboxylated Branched Poly(β-Amino Ester) Nanoparticles Enable Robust Cytosolic Protein Delivery and CRISPR-Cas9 Gene Editing. *Sci. Adv.* **2019**, *5* (12). https://doi.org/10.1126/sciadv.aay3255.

(27) Backlund, C. M.; Hango, C. R.; Minter, L. M.; Tew, G. N. Protein and Antibody Delivery into Difficult-to-Transfect Cells by Polymeric Peptide Mimics. *ACS Appl. Bio Mater.* **2020**, *3* (1), 180–185. https://doi.org/10.1021/acsabm.9b00876.

(28) Zhang, Z.; Shen, W.; Ling, J.; Yan, Y.; Hu, J.; Cheng, Y. The Fluorination Effect of Fluoroamphiphiles in Cytosolic Protein Delivery. *Nat. Commun.* **2018**, *9* (1). https://doi.org/10.1038/s41467-018-03779-8.

(29) Wu, D.; Qin, M.; Xu, D.; Wang, L.; Liu, C.; Ren, J.; Zhou, G.; Chen, C.; Yang, F.; Li, Y.; et al. A Bioinspired Platform for Effective Delivery of Protein Therapeutics to the Central Nervous System. *Adv. Mater.* **2019**, *31* (18), 1–7. https://doi.org/10.1002/adma.201807557.

(30) Kleinmaier, R.; Keller, M.; Igel, P.; Buschauer, A.; Gschwind, R. M. Conformations, Conformational Preferences, and Conformational Exchange of N′-Substituted N -Acylguanidines: Intermolecular Interactions Hold the Key. *J. Am. Chem. Soc.* **2010**, *132* (32), 11223–11233. https://doi.org/10.1021/ja103756y.

(31) Keller, M.; Kuhn, K. K.; Einsiedel, J.; Hübner, H.; Biselli, S.; Mollereau, C.; Wifling, D.; Svobodová, J.; Bernhardt, G.; Cabrele, C.; et al. Mimicking of Arginine by Functionalized Nω-Carbamoylated Arginine As a New Broadly

Applicable Approach to Labeled Bioactive Peptides: High Affinity Angiotensin, Neuropeptide Y, Neuropeptide FF, and Neurotensin Receptor Ligands As Examples. *J. Med. Chem.* **2016**, *59* (5), 1925–1945. https://doi.org/10.1021/acs.jmedchem.5b01495.

(32) Li, M.; Schlesiger, S.; Knauer, S. K.; Schmuck, C. A Tailor-Made Specific Anion-Binding Motif in the Side Chain Transforms a Tetrapeptide into an Efficient Vector for Gene Delivery. *Angew. Chemie - Int. Ed.* **2015**, *54* (10), 2941–2944. https://doi.org/10.1002/anie.201410429.

(33) Lv, J.; Tan, E.; Wang, Y.; Fan, Q.; Yu, J.; Cheng, Y. Tailoring Guanidyl-Rich Polymers for Efficient Cytosolic Protein Delivery. *J. Control. Release* **2020**, *320* (January), 412–420. https://doi.org/10.1016/j.jconrel.2020.01.056.

(34) Posey, N. D.; Hango, C. R.; Minter, L. M.; Tew, G. N. The Role of Cargo Binding Strength in Polymer-Mediated Intracellular Protein Delivery. *Bioconjug. Chem.* **2018**, *29* (8), 2679–2690. https://doi.org/10.1021/acs.bioconjchem.8b00363.

(35) Sgolastra, F.; Backlund, C. M.; Ilker Ozay, E.; deRonde, B. M.; Minter, L. M.; Tew, G. N. Sequence Segregation Improves Non-Covalent Protein Delivery. *J. Control. Release* **2017**, *254* (March), 131–136. https://doi.org/10.1016/j.jconrel.2017.03.387.

(36) Ahmed, M. S.; Dutta, R. K.; Manandhar, P.; Li, X.; Torabi, H.; Barrios, A.; Wang, P.; Chinnapaiyan, S.; Unwalla, H. J.; Moon, J. H. A Guanylurea-Functionalized Conjugated Polymer Enables RNA Interference in: Ex Vivo Human Airway Epithelium. *Chem. Commun.* **2019**, *55* (54), 7804–7807. https://doi.org/10.1039/c9cc02856k.

(37) Salis, A.; Boström, M.; Medda, L.; Cugia, F.; Barse, B.; Parsons, D. F.; Ninham, B. W.; Monduzzi, M. Measurements and Theoretical Interpretation of Points of Zero Charge/Potential of BSA Protein. *Langmuir* **2011**, *27* (18), 11597–11604. https://doi.org/10.1021/la2024605.

(38) Van Guyse, J. F. R.; Xu, X.; Hoogenboom, R. Acyl Guanidine Functional Poly(2-Oxazoline)s as Reactive Intermediates and Stimuli-Responsive Materials. *J. Polym. Sci. Part A Polym. Chem.* **2019**, *57* (24), 2616–2624. https://doi.org/10.1002/pola.29542.

(39) Wilson, D. R.; Rui, Y.; Siddiq, K.; Routkevitch, D.; Green, J. J. Differentially Branched Ester Amine Quadpolymers with Amphiphilic and PH-Sensitive Properties for Efficient Plasmid DNA Delivery. *Mol. Pharm.* **2019**, *16* (2), 655–668. https://doi.org/10.1021/acs.molpharmaceut.8b00963.

(40) Zhang, S.; Lv, J.; Gao, P.; Feng, Q.; Wang, H.; Cheng, Y. A PH-Responsive Phase-Transition Polymer with High Serum Stability in Cytosolic Protein Delivery. *Nano Lett.* **2021**. https://doi.org/10.1021/acs.nanolett.1c03031.

(41) Nel, A. E.; Mädler, L.; Velegol, D.; Xia, T.; Hoek, E. M. V.; Somasundaran, P.; Klaessig, F.; Castranova, V.; Thompson, M. Understanding Biophysicochemical Interactions at the Nano-Bio Interface. *Nat. Mater.* **2009**, *8* (7), 543–557. https://doi.org/10.1038/nmat2442.

(42) Lättig-Tünnemann, G.; Prinz, M.; Hoffmann, D.; Behlke, J.; Palm-Apergi, C.; Morano, I.; Herce, H. D.; Cardoso, M. C. Backbone Rigidity and Static Presentation of Guanidinium Groups Increases Cellular Uptake of Arginine-Rich Cell-Penetrating Peptides. *Nat. Commun.* **2011**, *2* (1). https://doi.org/10.1038/ncomms1459.

(43) Sun, J.; Zhang, L.; Wang, J.; Feng, Q.; Liu, D.; Yin, Q.; Xu, D.; Wei, Y.; Ding, B.; Shi, X.; et al. Tunable Rigidity of (Polymeric Core)-(Lipid Shell) Nanoparticles for Regulated Cellular Uptake. *Adv. Mater.* **2015**, *27* (8), 1402–1407. https://doi.org/10.1002/adma.201404788.

(44) Polito, L.; Bortolotti, M.; Mercatelli, D.; Battelli, M. G.; Bolognesi, A. Saporin-S6: A Useful Tool in Cancer Therapy. *Toxins (Basel).* **2013**, *5* (10), 1698–1722. https://doi.org/10.3390/toxins5101698.

(45) Gotte, G.; Menegazzi, M. Biological Activities of Secretory RNases: Focus on Their Oligomerization to Design Antitumor Drugs. *Front. Immunol.* **2019**, *10* (November), 1–26. https://doi.org/10.3389/fimmu.2019.02626.

(46) Liu, R.; Chen, Y.; Liu, G.; Li, C.; Song, Y.; Cao, Z.; Li, W.; Hu, J.; Lu, C.; Liu, Y. PI3K/AKT Pathway as a Key Link Modulates the Multidrug Resistance of Cancers. *Cell Death Dis.* **2020**, *11* (9). https://doi.org/10.1038/s41419-020-02998-6.

(47) Dutta, K.; Kanjilal, P.; Das, R.; Thayumanavan, S. Synergistic Interplay of Covalent and Non-Covalent Interactions in Reactive Polymer Nanoassembly Facilitates Intracellular Delivery of Antibodies. *Angew. Chemie - Int. Ed.* **2021**, *60* (4), 1821–1830. https://doi.org/10.1002/anie.202010412.

CHAPTER III

Effects of Sidechain Isomerism on Polymer-Based Non-Covalent Protein Delivery

This chapter has been published in full in Chemical Communications, **2022**, DOI: 10.1039/d2cc02343a.

Alfonso Barrios,[a] Mario Milan Diaz,[b] Elianny Perozo, Md Lokman Hossen,[b] Prem Chapagain,[b,c] and Joong Ho Moon[a,c]

[a]Department of Chemistry and Biochemistry, Biomolecular Sciences Institute, Florida International University, 11200 SW 8th St., Miami, FL 33199, USA
[b]Department of Physics, Florida International University, 11200 SW 8th St., Miami, FL 33199, USA
[c]Biomolecular Sciences Institute, Florida International University, 11200 SW 8th St., Miami, FL 33199, USA

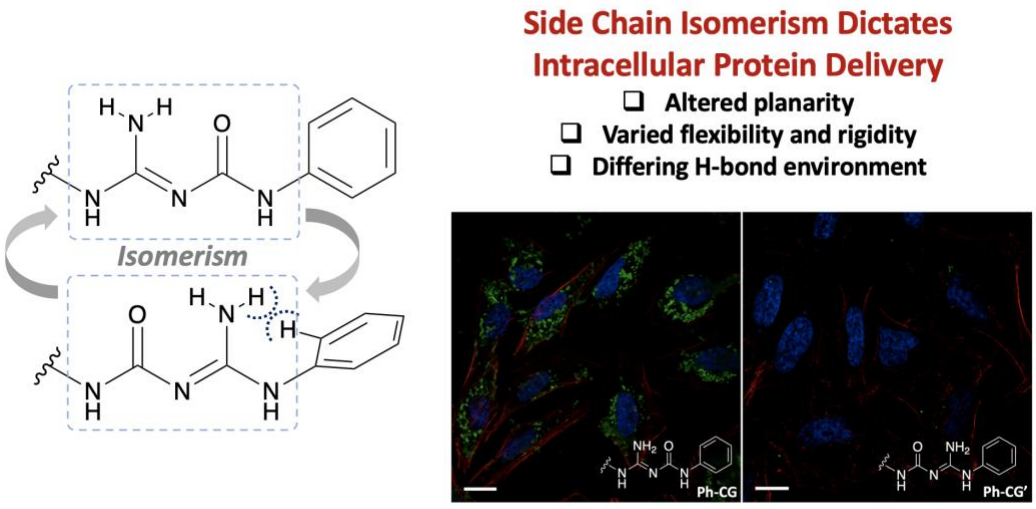

3.1. Abstract

We present the importance of functional group isomerism on intracellular protein delivery using polymers containing different isomeric side chains. While the physical properties of polymer/protein complexes are relatively similar, different planarity of the isomers greatly influences the cellular entry efficiency.

3.2. Introduction

Protein-based therapeutics have gained much recent attention for treating or curing various diseases. Their therapeutic success is due to high specificity, low side effects, less immunogenicity, and relatively short regulatory approval time than small molecular drugs.[1] Despite their advantages, the cell impermeability of most proteins has limited their applications to extracellular targets.[2] As more than 60% of intracellular protein signaling pathways control cellular functions, the intervention of disease-causing or -related signaling pathways would contribute to treating various diseases, including traditionally uncurable diseases using molecular drugs.[1,3–5] Therefore, there have been extensive efforts to develop efficient intracellular protein delivery systems.

Polymer-based non-covalent protein delivery systems have gained significant attention owing to the versatile tunability of the functional groups, compositions, and architectures.[6–8] Numerous structural (i.e., backbones) and functional groups (i.e., sidechains) for ionic, hydrogen bonding (HB), and hydrophobic interactions have been developed for facile protein complexation, cellular entry, and cytosolic release of functional proteins. The efficient protein delivery critically relies on optimized and balanced inter-macromolecular interactions. Without sufficient protein binding affinity, a premature dissociation of the complex occurs in the presence of excess serum proteins and

upon interaction with the cellular membranes.[9,10] With excessively high affinity, structural deformations and retarded desorption of polymers from the protein surface result in decreased concentrations of active proteins in the cytosol.[11]

Both structural and functional groups collectively influence the interactions with lipid membranes and entry pathways during cellular entry. While differences in cellular uptakes arising from tailored polymer backbone architecture have been reported,[12–14] little is known about the effects of subtle differences in the functional groups' conformation, isomerism, rigidity, and planarity. Most recently, Johnson et al. reported polymers with enantiomeric side chains displaying changed cellular uptakes and pharmacokinetic properties due to their different chiral recognition.[15] Our group also observed significant changes in the protein delivery efficiency from modified guanidine groups. Using various carbamoylated guanidine (CG) derivatives, we demonstrated the importance of the newly developed functional group for complex serum stability, cellular entry, and cytosolic availability of proteins.[16] While CG derivatives benefited from enhanced serum stability, the direct attachment of the phenyl group to CG contributed most to efficient protein delivery, presumably due to its planar structure. CG derivatives lacking planarity due to free rotating benzyl groups exhibited poor protein delivery, prompting us to explore how these subtle changes govern biological functions.

3.3. Results and Discussion

Herein, we report the effects of the constitutional isomerism of the Ph-CG group on functional protein delivery (Figure 3.1). From the backbone of polynorbornene (PN), the order of connectivity in phenyl-CG (Ph-CG) was altered to make an isomeric Ph-CG'. An isomer (Bn-CG') of benzyl-CG (Bn-CG) was also tested to expand the concept of the

isomer effect. Molecular dynamics simulations reveal that the isomeric functional group (i.e., Ph-CG') has a non-planar structure with less rotational freedom along the bond between nitrogen and sp^2 carbon in the phenyl group, while Ph-CG exhibits the planarity. Strikingly, while the complex sizes, protein loading, and serum stability are not significantly affected by the different planarity of the isomers, the cellular entry of the resulting complex and intracellular protein activities were significantly influenced by the connectivity. This approach demonstrates the importance of a key structural component of polymeric carriers required for highly efficient functional intracellular protein delivery.

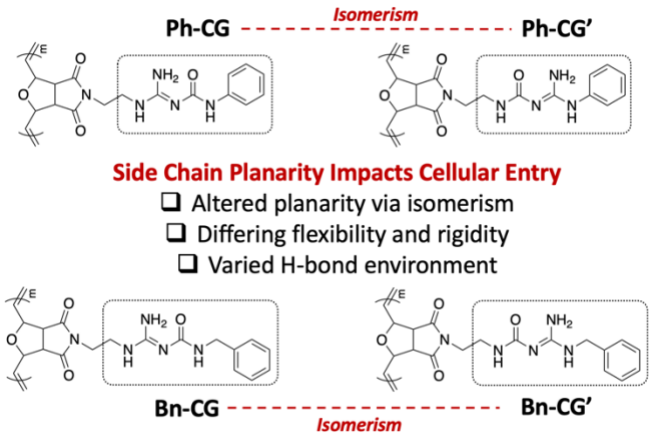

Figure 3.1. Chemical structure of polymers. Ph: Phenyl, Bn: Benzyl, CG: Carbamoylated Guanidine. Isomers are denoted with a prime (i.e., ') for simplicity.

Previously reported polynorbornes (PNs)-containing Ph-CG and Bn-CG, respectively, were used to study the effects of the functional group isomerism. In the case of Ph-CG' and Bn-CG', the respective monomers were prepared and polymerized (Scheme 3.1), leading to the pairs of constitutional isomers (Figure 3.1).

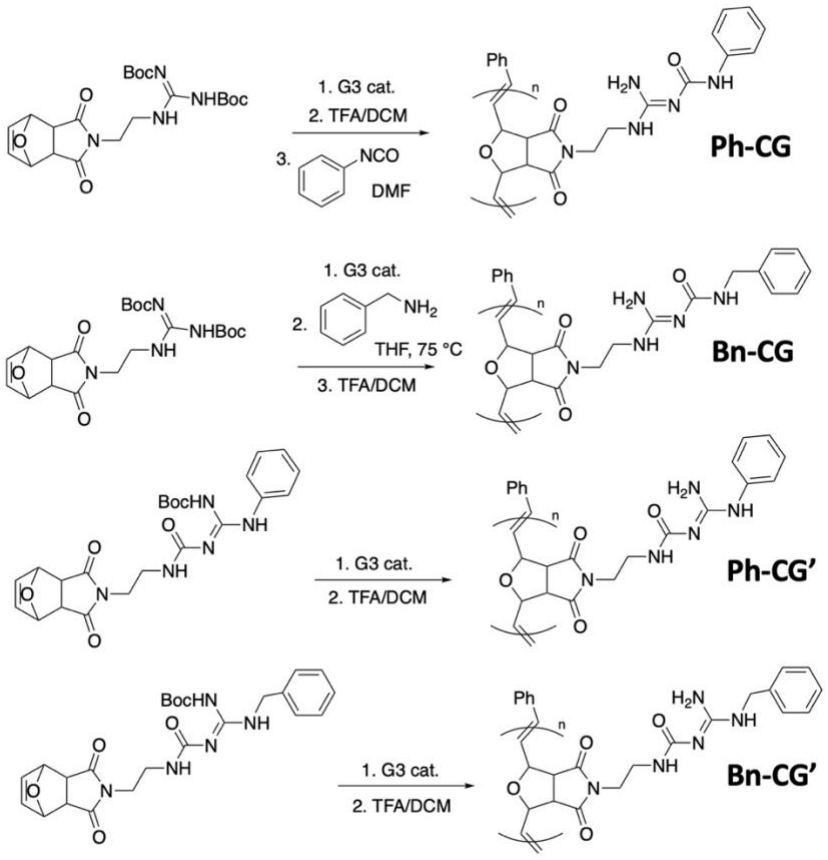

Scheme 3.1. General synthesis of carbamoylated polymers (Ph-CG, Bn-CG, Ph-CG', Bn-CG').

Molecular dynamics simulations were performed to investigate the flexibility and planarity of the isomeric functional groups in the side chains. The dihedral angles ϕ and ψ, as defined in Figure 3.2, were calculated. The dynamics of the bonds are given by the fluctuations in the measured dihedral angles as a function of the simulation time. As shown in Figure 3.3, Ph-CG shows high rotational flexibility along the sp^2 C-N bond, whereas the dihedrals of Ph-CG' are much more restricted and show less rotational flexibility. Although there is fast rotation, the Ph group in Ph-CG is mostly populated in conformations at the combinations of ϕ and ψ in the range of (0, ±180) and (±180, ±180), indicating higher planarity of Ph-CG. In contrast, the combinations of ϕ and ψ for Ph-CG' are close to ±90

and ±90, respectively, indicating the phenyl group is perpendicular (i.e., bent) to guanidine. It has been reported that the steric hindrance arising between the aryl and amine protons in Ph-CG' leads to a non-planar conformation.[17]

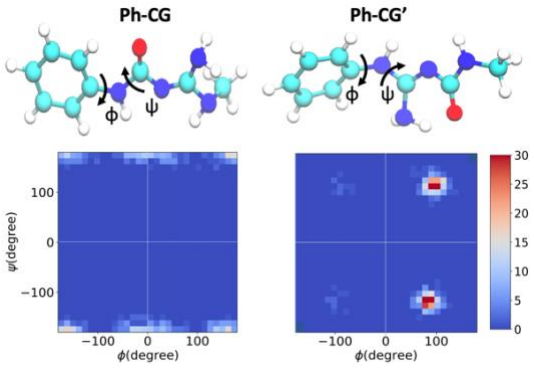

Figure 3.2. Conformational flexibility of polymer isomers. Structures of the compounds Ph-CG and Ph-CG' showing the dihedral angles (ϕ and ψ) and 2D histograms of the dihedral angles ϕ and ψ of the compounds. The color bar shows the frequency (%) of structures that occur during the simulation.

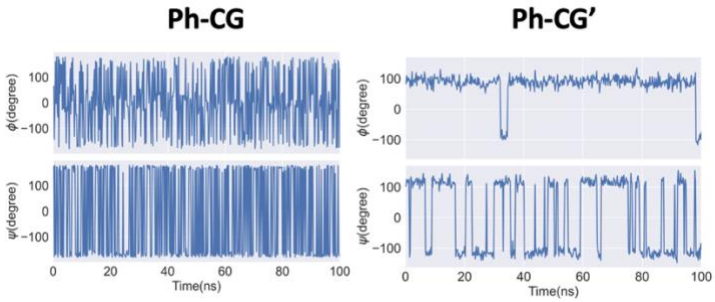

Figure 3.3. Fluctuations in dihedral angles ϕ and ψ as a function of simulation time.

Complexation with cargo proteins was achieved by mixing a PN solution in water containing a low percentage of dimethylsulfoxide (DMSO) and corresponding protein with different sizes and isoelectric points (pIs) in phosphate-buffered saline (PBS). Despite the broad size differences in proteins, all polymer-protein complexes exhibit similar hydrodynamic diameters (HDs) and zeta potentials (ζ), except Bn-CG showing relatively small HD (Table 3.1, Table 3.2, and Figure 3.4).

Table 3.1. Summary of physical characterization of PNs and PN/R-PE complexes.

PNs	M_n[a]	M_w[a]	pK_a[a]	HD[b]	ζ[c]	K_d[d]
Ph-CG	5.5	5.9	6.1	194 ± 49	-10.2 ± 0.8	219 ± 42
Bn-CG	5.7	6.1	6.1	159 ± 55	-6.0 ± 2.6	234 ± 37
Ph-CG'	5.8	6.4	5.4	212 ± 55	-5.2 ± 0.3	341 ± 51
Bn-CG'	6.1	7.0	6.0	210 ± 46	-7.4 ± 3.3	143 ± 27

[a] Molecular weights (M_n and M_w, kDa) and acidity constant (pK_a) of PNs. [b] Hydrodynamic diameters (HD, nm) of PN/R-PE complexes (10 µM/10 µg/mL). Values represent mean ± standard deviation of the arithmetic values calculated for all nanoparticles recorded by the NTA software. [c] Zeta potentials (mV) of PN/R-PE complexes in DPBS (345 µM NaCl), where R-PE is 0.625 µg/mL). [d] Dissociation constant (K_d, nM) of PN/R-PE complexes.

Table 3.2. Summary of hydrodynamic diameters (HD) for PN/protein complexes analyzed by NTA.

	Hydrodynamic diameter HD (nm)			
	BSA	**IgG**	**R-PE**	**β-Gal**
Ph-CG	215 ± 65	214 ± 60	194 ± 49	198 ± 43
Bn-CG	164 ± 49	238 ± 72	159 ± 55	173 ± 47
Ph-CG'	212 ± 80	223 ± 57	212 ± 55	169 ± 40
Bn-CG'	176 ± 40	260 ± 73	210 ± 46	291 ± 93

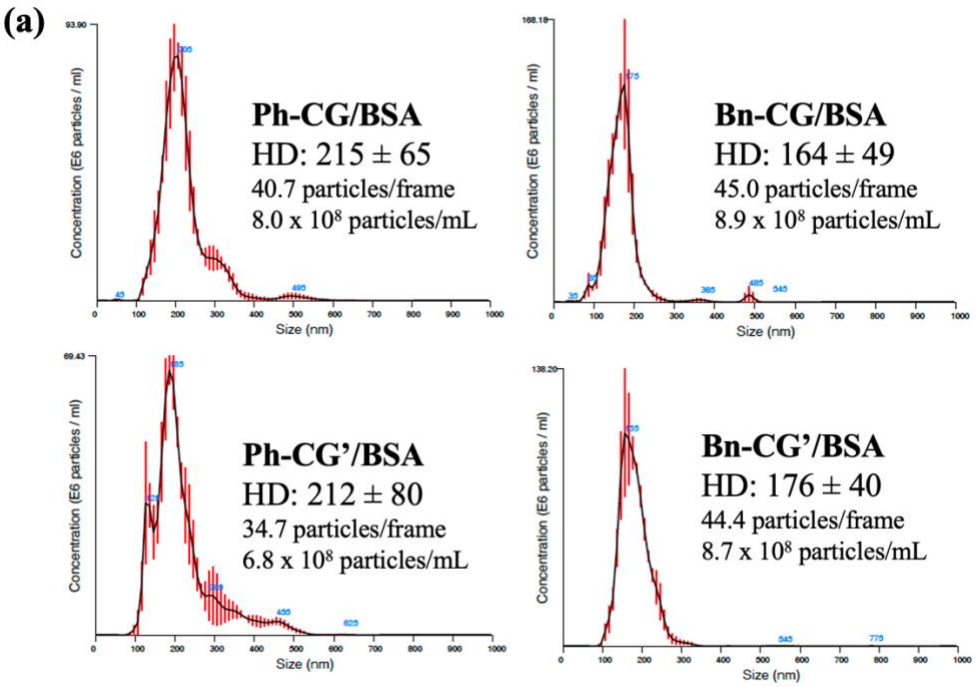

(b)

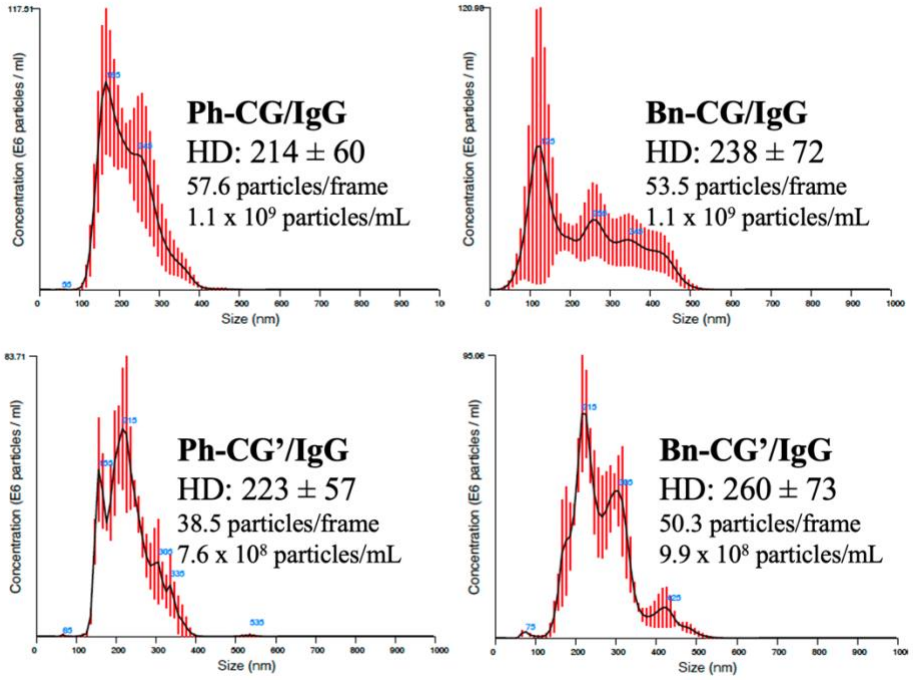
Concentration (E6 particles / ml)
Size (nm)
Ph-CG/IgG
HD: 214 ± 60
57.6 particles/frame
1.1 x 10⁹ particles/mL
Bn-CG/IgG
HD: 238 ± 72
53.5 particles/frame
1.1 x 10⁹ particles/mL
Ph-CG'/IgG
HD: 223 ± 57
38.5 particles/frame
7.6 x 10⁸ particles/mL
Bn-CG'/IgG
HD: 260 ± 73
50.3 particles/frame
9.9 x 10⁸ particles/mL

(c)

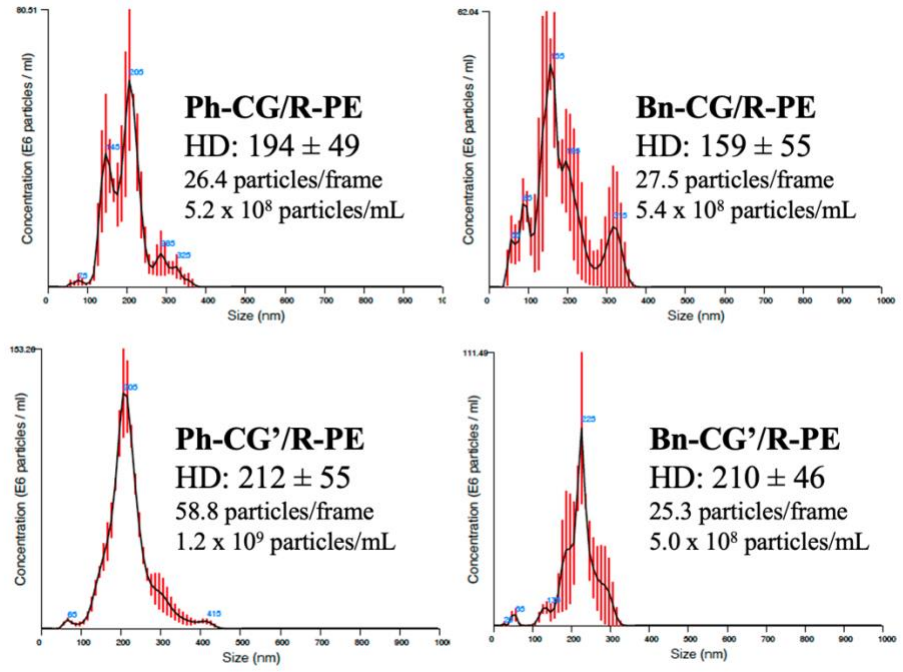
Concentration (E6 particles / ml)
Size (nm)
Ph-CG/R-PE
HD: 194 ± 49
26.4 particles/frame
5.2 x 10⁸ particles/mL
Bn-CG/R-PE
HD: 159 ± 55
27.5 particles/frame
5.4 x 10⁸ particles/mL
Ph-CG'/R-PE
HD: 212 ± 55
58.8 particles/frame
1.2 x 10⁹ particles/mL
Bn-CG'/R-PE
HD: 210 ± 46
25.3 particles/frame
5.0 x 10⁸ particles/mL

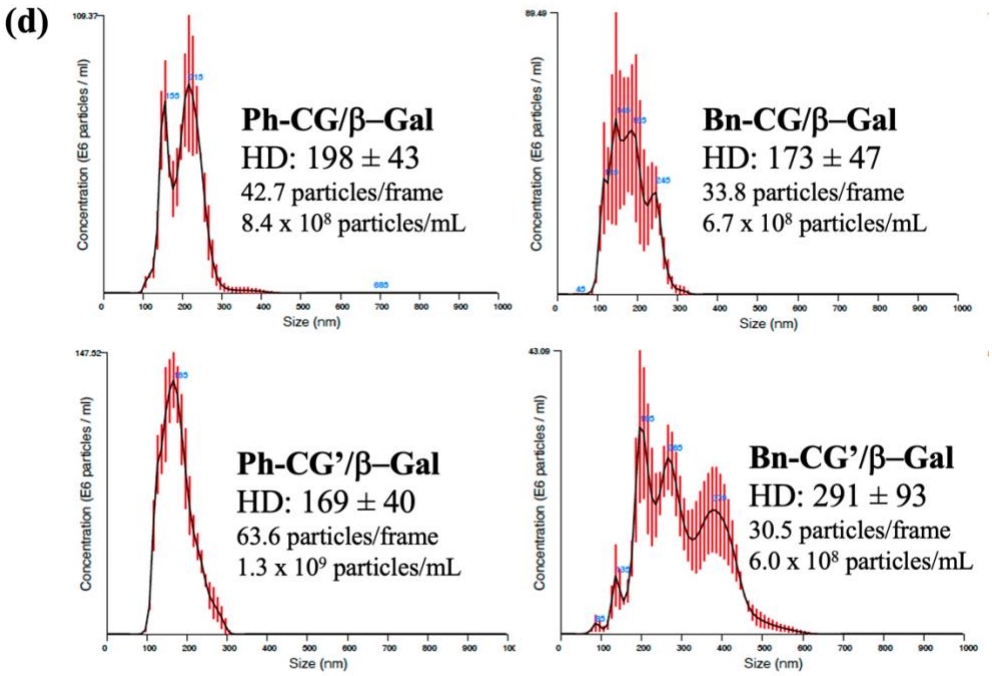

Figure 3.4. HD plots for PN/protein complexes for BSA (a), IgG (b), R-PE (c), and β-Gal (d), demonstrating the formation of relatively monodisperse nanoparticles after complexation.

Similarly, the pK_a values of the isomeric functional groups were measured to be between 5.4 and 6.1. Notably, Ph-CG' exhibited a lower pK_a of 5.4, presumably due to the resonance contribution of the adjacent phenyl ring next to the protonatable group. Acylation in guanidine has been reported and used to tune the pK_a of guanidine-containing small molecules.[18,19] Through conjugation of the electron-withdrawing acyl group, the pKa of acyl guanidine was reported to be ~8.[19] Previously, we also reported that the carbamoylation of guanidine led to a sharp pK_a decrease in guanidine.[16] All CG-containing PNs exhibit a charge-neutral state in the physiological environment. Despite the lack of positive charge, synergistic HB and hydrophobic interactions have been reported as the major driving forces for non-ionic protein complexation.[10,20–22] With the increased number of HB donors, the hydrophobic aromatic group introduced at the close vicinity of CG is

believed to favorably contribute to stable complex formation. Calculation of K_d for PN/protein complexes indicates that the binding affinity of PNs to fluorescent proteins (FPs) with different sizes is in a nanomolar concentration range (Table 3.1, Figure 3.5, and Table 3.3).

Table 3.3. Summary of dissociation constants (K_d) for PN/protein complexes

	Dissociation Constant K_d (nM)		
	BSA	**IgG**	**R-PE**
Ph-CG	276 ± 51	352 ± 52	219 ± 42
Bn-CG	417 ± 44	733 ± 81	234 ± 37
Ph-CG'	695 ± 104	312 ± 55	341 ± 51
Bn-CG'	801 ± 106	454 ± 71	143 ± 27

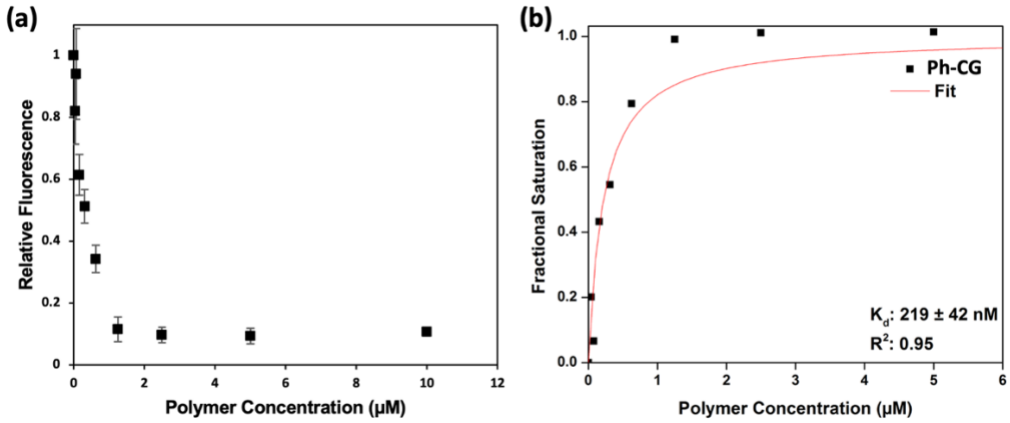

Figure 3.5. Representative example of relative fluorescence of free R-PE (a) and fractional saturation (b) at various concentrations of Ph-CG. Data shown represents the mean of three independent experiments ± standard deviation.

The protein loading efficiency in the complex was estimated by measuring the amounts of free FPs in the supernatant after centrifugation of complexes. Regardless of the protein sizes, all PNs show similar high protein loading efficiency at the concentration used for cellular delivery (i.e., above 2.5 mM) (Figure 3.6). Lastly, the complex stability in PBS containing 10% fetal bovine serum (FBS) was also very similar among the isomers (Figure

3.7). Overall, all the HDs, ζ, protein loading efficiency, K_d, and complex serum stability data indicate that the protein complexation behaviors of CG-containing PNs, regardless of the isomerism and planarity, are similar due to the CG group enhancing the inter-macromolecular interactions. All PNs exhibit no cell viability inhibition on HeLa cells at the concentrations tested (Figure 3.8).

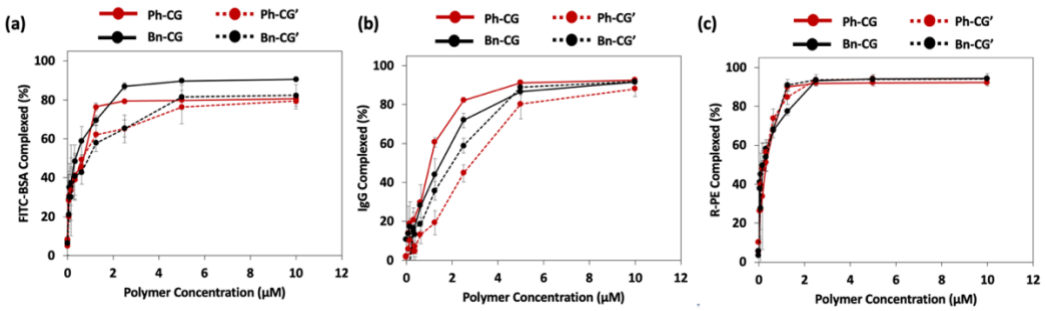

Figure 3.6. Complexation ratio of FITC-BSA (a), FITC-IgG (b), and R-PE (c) at various concentrations of PNs. Data shown represents the mean of three independent experiments ± standard deviation.

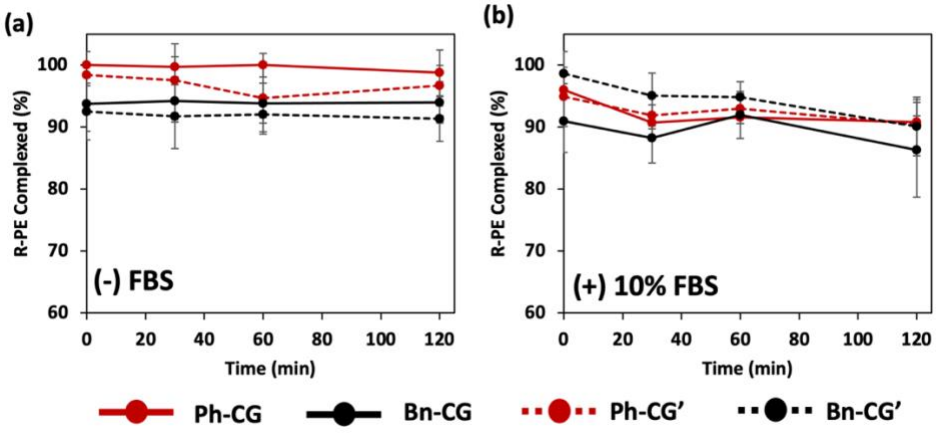

Figure 3.7. Stability of PN/R-PE complexes in PBS (a) and PBS containing 10% FBS (b). Data represents the mean of three independent experiments +/- standard deviation.

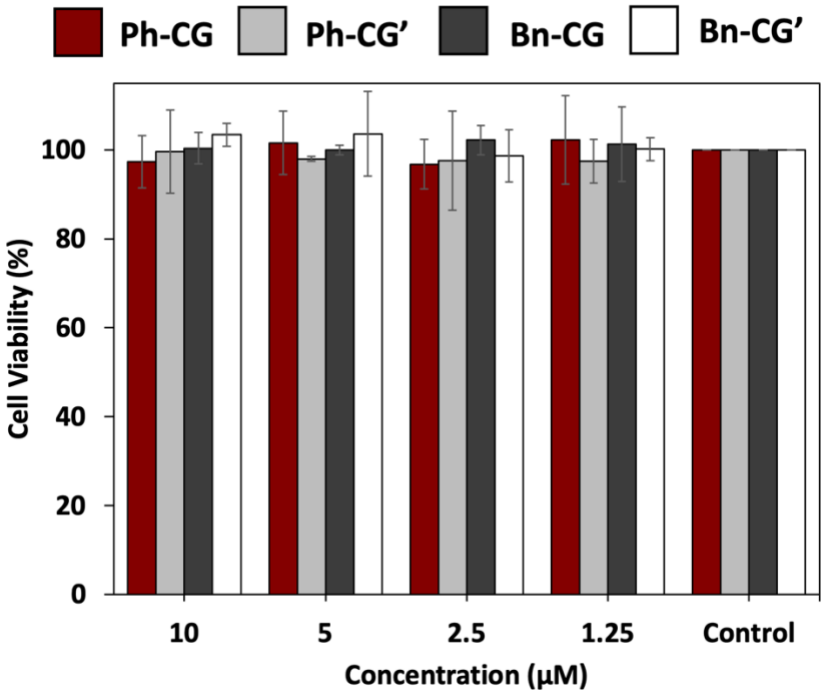

Figure 3.8. Cell viability assay of PNs. Data represents mean of three independent experiments ± standard deviation.

While the physical properties of the complexes are similar, the cellular protein delivery efficiency of PNs, measured by flow cytometry, is quite different. The mean fluorescent intensity (MFI) of HeLa cells treated with PN/R-PE complex formed at various PN to R-PE ratios was monitored to study the optimum formulation yielding the highest intracellular R-PE concentration (Figure 3.9). R-PE is a red fluorescent protein isolated from red algae and used as a model protein for cellular delivery. The membrane adsorbed R-PE fluorescence signals were quenched by treating with trypan blue (TB) (see below discussion without TB treatment). As shown in Figure 3.10, Ph-CG has a higher MFI (i.e., four folds) and percent R-PE positive cells than Ph-CG', its constitutional isomer. Considering the similar complex size, serum stability, and loading efficiency, the differences observed can be attributed to different cellular entry abilities of the complex,

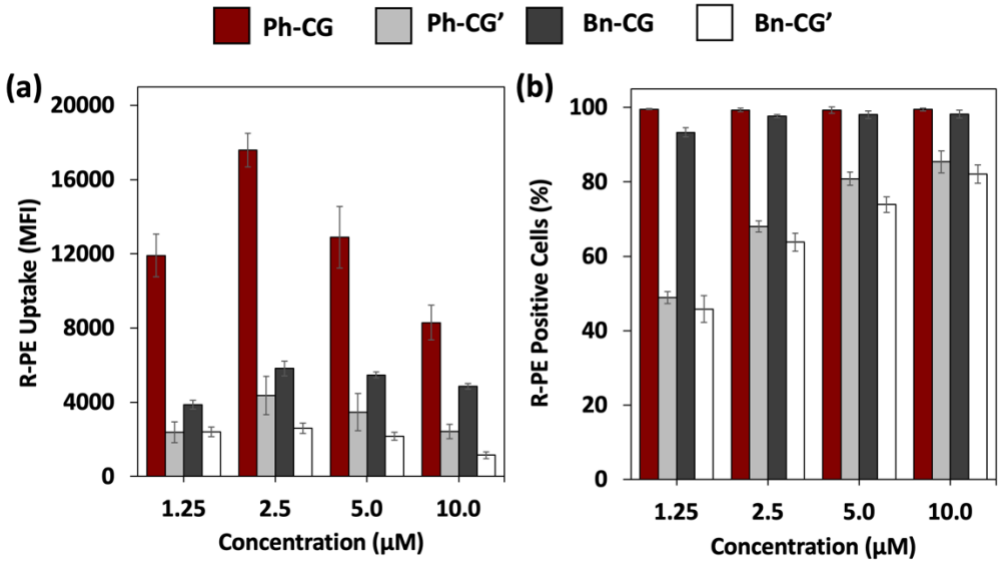

Figure 3.9. Median fluorescence intensity (a) and percent R-PE positive (b) of HeLa cells treated with PN/R-PE complexes for 18 h at various concentration of PNs. The concentration of R-PE was fixed at 0.5 μg/mL. Extracellular fluorescence was quenched with the addition of TB. Data shown is the mean of three independent experiments ± standard deviation.

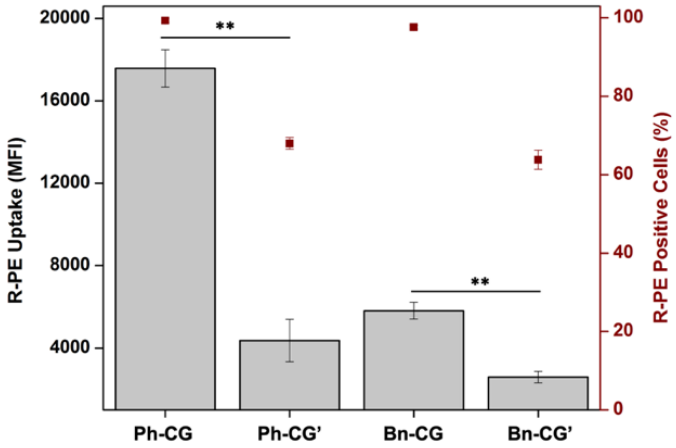

Figure 3.10. MFI and percent positive cells of HeLa cells treated with PN/R-PE complexes for 18 h. The concentrations of polymer and R-PE were 2.5 μM and 0.5 μg/mL, respectively. Membrane adsorbed R-PE signal was quenched with TB. Data shown are the mean of three independent experiments ± standard deviation. ** $p<0.01$.

presumably due to the planarity of Ph-CG. The non-planar and bent conformation of Ph-CG' could be tied with the decreased cellular interactions and/or internalization, resulting in low protein delivery ability. A similar trend was also observed between Bn-CG and Bn-

CG', in which Bn-CG shows a 2-fold higher MFI than Bn-CG'. From the different cellular delivery efficiencies between Bn-CG and Bn-CG', in which both functional groups have no coplanarity with the Bn group due to the free-rotating methylene spacers, the isomeric relationship of Bn-CG and Bn-CG' also influences cellular delivery. The concentrations of internalized proteins were gradually increased as the incubation time increased (Figure 3.11), and similar delivery efficiency of R-PE to different cell types was also observed (Figure 3.12).

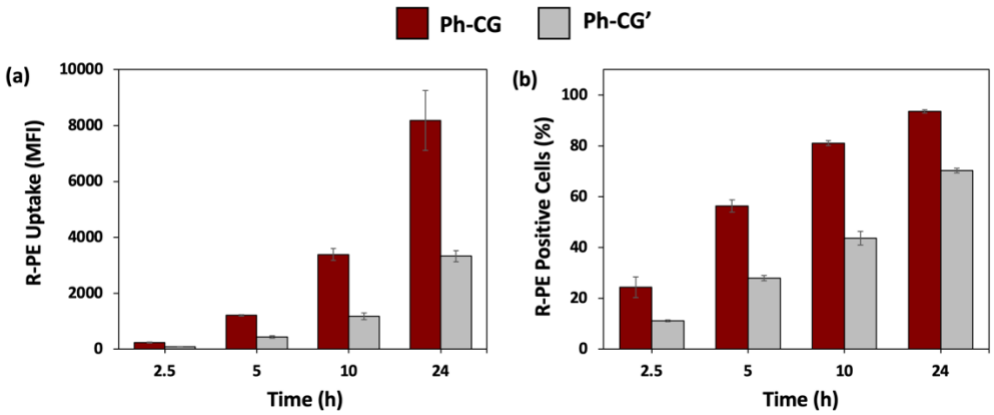

Figure 3.11. Median fluorescence intensity (a) and percent R-PE positive (b) of HeLa cells treated with PN/R-PE complexes for various time frames. The concentration of PNs and R-PE were 5.0 μM and 0.5 μg/mL, respectively. Extracellular fluorescence was quenched with the addition of TB. Data shown is the mean of three independent experiments ± standard deviation.

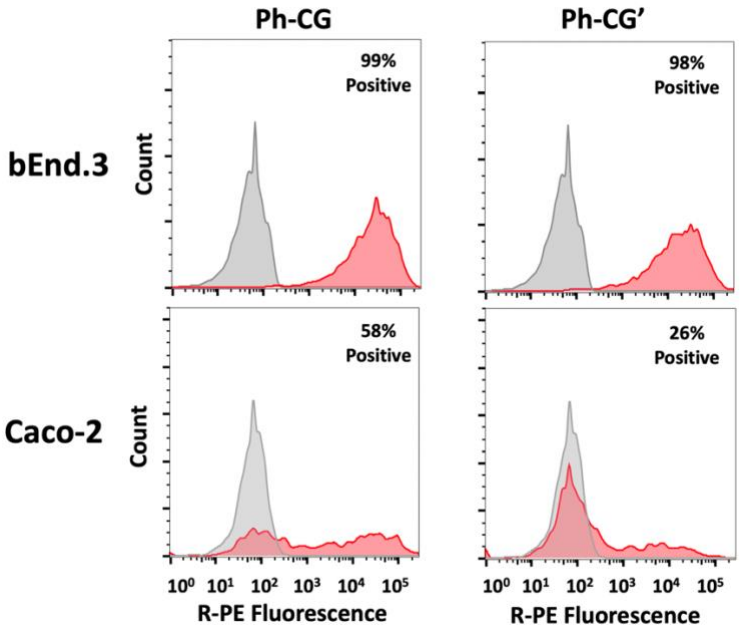

Figure 3.12. Flow cytometry histograms of Ph-CG and Ph-CG' mediated delivery of R-PE to bEnd.3 and Caco-2 cells after overnight incubation. The concentration of polymer and R-PE were 5.0 μM and 0.5 μg/mL, respectively.

Considering the similar physical properties of complex, the substantial differences in the R-PE internalization efficacy are pretty interesting. To examine the degree of internalized protein and protein adsorbed on the membranes, the MFI of HeLa cells with and without TB treatment was measured.[20] Before the TB treatment, the complex-treated cells were thoroughly rinsed with PBS (three times) and a heparin sulfate solution. As shown in Figure 3.13, both Ph-CG and Ph-CG' demonstrate relatively similar MFI without the TB treatment at 5 mM of PNs. However, while Ph-CG only shows a ~2-fold decrease in fluorescence quenching upon TB treatment, the isomer Ph-CG' has ~5-fold decreased MFI. Assuming the similar colloidal stability of the complexes (i.e., a similar range of ζ), this observation implies that initial membrane interactions of Ph-CG/R-PE and Ph-CG' could be similar at the same complexation ratio (i.e., 5 mM PN/0.5 μg/ml R-PE) (i.e., similar fluorescent intensity before the TB treatment). However, when the fluorescent intensity from the

membrane adsorbed PN/R-PE complex was quenched, the higher internalized R-PE signals imply that Ph-CG with planarity internalizes R-PE more efficiently than non-planar Ph-CG'. Interestingly, the proportions of internalized R-PE after TB treatment were also decreased when excess amounts of PNs were used (Figure 3.13), which could be due to poor aqueous solubility of PNs causing/contributing aggregations and/or reducing the proportion of the PN/protein complex interacting the cell membranes, implying that there might be an optimum PN concentration needed for facilitating the internalization process.

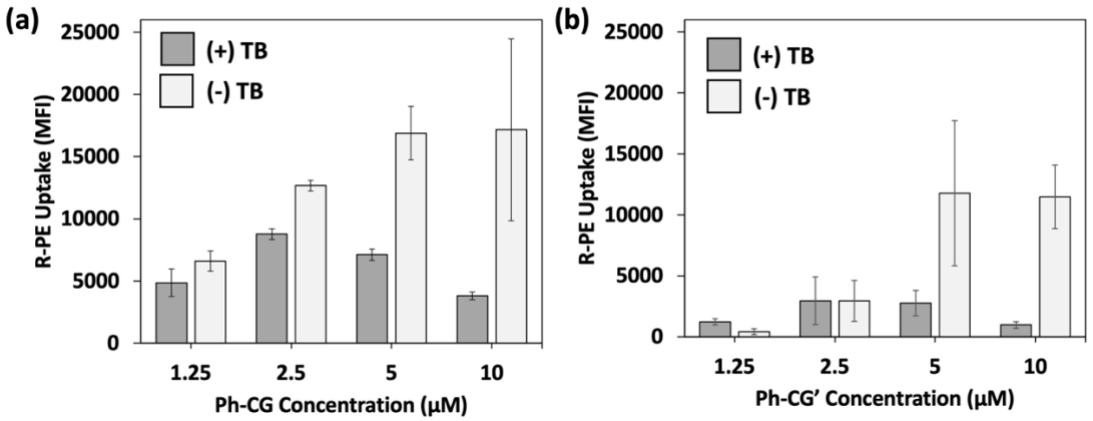

Figure 3.13. Median fluorescence intensity of HeLa cells treated with PN/R-PE complexes for 18 h with or without the addition of TB. The concentration of R-PE was fixed at 0.5 μg/mL. Data shown is the mean of three independent experiments ± standard deviation.

Cellular entry pathway studies demonstrate that the internalization of R-PE by both Ph-CG and Ph-CG' primarily occurs via energy-dependent pathways, as the treatment at 4 °C and ATP-depleted conditions significantly decrease the uptakes. Pretreatment with various chemical endocytosis inhibitors implies that macropinocytosis is the primary entry pathway along with other pathways. There are negligible differences in the inhibition pattern between both isomeric carriers (Figure 3.14). As revealed by the confocal images in Figure 3.15, FITC-BSA delivered by Ph-CG is dispersed inside the cell, within the boundaries of the membrane stained with Actin Red, while Ph-CG' exhibits almost no

green signals under the same incubation condition. To determine whether FITC-BSA delivered by Ph-CG and Ph-CG', respectively, is located in the endosome/lysosome, a counter-staining was done with Lysotracker Red, and Pearson's correlation coefficient (PCC) scorning was conducted to quantitatively analyze the overlap between two colors. As seen in Figure 3.16, PCC values of 0.356 and 0.128 were found for Ph-CG and Ph-CG', respectively. The higher PCC value for Ph-CG is likely due to significantly higher green signals from the delivered FITC-BSA than Ph-CG', and not necessarily due to higher endosomal entrapment.

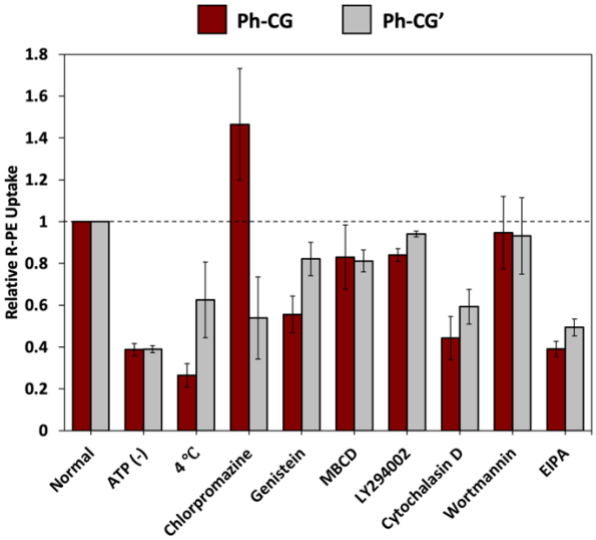

Figure 3.14. Relative median fluorescence intensity of HeLa cells in energy-independent conditions (ATP depletion and 4 ℃) or pre-treated with various pharmacological endocytosis inhibitors followed by incubation with Ph-CG and Ph-CG'/R-PE complex for 1 h. The concentration of polymer and R-PE were 20 μM and 16 nM, respectively. Data shown is the mean of three independent experiments +/- standard deviation.

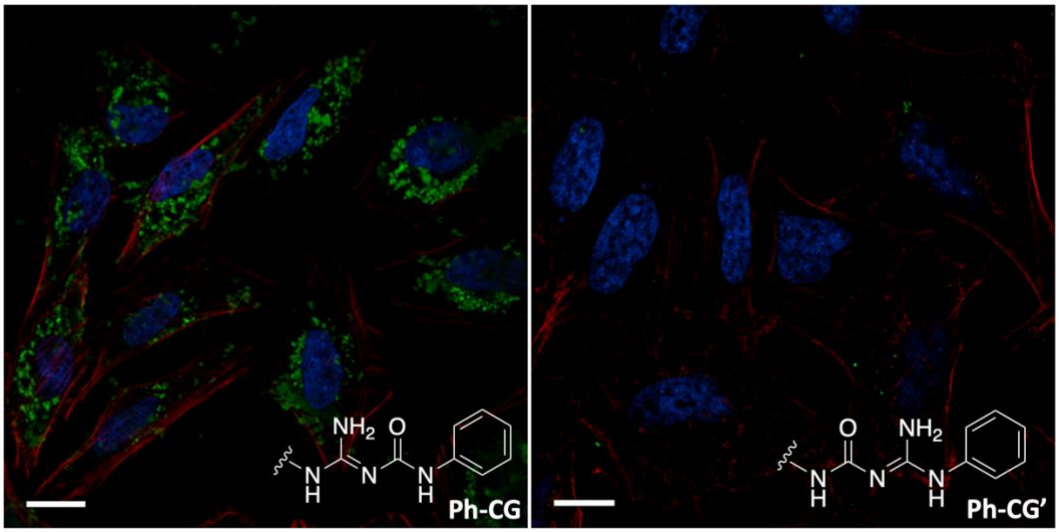

Figure 3.15. Confocal microscope images of HeLa cells incubated with Ph-CG and Ph-CG'/R-PE. Concentrations of PN and FITC-BSA were 10 µM and 40 nM, respectively. The mebrane was stained with ActinRed.

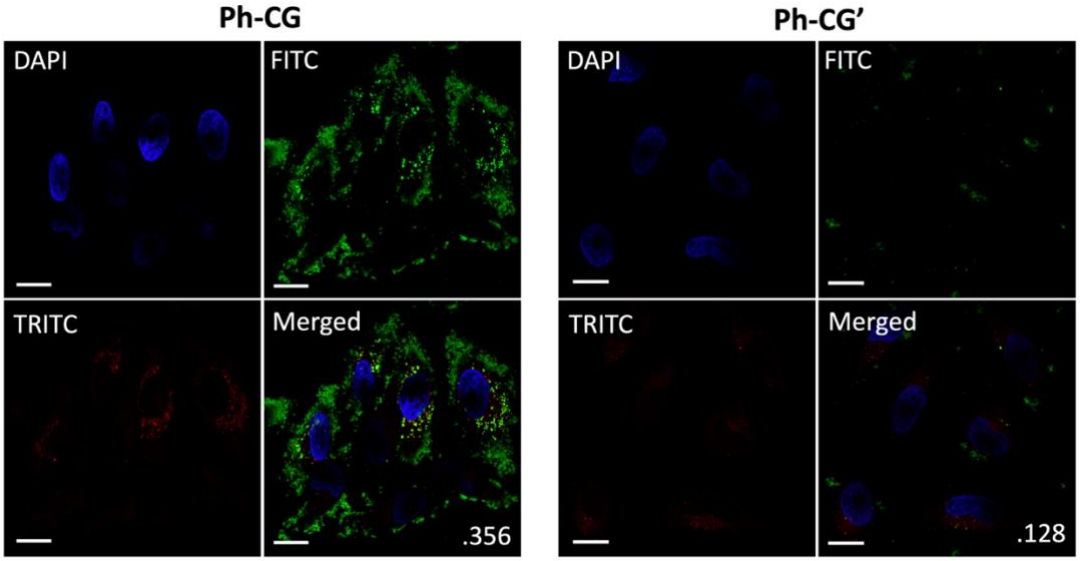

Figure 3.16. Confocal microscope images of HeLa cells incubated with Ph-CG and Ph-CG'/R-PE. Concentrations of PN and FITC-BSA were 10 µM and 40 nM, respectively. Lysotracker Red was used according to manufacturer guidelines. PCC values are given on the bottom right corner.

Maintaining the structure and function of the complexed and delivered proteins is crucial in the development of protein carriers. A large enzyme, β-Galactocidase (β-Gal), was intracellularly delivered by Ph-CG. Generation of blue color in the cells upon

treatment of the enzyme-substrate 5-bromo-4-chloro-3-indolyl β-D-galactopyranoside (X-Gal) indicates that the delivered proteins maintain their enzymatic activities.[23] As seen in Figure 3.17a, cells treated with Ph-CG/β-Gal complexes demonstrate a clear blue color compared to controls. We further tested the efficacy in functional protein delivery using an anti-apoptotic antibody, anti-pAkt. Protein kinase B (Akt) is involved in cellular survival pathways by inhibiting apoptotic processes. Therefore, blocking the pathway inhibits cell growth and proliferation.[23,24] While the cell membrane-impermeable antibody alone shows negligible cell viability inhibition, an exponential decrease in viability was observed when anti-pAkt was delivered by Ph-CG. The isomeric Ph-CG' mediated delivery also exhibits a decrease in viability but has relatively poor activity (Figure 3.17b). The cell viability inhibition results support that the delivered antibody maintains its activity and reaches its epitope in the cytosol. The functional antibody delivery also confirmed the difference in the intracellular entry efficiency between the isomeric complexes.

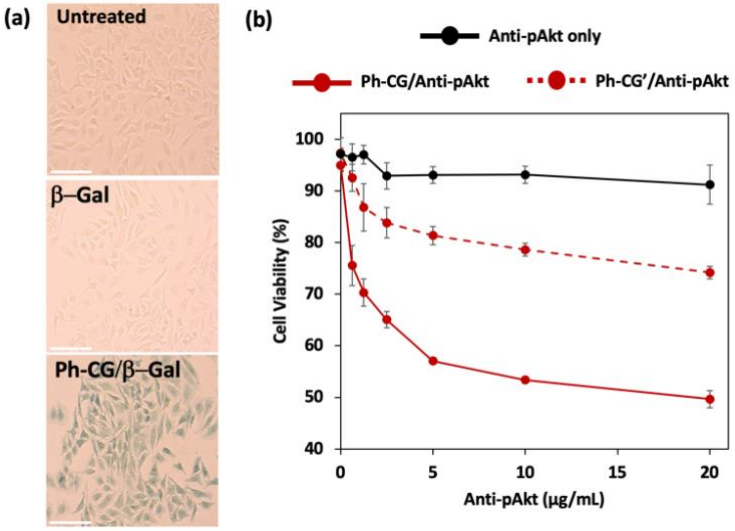

Figure 3.17. (a) X-Gal staining of treated HeLa cells. Final concentrations of Ph-CG and β-Gal were 2.5 μM and 0.5 μg/mL. Untreated cells and β-Gal alone are shown as controls. Scale bar: 150 μm (b) Viability of HeLa cells treated with PN/anti-pAkt complexes or anti-pAkt alone at various antibody concentrations. The concentration of PN was kept constant at 10 μM. Data represent the mean ± standard deviation.

3.4. Conclusion

In conclusion, we report a dramatic influence of the functional group isomerism on intracellular protein delivery. Remarkable differences were observed in terms of rigidity, planarity, and ultimately protein delivery behavior for pairs of polymers with isomeric side chains. While electrostatic, hydrogen bonding, and hydrophobic inter-macromolecular interactions are relatively similar in the tested polymers, the PN containing a planar Ph-CG moiety demonstrated significantly improved cellular entry and protein delivery ability. Overall, this work establishes the importance of rigidity, planarity, and conformation as parameters of the functional group for designing protein delivery carriers. Studying the entry efficiency and mechanism of fluorescently-labeled PN-containing different isomeric side chains should also provide useful insights into how the carriers interact with proteins and membranes. To the best of our knowledge, this is the first report on the effect of polymer side chain isomerism on protein delivery.

3.5. Experimental and Supporting Information

3.5.1. Physical Characterization of PNs and PN/Protein Complexes

Molecular Weight Determination - Aliquots of polymer solutions in tetrahydrofuran (THF) or dichloromethane (DCM) were diluted in 1 mL of HPLC-grade THF and filtered through a 0.45 μm polytetrafluoroethylene (PTFE) syringe filter prior to injection.

Molecular Dynamic Simulations - The structures of the Ph-CG and Ph-CG' polymers were generated from the ligand reader interface of the CHARMM-GUI.[25] Simulation systems were prepared for the four compounds using the Solution Builder plugin of the CHARMM-GUI.[26] The compounds were solvated in TIP3 water and 150 mM of KCl.[27] A GPU version of NAMD 2.14 was used to perform all-atom molecular dynamics (MD) simulations with

CHARMM36 force field at 303.15 K temperature.[28] The systems were minimized for 10,000 steps, followed by 0.25 ns equilibration with position restraints. Finally, 100 ns unconstrained production run was performed with a timestep of 2 fs for each system. The covalent bonds involving hydrogen atoms were restrained with SHAKE algorithm and the long-range electrostatic interactions were treated with particle mesh Ewald method. Temperature was controlled by Langevin temperature coupling with 1 ps of friction coefficient and the pressure was controlled by Langevin piston. The visualization and data analysis were performed using VMD.1.9.3.

Measurement of Hydrodynamic Diameters and Zeta Potential - Nanoparticle tracking analysis (NTA) was used to determine the hydrodynamic diameter (HD) of PN/protein complexes. Briefly, PN stock solutions were prepared by dissolving dried PN powders in DMSO and diluting to final concentrations of 1 mM in DMSO. Adequate volmes of PN stock solutions were diluted in water (20% v/v) and mixed with equal volumes of BSA solution for a final complex volume of 100 μL. Complexes were incubated for 30 min at room temperature before a ten-fold dilution in PBS to a final volume of 1 mL (final PN/protein concentration was 10 μM and 10 μg/mL, respectively). 1 mL of this solution was then injected into the NTA chamber and videos of the scattering particles was recorded for 30 seconds. The software identified each individual particle and tracked its motion, relating the particle displacement as a function of Brownian motion, which relates to the particle size through the Stokes-Einstein equation. The concentrations of samples were chosen to meet the manufacturers' recommendation of 20-100 particles per frame and a concentration of 10^7-10^9 particles/mL. All measurements were performed in triplicate at 25 °C. HD plots are listed below for PN/BSA complexes, demonstrating the formation of

monodisperse nanoparticles. Values given are the mean HD of three readings +/- mean standard deviation (SD). In this study, SD is defined as the arithmetic value calculated with the sizes of all of the particles analyzed by the software. Zeta Potential was acquired by preparing samples in the same way as for NTA prior to analysis.

3.5.2. pKa Determination

pKa was determined for the different PNs using previously described methods.[16] Briefly, a 2 mM polymer solution in 1 mL of acidified (pH ~3) 100 mM NaCl solution was preared and titrated from pH ~3 to 11 with 5 μL increments of a 25 mM KOH solution. For the titration, the pH was determined using a Mettler Toledo InLab Ultra-Micro pH Probe. pKa value for each polymer was determined by plotting the ΔpH/volume of KOH and identifying the largest ΔpH. For polymers with two maxima, the volume of the median point between the two maxima was chosen as the point where pH = pKa.

3.5.3. Complexation Ratio

The loading ratio of various FPs (FITC-BSA, FITC-IgG, and R-PE) was determined by measuring the fluorescence of non-complexed FPs in centrifuged complexes. PN stock solutions were prepared by dissolving dried PN powders in DMSO and diluting to final concentrations of 1 mM in DMSO. 1 mM stock solutions were serially diluted in DMSO to a final concentration of 3.91 μM. Adequate volumes of each PN stock solution was diluted in water (20% v/v) and mixed with equal volumes of FP solution for a final complex volume of 50 μL. Complexes were incubated for 30 min at room temperature before a ten-fold dilution in PBS to a final volume of 500 μL (final concentration of BSA, IgG, and R-PE was 0.5 μg/mL, 5.0 μg/mL and 0.5 μg/mL, respectively). The final concentration of PNs ranged from 10 μM to 0 μM. The solutions were centrifuged at 22,000 x g for 10 min.

The supernatant was collected in a cuvette and the fluorescence intensity of FPs in the supernatant was measured at their emission λ_{max}. The amount of FP in supernatant was calculated according to the standard curve of FP in the same solvent composition.

3.5.4. Dissociation Constant Determination

PN stock solutions were prepared by dissolving dried PN powders in DMSO and diluting to final concentrations of 1 mM in DMSO. 1 mM stock solutions were serially diluted in DMSO to a final concentration of 3.91 μM. Adequate volumes of each PN stock solution was diluted in water (20% v/v) and mixed with equal volumes of FP solution for a final complex volume of 50 μL. Complexes were incubated for 30 min at room temperature before a ten-fold dilution in PBS to a final volume of 500 μL (final concentration of BSA, IgG, and R-PE was 0.5 μg/mL, 5.0 μg/mL and 0.5 μg/mL, respectively). Final concentration of PNs ranged from 10 μM to 0 μM. The solutions were centrifuged at 22,000 x g for 10 min. The supernatant was collected in a cuvette and the fluorescence intensity of FPs in the supernatant was measured at their emission λ_{max}. The fluorescence intensity of each supernatant solution was related to 0 μM of PN yielding relative fluorescence curves. The relative fluorescence plots were converted to fractional saturation plots using equation 1 below:

$$Fractional\ Saturation\ (y) = \frac{F_P - F_0}{F_{sat} - F_0} \qquad (1)$$

where F_0, F_P, and F_{sat} were the relative emission intensities of FP only, free FP in supernatant at the various concentrations tested, and free FP at saturation. The dissociation constant was determined by equation 2 below:

$$y = \frac{(P + c + K_d) - \sqrt{(P + c + K_d)^2 - 4Pc}}{4c} \qquad (2)$$

where y is the fractional saturation plot obtained with equation 1, P is the polymer concentration (x-axis) and c is the constant FP concentration. K_d was determined using the non-linear curve fitting module of Origin 8.5 and equation 2. All R^2 from fitting curves >0.91.

3.5.5. Serum Stability Assay

The stability of complexes was studied by monitoring the fluorescence of the R-PE released from complexes. PN stock solutions were prepared by dissolving dried PN powders in DMSO and diluting to final concentrations of 1 mM in DMSO. Adequate volumes of PN stock solutions were diluted in water (20% v/v) and mixed with equal volumes of R-PE solution for a final complex volume of 50 μL. Complexes were incubated for 30 min at room temperature before a ten-fold dilution in PBS with 10% FBS to a final volume of 500 μL (final PN/R-PE concentration was 5 μM and 2 nM, respectively). The solutions were incubated at room temperature for the respective amounts of time before being centrifuged at 22,000 x g for 10 min. The supernatant was collected in a cuvette and the fluorescence intensity of R-PE in the supernatant was measured at 574 nm. The amount of R-PE in supernatant was calculated according to the standard curve of R-PE in the same solvent composition.

3.5.6. Cell Culture

HeLa cells were cultured in Gibco DMEM High Glucose medium supplemented with 10% (v/v) FBS and 1% (v/v) Penicillin-Streptomycin mixture.

3.5.7. Protein Delivery Experiments

Flow Cytometry Analysis - Hela cells were seeded into 12 well plates (~100,000/well) in complete media and allowed to attach for one day at 37 °C under a humidified atmosphere of 5% CO_2 prior to sample treatment. R-PE stock solution was diluted to working concentration with 1X PBS. Polymer stock solutions were prepared at 1 mM in DMSO. 40 μL of polymer/protein complexes were prepared by mixing appropriate volumes of polymer and protein sub-stock solutions and incubating for 30 min at room temperature in the dark. Complexes were added dropwise to each well to the cells in complete media and incubated for varying periods of time, depending on the experiment. After the incubation periods required, adherent cells were rinsed three times with full volumes of PBS, followed by washing with 1 μM heparan sulfate solution to remove any extracellular surface-bound complexes.[9,29] The cells were harvested with TrypLE, transferred to centrifuge tubes, rinsed an additional three times with PBS and once with a 0.1% Trypan Blue solution before being finally resuspended in 300 μL of PBS. Cells were analyzed by flow cytometry, in which data for 10,000 events were collected.

Internalization of PN/R-PE Complexes - In order to study the internalization or adsorption of PN/R-PE on the cellular membrane, flow cytometry analysis was done with or without the addition of trypan blue.

3.5.8. Cellular Entry Pathway

In order to study the mechanism of uptake, HeLa cells were treated with Ph-CG and Ph-CG'/R-PE complexes (10 μM/2 nM) for 1 h under energy-independent conditions or under pre-treatment with various pharmacological inhibitors. Briefly, HeLa cells were seeded the day prior to sample treatment in 12-well plates (100,000/well). The day of experiment,

cells were equilibrated for 30 minutes under 4 °C, ATP depletion conditions (NaN_3: 10 mM & 2-deoxyglucose: 50 mM), chlorpromazine (28 μM), LYS 294003 (3 μM), Cytochalasin D (10 μM), methyl-B-cyclodextrin (1 mM), wortmannin (500 nM), EIPA (100 μM) and genistein (200 μM) or normal culture conditions. Complexes were added dropwise, and cells were incubated for 1 h prior to analysis via flow cytometry as described previously.[16]

3.5.9. Confocal Imaging

Hela cells were seeded on 12-well plates (~60,000/well) containing glass coverslips one day before sample treatment. Complexes were prepared as described previously. After incubation for varying periods of time using the same culture conditions discussed earlier, the medium was removed, and cells were washed three times with PBS and once with heparan sulfate. Cells were fixed with 4% PFA for 10 minutes and rinsed once with PBS. Nuclei were stained with Hoechst 33342 at a final concentration of 1 μg/mL for 7 minutes. For cells with Lysotracker Red and ActinRed staining, the manufacturers' protocol was followed. The coverslips were mounted on microscope slides using 1:1 glycerol/PBS mounting medium.

3.5.10. Functional Protein Delivery

Anti-pAkt Delivery - MTT (methylthiazole tetrazolium) assay was performed with PN/protein complexes are described previously.[16] HeLa cells were seeded in a 96-well plate (~10,000/well) in 200 μL of complete medium and allowed to attach for one day at 37 °C under a humidified atmosphere of 5% CO_2 prior to sample treatment. Serial dilutions of anti-pAkt were prepared and complexed with various PNs. Complexes or anti-pAkt alone were added to HeLa cells (final concentration of anti-pAkt of 20, 10, 5, 2.5, 1.25,

0.625, and 0 μg/mL) and incubated for 48 h prior to MTT treatment. 10 μL of MTT solution (5 mg/mL in PBS) was added and incubated for 4 h at 37 °C. After incubation, 200 μL of medium was gently removed and 100 μL of biological grade DMSO was added to solubilize the purple formazan crystals. Absorbance was measured using a microwell plate reader. Cell viability was determined as a function of the absorbance of each sample relative to control wells. All measurements represent the average of three measurements ± standard deviation.

Intracellular β-Gal Delivery - Intracellular β-Gal activity was visualized with X-Gal staining. HeLa cells were seeded in a 12-well plate (~40,000/well) in 800 μL of complete medium and allowed to attach for one day at 37 °C under a humidified atmosphere of 5% CO_2 prior to sample treatment. Dilutions of β-Galactosidase were prepared and complexed with Ph-CG for 30 min prior to addition to cells. Cells were incubated with complexes (2.5 μM and 0.5 μg/mL of PN and β-Gal, respectively) or β-Gal alone (0.5 μg/mL) overnight. After incubation, the medium was removed and cells were thoroughly rinsed with PBS (3x) and heparin Sulfate (1x, 1 mg/mL) and fixed with 4% PFA for 15 min. The X-Gal staining solution was prepared by dissolving X-Gal in DMSO (10 mg/mL) and making a 5% solution in PBS. 500 μL of the X-Gal staining solution was added to the fixed cells and incubated overnight at 37 °C in the absence of CO_2. The wells were rinsed thoroughly with PBS and imaged.

3.5.11. Synthesis

Monomer Synthesis -

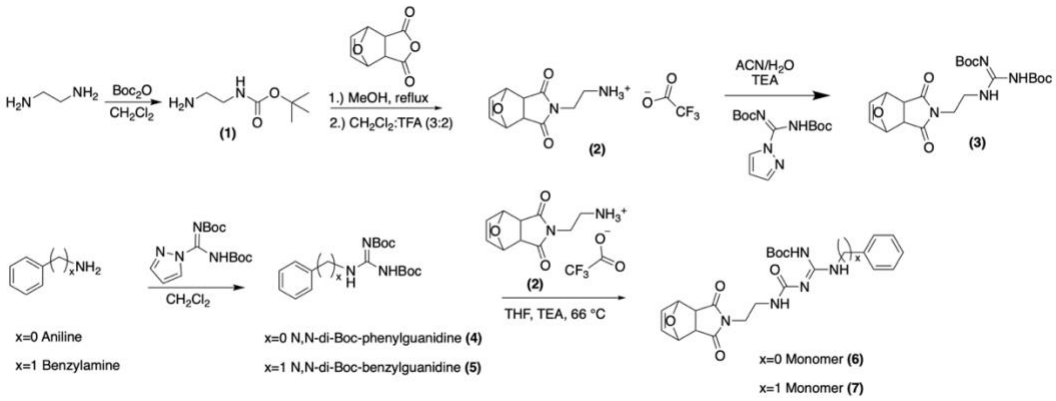

Scheme 3.2. Synthesis of monomers used for polymerization.

Synthesis of 1. To a round bottom flask containing a solution of ethylenediamine (1.0 mol, 66.6 mL) in 800 mL of methylene chloride, di-*tert*-butyl dicarbonate anhydrous (0.15 mol, 32.7 g) pre-mixed in 300 mL of methylene chloride was added dropwise over 2 hours. The reaction continued for 16 hours; then, the organic phase was washed with H_2O (2x 800 mL), brine (1x 800 mL), dried ($MgSO_4$ anhydrous), and filtered. The solvent was removed in vacuo, and a light-yellow viscous liquid was obtained.

1: Yield: 78%. ^{1}H NMR (400 MHz, $CDCl_3$): δ 5.44 (br s, 1H), 2.96 (s, 2H), 2.59 (t, 2H), 1.25 (s, 9H), 1.04 (s, 2H).

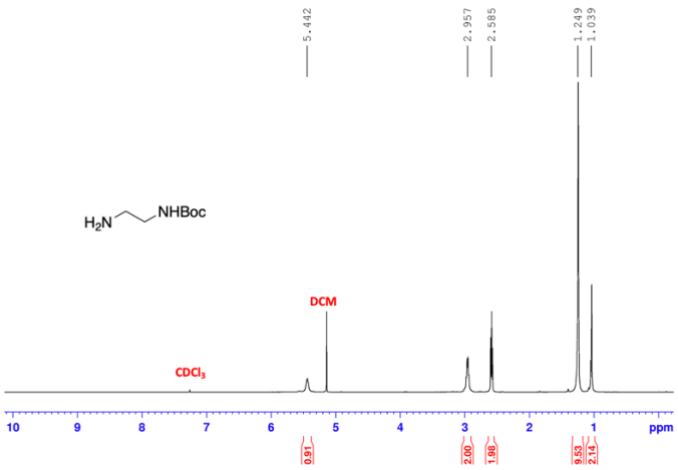

Synthesis of 2. *N*-Boc-ethylenediamine (39.2 mmol, 6.35 g) and exo-7-oxabicyclo [2.2.1] hept-5-ene-2,3-dicarboxylic anhydride (30.1 mmol, 5 g) were dissolved in 100 mL of MeOH. Then, triethylamine (72 mmol, 10 mL) was added, and the reaction mixture was stirred in reflux. The heating stopped after 20 hours, and the compound precipitated once the crude reached room temperature. The product was purified by recrystallization using methylene chloride and methanol mixture. The solid obtained was deprotected using methylene chloride: trifluoracetic acid mixture (3:2). The solvent was removed in vacuo, and the crude was purified by precipitation in ether solution yielding pure compound 2.

2 (protected): Yield: 62%. ^{1}H NMR (400MHz, $CDCl_3$): δ 6.51 (s, 2H), 5.26 (s, 2H), 4.77 (br s, 1H), 3.62 (t, 2H), 3.30 (br q, 2H), 2.85 (s, 2H), 1.41 (br s, 9H).

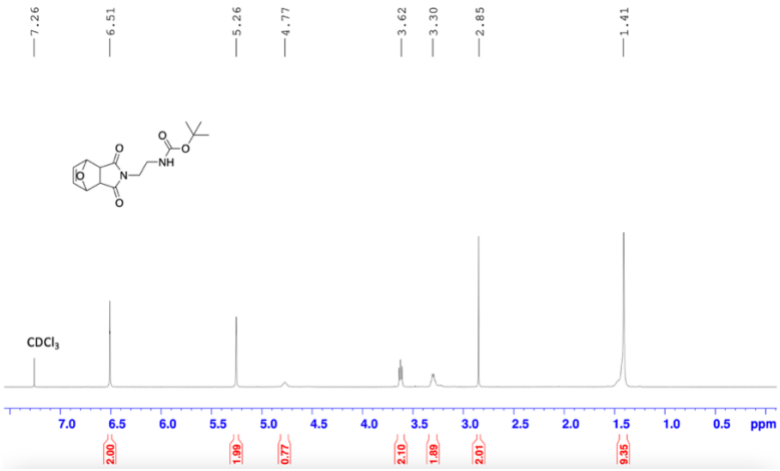

2: Yield: 59%. ^{1}H NMR (400MHz, DMSO-d_6): δ 7.91 (s, 3H), 6.58 (s, 2H), 5.14 (s, 2H), 3.61 (t, 2H), 2.96 (br s, 4H).

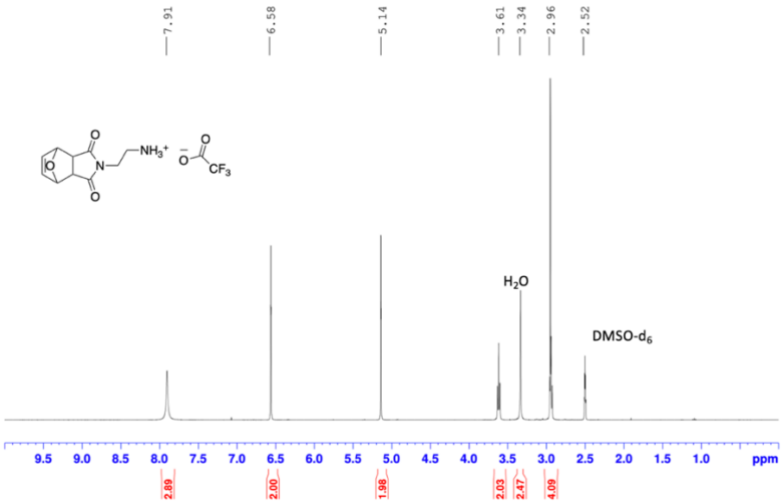

Synthesis of 3. Compound 2 was deprotected using TFA and the free amine was converted to Boc-protected guanidine using *N,N′*-Di-Boc-1*H*-pyrazole-1-carboxamidine.

3: Yield: 68%. ^{1}H NMR (400 MHz, $CDCl_3$): δ 11.40 (s, 1H), 8.39 (s, 1H), 6.48 (s, 2H), 5.23 (s, 2H), 3.67 (t, 2H), 3.60 (t, 2H), 2.84 (s, 2H), 1.44 (m, 18H).

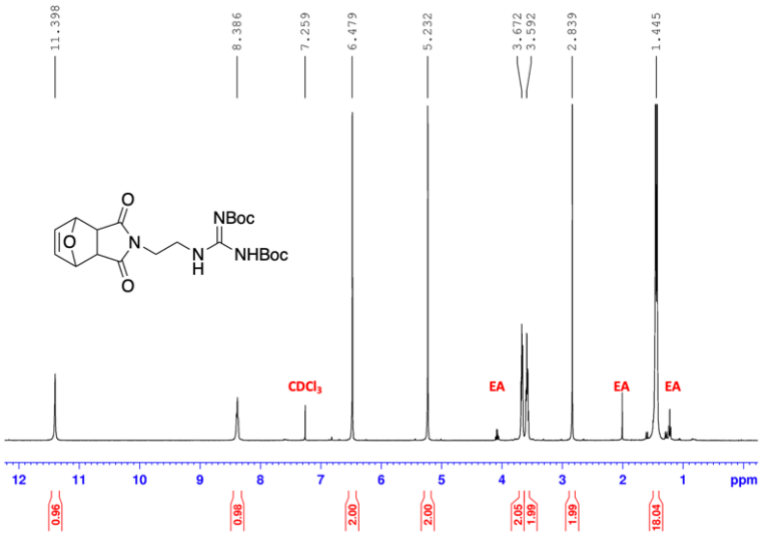

Synthesis of 4. *N, N'*-di-Boc-1*H*-pyrazole-1-carboxamidine (3.22 mmol, 1 g) was added to a round bottom flask and dissolved in methylene chloride. Aniline (4.2 mmol, 0.38 mL) was added to the flask, and the reaction mixture was heated at 50 °C and stirred for 16 hours. The crude was diluted to 80 ml of methylene chloride and washed with H_2O (2x100 mL), brine (1x100 mL), dried ($MgSO_4$ anhydrous), and filtered. The solvent was removed in vacuo, and the crude was purified by recrystallization using hot MeOH, compound 4.

4: ^{1}H NMR (400MHz, $CDCl_3$): δ 11.65 (s, 1H), 10.32 (s, 1H), 7.60 (d, 2H), 7.32 (t, 2H), 7.11 (t, 1H), 1.54 and 1.51 (br s, 18H).

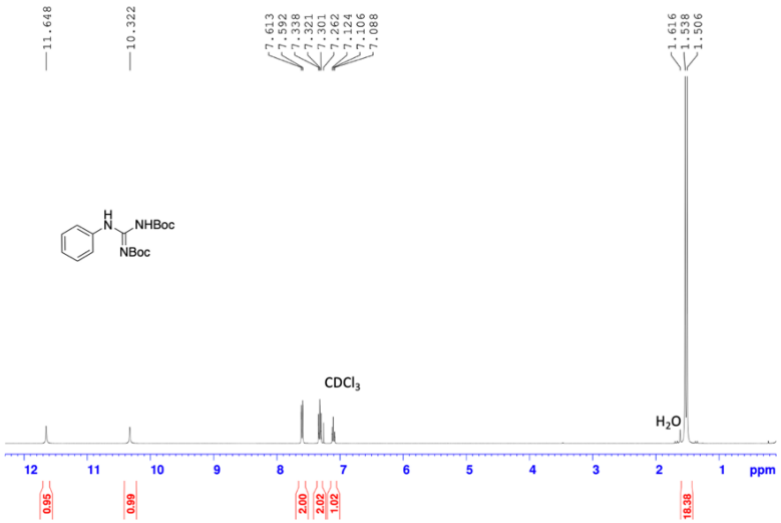

Synthesis of 5. *N, N'*-di-Boc-1*H*-pyrazole-1-carboxamidine (11 mmol, 3.4 g) was added to a round bottom flask and dissolved in methylene chloride. Triethylamine (9.3 mmol, 1.3 mL) and Benzylamine (9.3 mmol, 1.02 mL) were added to the flask, and the reaction mixture was stirred for 16 hours at room temperature. The crude was diluted to 80 ml of methylene chloride and washed with H_2O (2x100 mL), brine (1x100 mL), dried ($MgSO_4$ anhydrous), and filtered. The solvent was removed in vacuo, and the crude was purified by recrystallization using methylene chloride:MeOH, yielding compound 5.

5: Yield: 63%. ^{1}H NMR (400MHz, $CDCl_3$): δ 11.53 (s, 1H), 8.60 (s, 1H), 7.33 (br m, 5H), 4.63 (s, 2H), 1.52 and 1.48 (br s, 18H).

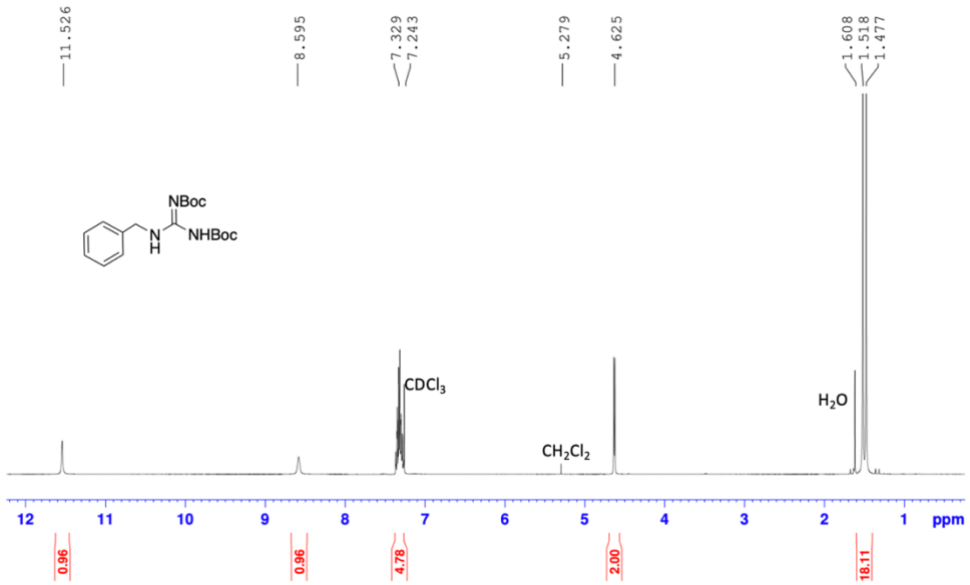

Synthesis of 6. Compound 2 (1.24 mmol, 400 mg) and *N*, *N*-di-Boc-phenylguanidine **4** (0.992 mmol, 333 mg) were added to a round bottom flask and dissolved in 6 mL of THF and triethylamine (7.44 mmol, 1 mL). The mixture was stirred at reflux for 16 hours. Then, the solvent was removed in vacuo, and the crude was diluted in methylene chloride and washed with NH_4Cl (1x10 mL), brine (1x10 mL), dried ($MgSO_4$ anhydrous), and concentrated in vacuo. The crude was purified by flash column using n-Hexane: Ethyl Acetate (9:1) and then (4:1), yielding monomer 6.

6: Yield: 52%. ^{1}H NMR (400MHz, $CDCl_3$): δ 12.14 (s, 1H), 10.11 (s, 1H), 7.56 (d, 2H), 7.27 (t, 2H), 7.07 (t, 1H), 6.49 (s, 2H), 5.53 (t, 1H), 5.25 (s, 2H), 3.69 (t, 2H), 3.40 (m, 2H), 2.84 (s, 2H), 1.50 (s, 9H).

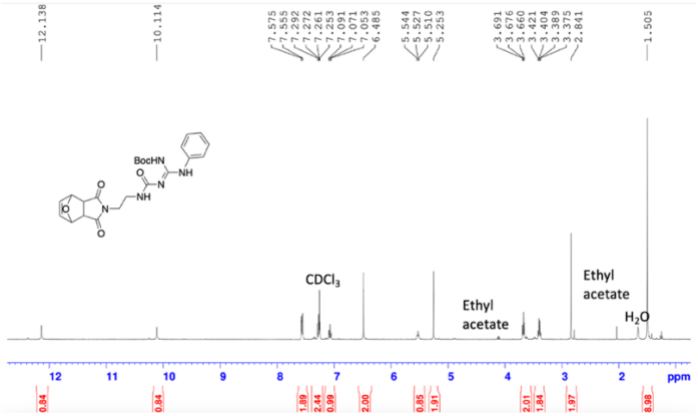

Synthesis of 7. Compound 2 (1.24 mmol, 400 mg) and *N*, *N*-di-Boc-benzylguanidine 5 (0.992 mmol, 346.6 mg) were added to a round bottom flask and dissolved in 6 mL of THF and triethylamine (7.44 mmol, 1 mL). The mixture was stirred at reflux for 16 hours. Then, the solvent was removed in vacuo, and the crude was diluted in methylene chloride and washed with NH_4Cl (1x10 mL), brine (1x10 mL), dried ($MgSO_4$ anhydrous), and concentrated in vacuo. The crude was purified by flash column using n-Hexane: Ethyl Acetate (2x 4:1) and (1x 1:1) yielding monomer 7.

7: Yield: 45%. ^{1}H NMR (400MHz, $CDCl_3$): δ 12.00 (s, 1H), 8.37 (s, 1H), 7.32 (br m, 5H), 6.47 (s, 2H), 5.37 (t, 1H), 5.21 (s, 2H), 4.50 (s, 2H), 3.67 (t, 2H), 3.37 (m, 2H), 2.83 (s, 2H), 1.45 (s, 9H).

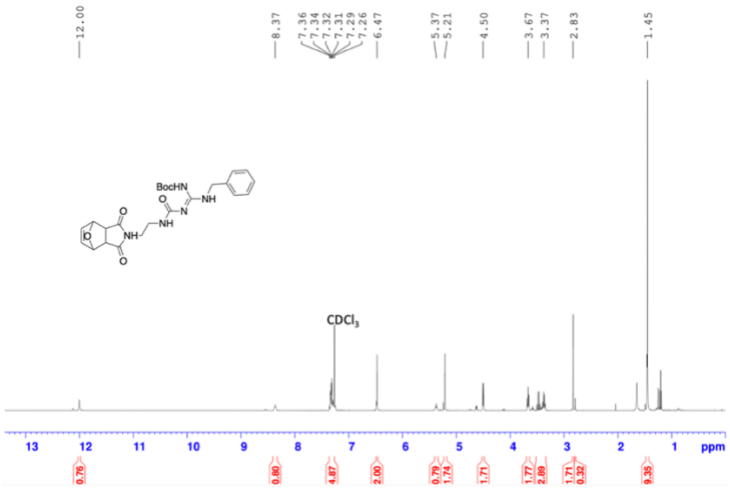

Polymer Synthesis –

Synthesis of Ph-CG. Monomer 3 was dissolved in DCM. Grubbs 3rd generation catalyst was dissolved in DCM and added to the stirring monomer solution. After 60 min, the living polymer was end-capped with 1 mL of ethyl vinyl ether. The polymer solution was precipitated into stirring diethyl ether (3x) and dried. The dried solid was dissolved in a DCM/TFA mixture (1:1, v/v) and deprotected overnight. The reaction mixture was precipitated (3x) and collected via centrifugation. Deprotected polymer was dissolved in dry DMF. 5 equivalents of phenyl isocyanate were added. The mixture was sealed in a vial and allowed to react overnight at 75 °C. The reaction mixture was precipitated into diethyl ether (3x) and the polymer was collected via centrifugation.

Ph-CG: ^{1}H NMR (400 MHz, DMSO-d_6): δ 11.70 (br, 1H), 9.59 (br, 1H), 9.15 (br, 2H), 7.91 (br, 2H), 7.69 (br, 1H), 7.55 (br, 2H), 5.75 (br, 2H), 4.91 (br, 1H), 4.41 (br, 1H), 3.60 (br, 4H), 3.24 (br, 2H).

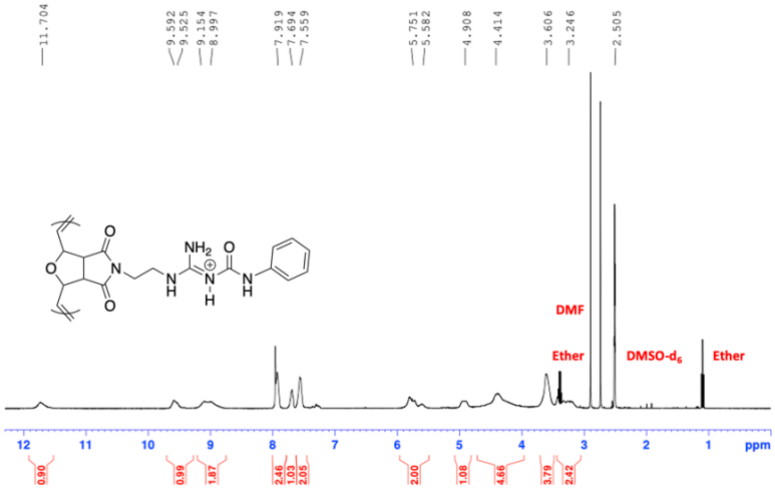

Synthesis of Bn-CG. Monomer 3 was dissolved in DCM. Grubbs 3rd generation catalyst was dissolved in DCM and added to the stirring monomer solution. After 60 min, the living polymer was end-capped with 1 mL of ethyl vinyl ether. The polymer solution was precipitated into stirring diethyl ether (3x) and dried. The dried polymer was dissolved in THF to which 2.5 equivalents of benzylamine were added. The mixture was sealed in a vial and allowed to react overnight at 75 °C. The reaction mixture was precipitated into diethyl ether (3x) and then deprotected in DCM/TFA mixture (1:1, v/v). Deprotected polymer solution was precipitated into diethyl ether (3x) and polymer was collected via centrifugation.

Bn-CG protected: ^{1}H NMR (400 MHz, $CDCl_3$): δ 12.04 (br, 1H), 8.14 (br, 1H), 7.20 (br, 5H), 5.97 (br, 1H), 5.67 (br, 1H), 4.97 (br, 1H), 4.33 (br, 3H), 3.56 (br, 4H), 3.17 (br, 2H), 1.44 (s, 9H).

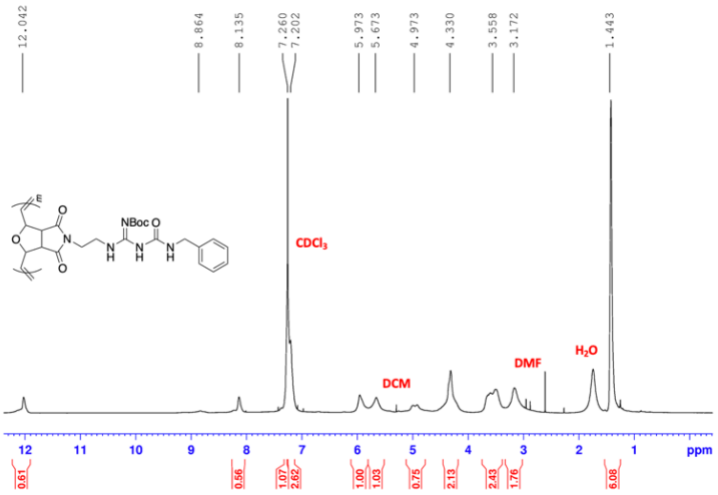

Bn-CG: ^{1}H NMR (400 MHz, DMSO-d$_6$): δ 9.15 (br, 1H), 8.61 (br, 2H), 7.99 (br, 1H), 7.27 (br, 5H), 5.92 (br, 1H), 5.71 (br, 2H), 4.94 (br, 1H), 4.41 (br, 1H), 4.25 (br, 4H), 3.75 (br, 4H).

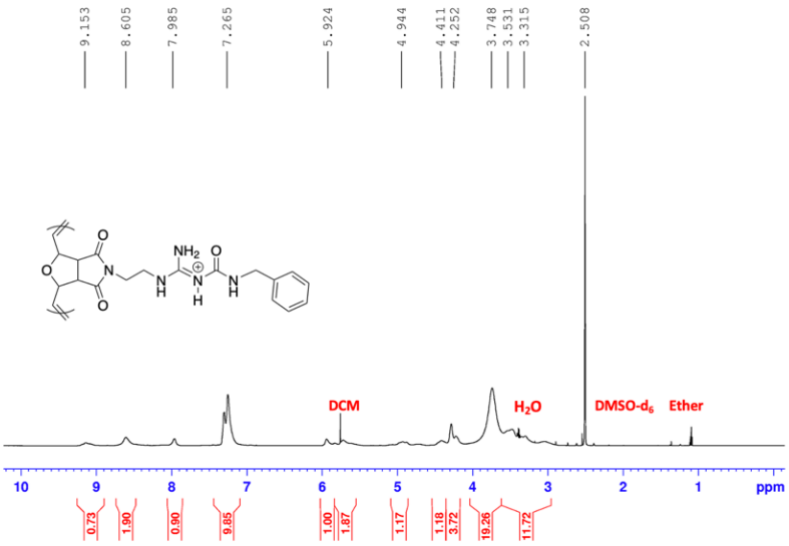

Synthesis of Ph-CG' and Bn-CG'. Grubb's catalyst 3rd generation was dissolved in dry DCM and added to a stirring solution containing monomer 6 (Ph-CG') or 7 (Bn-CG'). After 60 min, the living polymer was end-capped with 1 mL of ethyl vinyl ether. The polymer solution was precipitated into stirring diethyl ether (3x) and dried. The protected

polymer Ph-CG' was deprotected by mixing it with methylene chloride and trifluoroacetic acid (3:2) for 4 hours. Then, the deprotected polymer was precipitated in diethyl ether (3x) and dried.

Ph-CG' (protected): ^{1}H NMR (400MHz, $CDCl_3$): δ 12.15 (br s, 1H), 10.04 (br m, 1H), 7.50 (br m, 2H), 7.30 (br m, 3H), 7.05 (br s, 1H), 5.95 (br s, 1H), 5.73 (br s, 1H), 5.03 (br m, 1H), 4.46 (br s, 1H), 3.36 (br m, 6H), 1.49 (br s, 9H).

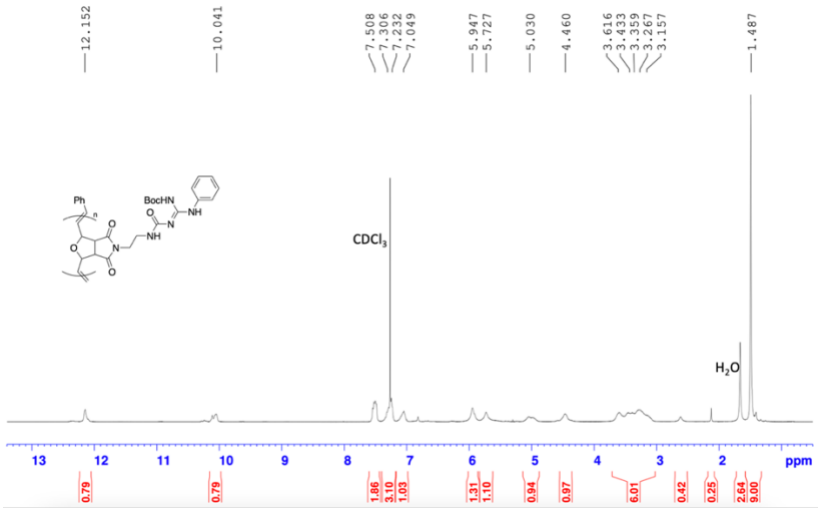

Bn-CG' (protected): ^{1}H NMR (400MHz, $CDCl_3$): δ 12.03 (br m, 1H), 8.36 (br s, 1H), 7.26 (br m, 5H), 6.02 (br s, 1H), 5.76 (br s, 1H), 5.08 (br m, 1H), 4.50 (br m, 3H), 3.60 (br m, 2H), 3.29 (br m, 4H), 1.43 (br s, 9H).

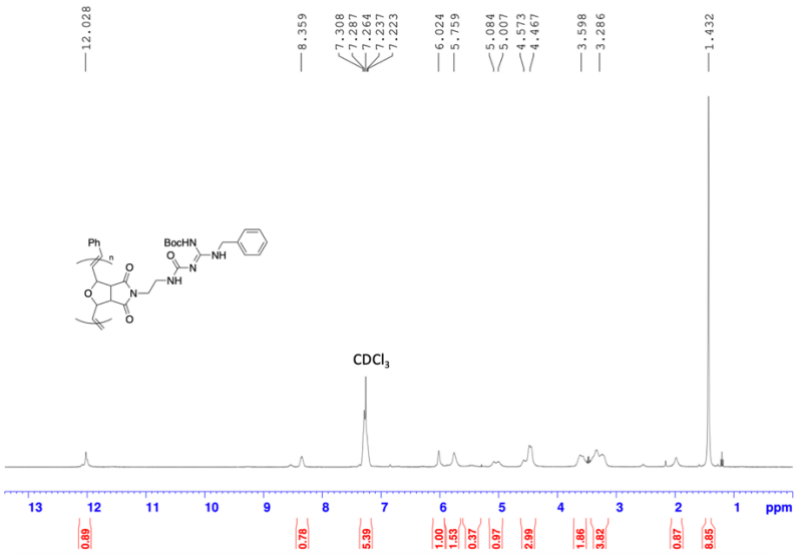

3.6. References

(1) Benjamin Leader, Q. J. B. and D. E. G. Protein Therapeutics: A Summary and Pharmacological Classification. *Nat. Rev. Drug Discov.* **2008**, *7* (1), 21–39.

(2) Fu, A.; Tang, R.; Hardie, J.; Farkas, M. E.; Rotello, V. M. Promises and Pitfalls of Intracellular Delivery of Proteins. *Bioconjug. Chem.* **2014**, *25* (9), 1602–1608. https://doi.org/10.1021/bc500320j.

(3) Carter, P. J.; Lazar, G. A. Next Generation Antibody Drugs: Pursuit of the "High-Hanging Fruit." *Nat. Rev. Drug Discov.* **2018**, *17* (3), 197–223. https://doi.org/10.1038/nrd.2017.227.

(4) Slastnikova, T. A.; Ulasov, A. V.; Rosenkranz, A. A.; Sobolev, A. S. Targeted Intracellular Delivery of Antibodies: The State of the Art. *Front. Pharmacol.* **2018**, *9* (OCT), 1–21. https://doi.org/10.3389/fphar.2018.01208.

(5) Diehn, M.; Bhattacharya, R.; Botstein, D.; Brown, P. O. Genome-Scale Identification of Membrane-Associated Human MRNAs. *PLoS Genet.* **2006**, *2* (1), 39–50. https://doi.org/10.1371/journal.pgen.0020011.

(6) Fu, A.; Tang, R.; Hardie, J.; Farkas, M. E.; Rotello, V. M. Promises and Pitfalls of Intracellular Delivery of Proteins. *Bioconjug. Chem.* **2014**, *25* (9), 1602–1608. https://doi.org/10.1021/bc500320j.

(7) Lv, J.; Fan, Q.; Wang, H.; Cheng, Y. Polymers for Cytosolic Protein Delivery. *Biomaterials* **2019**, *218* (July), 119358. https://doi.org/10.1016/j.biomaterials.2019.119358.

(8) Qin, X.; Yu, C.; Wei, J.; Li, L.; Zhang, C.; Wu, Q.; Liu, J.; Yao, S. Q.; Huang, W. Rational Design of Nanocarriers for Intracellular Protein Delivery. *Adv. Mater.* **2019**, *31* (46), 1–32. https://doi.org/10.1002/adma.201902791.

(9) Backlund, C. M.; Hango, C. R.; Minter, L. M.; Tew, G. N. Protein and Antibody Delivery into Difficult-to-Transfect Cells by Polymeric Peptide Mimics. *ACS Appl. Bio Mater.* **2020**, *3* (1), 180–185. https://doi.org/10.1021/acsabm.9b00876.

(10) Davis, H. C.; Posey, N. D.; Tew, G. N. Protein Binding and Release by Polymeric Cell-Penetrating Peptide Mimics. *Biomacromolecules* **2022**, *23* (1), 57–66. https://doi.org/10.1021/acs.biomac.1c00929.

(11) Hango, C. R.; Backlund, C. M.; Davis, H. C.; Posey, N. D.; Minter, L. M.; Tew, G. N. Non-Covalent Carrier Hydrophobicity as a Universal Predictor of Intracellular Protein Activity. *Biomacromolecules* **2021**, *22* (7), 2850–2863. https://doi.org/10.1021/acs.biomac.1c00242.

(12) Lättig-Tünnemann, G.; Prinz, M.; Hoffmann, D.; Behlke, J.; Palm-Apergi, C.; Morano, I.; Herce, H. D.; Cardoso, M. C. Backbone Rigidity and Static Presentation of Guanidinium Groups Increases Cellular Uptake of Arginine-Rich Cell-Penetrating Peptides. *Nat. Commun.* **2011**, *2* (1). https://doi.org/10.1038/ncomms1459.

(13) Sun, J.; Zhang, L.; Wang, J.; Feng, Q.; Liu, D.; Yin, Q.; Xu, D.; Wei, Y.; Ding, B.; Shi, X.; et al. Tunable Rigidity of (Polymeric Core)-(Lipid Shell) Nanoparticles for Regulated Cellular Uptake. *Adv. Mater.* **2015**, *27* (8), 1402–1407. https://doi.org/10.1002/adma.201404788.

(14) Kretzmann, J. A.; Luther, D. C.; Evans, C. W.; Jeon, T.; Jerome, W.; Gopalakrishnan, S.; Lee, Y. W.; Norret, M.; Iyer, K. S.; Rotello, V. M. Regulation of Proteins to the Cytosol Using Delivery Systems with Engineered Polymer Architecture. *J. Am. Chem. Soc.* **2021**. https://doi.org/10.1021/jacs.1c00258.

(15) Nguyen, H. V. T.; Jiang, Y.; Mohapatra, S.; Wang, W.; Barnes, J. C.; Oldenhuis, N. J.; Chen, K. K.; Axelrod, S.; Huang, Z.; Chen, Q.; et al. Bottlebrush Polymers with Flexible Enantiomeric Side Chains Display Differential Biological Properties. *Nat. Chem.* **2021**. https://doi.org/10.1038/s41557-021-00826-8.

(16) Barrios, A.; Estrada, M.; Moon, J. H. Carbamoylated Guanidine-Containing Polymers for Non-Covalent Functional Protein Delivery in Serum-Containing Media. *Angew. Chemie Int. Ed.* **2022**, *33199*. https://doi.org/10.1002/anie.202116722.

(17) Kelly, B.; McMullan, M.; Muguruza, C.; Ortega, J. E.; Meana, J. J.; Callado, L. F.; Rozas, I. A2-Adrenoceptor Antagonists: Synthesis, Pharmacological Evaluation, and Molecular Modeling Investigation of Pyridinoguanidine, Pyridino-2-Aminoimidazoline and Their Derivatives. *J. Med. Chem.* **2015**, *58* (2), 963–977. https://doi.org/10.1021/jm501635e.

(18) Kleinmaier, R.; Keller, M.; Igel, P.; Buschauer, A.; Gschwind, R. M. Conformations, Conformational Preferences, and Conformational Exchange of N′-Substituted N -Acylguanidines: Intermolecular Interactions Hold the Key. *J. Am. Chem. Soc.* **2010**, *132* (32), 11223–11233. https://doi.org/10.1021/ja103756y.

(19) Dardonville, C.; Caine, B. A.; Navarro De La Fuente, M.; Martín Herranz, G.; Corrales Mariblanca, B.; Popelier, P. L. A. Substituent Effects on the Basicity (p: K a) of Aryl Guanidines and 2-(Arylimino)Imidazolidines: Correlations of PH-Metric and UV-Metric Values with Predictions from Gas-Phase Ab Initio Bond Lengths. *New J. Chem.* **2017**, *41* (19), 11016–11028. https://doi.org/10.1039/c7nj02497e.

(20) Wang, M.; Liu, H.; Li, L.; Cheng, Y. A Fluorinated Dendrimer Achieves Excellent Gene Transfection Efficacy at Extremely Low Nitrogen to Phosphorus Ratios. *Nat. Commun.* **2014**, *5*, 1–8. https://doi.org/10.1038/ncomms4053.

(21) Li, M.; Schlesiger, S.; Knauer, S. K.; Schmuck, C. A Tailor-Made Specific Anion-Binding Motif in the Side Chain Transforms a Tetrapeptide into an Efficient Vector for Gene Delivery. *Angew. Chemie - Int. Ed.* **2015**, *54* (10), 2941–2944. https://doi.org/10.1002/anie.201410429.

(22) Hatai, J.; Schmuck, C. Diverse Properties of Guanidiniocarbonyl Pyrrole-Based Molecules: Artificial Analogues of Arginine. *Acc. Chem. Res.* **2019**, *52* (6), 1709–1720. https://doi.org/10.1021/acs.accounts.9b00142.

(23) Dutta, K.; Kanjilal, P.; Das, R.; Thayumanavan, S. Synergistic Interplay of Covalent and Non-Covalent Interactions in Reactive Polymer Nanoassembly Facilitates Intracellular Delivery of Antibodies. *Angew. Chemie - Int. Ed.* **2021**, *60* (4), 1821–1830. https://doi.org/10.1002/anie.202010412.

(24) Liu, R.; Chen, Y.; Liu, G.; Li, C.; Song, Y.; Cao, Z.; Li, W.; Hu, J.; Lu, C.; Liu, Y. PI3K/AKT Pathway as a Key Link Modulates the Multidrug Resistance of Cancers. *Cell Death Dis.* **2020**, *11* (9). https://doi.org/10.1038/s41419-020-02998-6.

(25) Kim, S.; Lee, J.; Jo, S.; Brooks, C. L.; Lee, H. S.; Im, W. CHARMM-GUI Ligand Reader and Modeler for CHARMM Force Field Generation of Small Molecules. *J. Comput. Chem.* **2017**, *38* (21), 1879–1886. https://doi.org/10.1002/jcc.24829.

(26) Lee, J.; Cheng, X.; Swails, J. M.; Yeom, M. S.; Eastman, P. K.; Lemkul, J. A.; Wei, S.; Buckner, J.; Jeong, J. C.; Qi, Y.; et al. CHARMM-GUI Input Generator

for NAMD, GROMACS, AMBER, OpenMM, and CHARMM/OpenMM Simulations Using the CHARMM36 Additive Force Field. *J. Chem. Theory Comput.* **2016**, *12* (1), 405–413. https://doi.org/10.1021/acs.jctc.5b00935.

(27) Jorgensen, W. L.; Chandrasekhar, J.; Madura, J. D.; Impey, R. W.; Klein, M. L. Comparison of Simple Potential Functions for Simulating Liquid Water. *J. Chem. Phys.* **1983**, *79* (2), 926–935. https://doi.org/10.1063/1.445869.

(28) Phillips, J. C.; Braun, R.; Wang, W.; Gumbart, J.; Tajkhorshid, E.; Villa, E.; Chipot, C.; Skeel, R. D.; Kalé, L.; Schulten, K. Scalable Molecular Dynamics with NAMD. *J. Comput. Chem.* **2005**, *26* (16), 1781–1802. https://doi.org/10.1002/jcc.20289.

(29) Tezgel, A. Ö.; Jacobs, P.; Backlund, C. M.; Telfer, J. C.; Tew, G. N. Synthetic Protein Mimics for Functional Protein Delivery. *Biomacromolecules* **2017**, *18* (3), 819–825. https://doi.org/10.1021/acs.biomac.6b01685.

CHAPTER IV

Perspectives and Future Outlook

The development of polymer-based carriers for protein delivery has made significant advances in recent times. The FDA and regulatory approvals of other macromolecule-based therapies offer significant promise looking forward and provide insight into the next steps for clinical applications. As many of the concept's surrounding protein delivery stem from the delivery of other macromolecules, key bottlenecks observed during translational research provides a path to advance this new era of protein-based therapeutics.

While fluorescent proteins are an excellent model system to test the efficacy of protein delivery systems, proteins with biological function offer a deeper understanding of protein-polymer interactions upon complexation, entry, and release. While the results discussed in Chapter 2 and 3 demonstrate the retained apoptotic function of various proteins, experiments demonstrating other biological activities would bolster our claims. In the field of stem cell therapy, bone marrow-derived mesenchymal stem cells (BM-MSCs) have potential to differentiate to osteoblasts and aid the treatment of bone diseases. The intracellular delivery of growth factors may up- or downregulate genes involved in differentiation. Bone morphogenic protein-2 (BMP-2) was intracellularly delivered using the best performing polymer discussed earlier to patient derived MSCs. Preliminary results indicate enhanced phenotypical changes, such as calcium mineralization, after intracellular delivery. These observations suggest the direct delivery of proteins, as opposed to traditional gene delivery, may be a promising technique for the engineering of stem cells prior to in vivo injection. Taken together, continued experiments aim to demonstrate the feasibility of this type of therapy for bone loss disease.

While the topic of protein delivery generally refers to the intracellular entry of the protein cargo, delivery may encompass the transport of the protein to the target site, cell type, or tissue. As discussed previously, the high stability of our polymer-cargo complexes provides promise to use these carriers in the harsh physiological environment. Oral delivery of proteins remains a major hurdle in the advancement of the field. Various model systems exist to mimic the human intestinal epithelium. Although these models have limitations, being able to study the stability of complexes in the mucosal lining and their transcytosis behaviors is of utmost importance. A model system composed of human colon carcinoma Caco-2 and mucus-producing HT-29 cells was established and used for protein delivery experiments. While transcytosis of polymer-protein complexes was not readily achieved, it was established more modifications were needed for carriers to pass through the single-cell layer epithelium. Further optimization in terms of polymer composition would elucidate the potential to cross through a major barrier for oral delivery.

Finally, a major avenue of future research to be explored is polymer biodegradability. The ROMP-based polymers discussed earlier have non-degradable backbones. Major questions remain regarding the fate of the polymer after cellular entry. Various biodegradable polymers have been used for macromolecule delivery, therefore the grafting of our developed functional group to biodegradable backbones may offer hope to avoid complications arising from our current platform.

Overall, the protein carriers discussed here have demonstrated the successful delivery of various proteins to multiple cell types. The polymer platform chosen allowed for probing the structure activity relationship in both polymer-protein interactions and the subsequent cellular entry. The designed functional group on the polymer side chains

demonstrated significant enhancement on protein delivery, providing insights that may be readily applied to other carriers. A vast wealth of opportunities exists to aid the advancement of this new era of protein-based therapeutics.

VITA

ALFONSO BARRIOS

abarr159@fiu.edu

EDUCATION

2017-2022	Ph.D. Candidate (expected graduation July 2022) Florida International University, Miami, FL, USA Dissertation Title: Modified Guanidine-Containing Polymers for Intracellular Protein Delivery Advisor: Joong Ho Moon, Ph.D.
2017-2020	Master of Science, Chemistry Florida International University, Miami, FL, USA
2012-2016	Bachelor of Science, Chemistry Florida International University, Miami, FL, USA

PATENTS AND PUBLICATIONS

Barrios, A.; Moon, J. H. Modulated guanidine-containing polymers or nanoparticles. *United States Patent* US 10 688 189 B1, 2020.

Barrios, A.; Diaz, M. M.; Moon, J. H. Modified guanidine-containing polymers for biological delivery. *United States Patent Application* 17/578,709, 2022.

Barrios, A.; Diaz, M. M.; Perozo, E.; Hossen, L.; Chapagain, P.; Moon, J. H. Effects of Sidechain Isomerism on Polymer-Based Non-Covalent Protein Delivery. *Chem. Commun*., 2022, DOI: 10.1039/d2cc02343a.

Barrios, A.; Estrada, M.; Moon, J.H. Carbamoylated Guanidine-Containing Polymers for Non-Covalent Functional Protein Delivery in Serum-Containing Media. *Angew. Chem. Int. Ed.* 2022, e202116722.

Ahmed, M.; Dutta, R.; Manandhar, P.; Li, X.; Torabi, H.; Barrios, A.; Wang, P.; Unwalla, H.; Moon, J.H. A guanylurea-functionalized conjugated polymer enables RNA interference in ex vivo human airway epithelium. *Chem. Commun*., 2019, 55, 7804-7807.